INVESTIGATION OF EFFECTIVE ELASTIC PROPERTIES OF FRAME-LIKE PERIODIC CELLULAR SOLIDS BY STRAIN-ENERGY-BASED HOMOGENIZATION

BY

KASEM THEERAKITTAYAKORN

A DISSERTATION SUBMITTED IN PARTIAL FULFILLMENT OF THE REQUIREMENTS FOR THE DEGREE OF DOCTOR OF PHILOSOPHY (ENGINEERING)
SIRINDHORN INTERNATIONAL INSTITUTE OF TECHNOLOGY
THAMMASAT UNIVERSITY
ACADEMIC YEAR 2015

INVESTIGATION OF EFFECTIVE ELASTIC PROPERTIES OF FRAME-LIKE PERIODIC CELLULAR SOLIDS BY STRAIN-ENERGY-BASED HOMOGENIZATION

BY

KASEM THEERAKITTAYAKORN

A DISSERTATION SUBMITTED IN PARTIAL FULFILLMENT OF
THE REQUIREMENTS FOR THE DEGREE OF DOCTOR OF
PHILOSOPHY (ENGINEERING)
SIRINDHORN INTERNATIONAL INSTITUTE OF TECH
THAMMASAT UNIVERSITY
ACADEMIC YEAR 2015

INVESTIGATION OF EFFECTIVE ELASTIC PROPERTIES OF FRAME-LIKE PERIODIC CELLULAR SOLIDS BY STRAIN-ENERGY-BASED HOMOGENIZATION

A Dissertation Presented

By

KASEM THEERAKITTAYAKORN

Submitted to

Sirindhorn International Institute of Technology

Thammasat University

In partial fulfillment of the requirements for the degree of

DOCTOR OF PHILOSOPHY (ENGINEERING)

Approved as to style and content by

Advisor and Chairperson of Thesis Committee _____
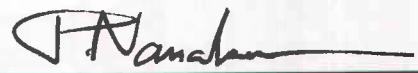
(Professor Pruettha Nanakorn, DEng)

Co-Advisor _____

(Kriskrai Sitthiseripratip, PhD)

Committee Member and
Chairperson of Examination Committee _____
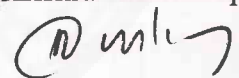
(Professor Somnuk Tangtermsirikul, DEng)

Committee Member _____
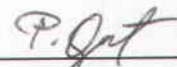
(Associate Professor Pakorn Opaprakasit, PhD)

Committee Member _____

(Assistant Professor Ekachai Chaichanasiri, PhD)

External Examiner: Professor Teerapong Senjuntichai, PhD

July 2016

i

Acknowledgements

Abstract

INVESTIGATION OF EFFECTIVE ELASTIC PROPERTIES OF FRAME-LIKE
PERIODIC CELLULAR SOLIDS BY STRAIN-ENERGY-BASED
HOMOGENIZATION

by

KASEM THEERAKITTAYAKORN

B.Sc. in Biotechnology, King Mongkut's Institute of Technology Ladkrabang, 2005

M.Sc. in Medical Science, Chulalongkorn University, 2009

Periodic cellular solids are used in various applications such as tissue-engineering scaffolds, lightweight structural sandwich panels, energy absorption devices, and thermal insulating containers. When periodic cellular solids are used as load-bearing structures, the effective elastic properties of periodic cellular solids are of significant interest, and are among the main considerations of cellular solid design. The desired effective elastic properties of a periodic cellular solid can be obtained by appropriate selection of the base material and the topology of its unit cell. Homogenization methods can be used to calculate the effective elastic properties of a periodic cellular solid from its unit-cell structure and the finite element method can be used to analyze the unit cell. Many useful periodic cellular solids are frame-like structures. For such periodic cellular solids, beam elements can be used to accurately model their struts. In this study, the exact forms of the effective elastic constants of arbitrary frame-like periodic cellular solids that can be modelled accurately by Euler beams are analytically derived by using the homogenization method based on equivalent strain energy. The exact forms are obtained in terms of some dimensionless factors, the characteristic length and volume of the unit cell, the area and moment of inertia of the struts, and Young's modulus of the base material. In general, the dimensionless factors can be functions of the area and moment of inertia of the struts. However, in many practical cases, these factors are constant. When the dimensionless factors are constant, they can be determined by exact curve fitting using finite element results with different areas and moments of inertia of the struts. In these cases, the closed-form solutions of the effective elastic constants will be obtained from exact curve fitting. By using the closed-form effective elastic constants obtained from exact curve fitting, mechanical characteristics of periodic cellular solids with various unit-cell topologies can be

iii

determined. This allows advantages and disadvantages of different unit-cell topologies to be studied. The closed-form effective elastic constants also allow the effect of strut sectional properties on the effective elastic constants to be thoroughly investigated. In addition to the closed-form effective elastic constants obtained from the exact forms with exact curve fitting, the closed-form effective elastic constants can also be derived in a symbolic computation platform. In summary, by using the closed-form effective elastic constants, unit-cell topologies and strut sectional properties can be appropriately chosen to suit different applications.

Keywords: Periodic cellular solid, Homogenization, Effective elastic property, Euler beam element

Table of Contents

List of Figures

List of Tables

Chapter 1

Introduction

1.1 General

Periodic cellular solids are cellular solids that are composed of repeating structures called unit cells (Fig. 1). The unit cells in a periodic cellular solids are joined to each other and regularly aligned to form the structure of the solid. Porous structures of cellular solids can provide advantageous properties such as light weight, low density, high permeability, low thermal conductivity, and high energy absorption. For periodic cellular solids, their complicated unit-cell structures can provide extraordinary properties over normal cellular solids. For instance, periodic cellular solids can exhibit extreme mechanical properties, such as Poisson's ratio close to -1, 0, and 0.5 (Milton, 1992; Sigmund, 1995). Due to these special properties that are difficult or impossible to find in natural materials, periodic cellular solids can be very useful in various engineering applications and are of interest to researchers.
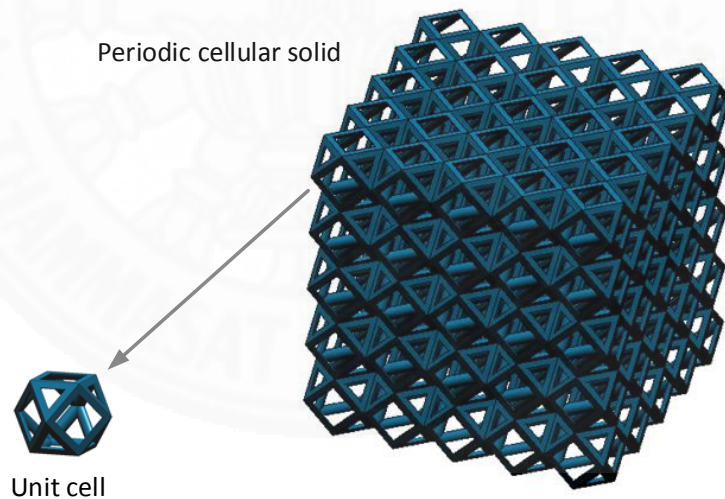
Fig. 1   A periodic cellular solid and its unit cell.

The properties of a periodic cellular solid depend on the base material and its unit cell topology. The desired effective elastic properties of a periodic cellular solid can be obtained by appropriate selection of the base material and the topology of its unit cell. There are a great variety of shapes that can be used as unit-cell topologies. Among them, polyhedrons are the shapes that are convenient to fabricate and use. A polyhedron is a 3D shape bounded by a set

of polygons that are joined at their edges to completely close a space. When polyhedrons are used as unit cells, they are often made of edges only in order that the resulting solids become open-cell structures. When unit cells are composed of only struts connected together at their ends, their periodic cellular solids resemble frame structures. Besides some common shapes, new topologies of unit cells can be designed and obtained from various methods in order to gain periodic cellular solids which possess desired properties.

A periodic cellular solid will behave as a homogeneous material when there are a significantly large number of unit cells in the solid. If the number of unit cells in a periodic cellular solid is small, the solid will not behave as a homogeneous material. If, however, the number of unit cells is continuously increased, the behavior of the solid will converge to that of a homogeneous material, and the apparent elastic properties of the solid will converge to constants, which are its effective elastic properties. In other words, if the size of the unit cell is sufficiently small when compared to the size of the whole solid, the apparent properties will converge to the effective properties. The effective elastic properties are important mechanical properties of periodic cellular solids especially when the periodic cellular solids are used as load-bearing structures.

The effective elastic properties of periodic cellular solids can be designed by changing their unit-cell topologies because their effective elastic properties are in fact defined by their unit cells. The effective elastic properties of periodic cellular solids can be determined from their unit cells by using homogenization methods (Suquet, 1987; Sigmund, 1995; Luxner, Stampfl, & Pettermann, 2005; Drago & Pindera, 2007). Generally, homogenization methods define the effective constitutive material law of a material as a relationship between some average stress and some average strain. The effective elastic constants can be obtained by analyzing the material under appropriate boundary conditions at far-field. When a periodic cellular solid is considered, periodic boundary conditions can be used and the average stress and average strain can be computed directly from the solid's unit cell due to the periodicity. The homogenization method based on equivalent strain energy (Zhang et al., 2007; Dai & Zhang, 2009; Alzebdeh, 2012) is a convenient method for finding the effective elastic constants of periodic cellular solids. The method determines the effective elastic constants of a periodic cellular solid from strain energy values of the solid's unit cell that is subjected to some prescribed strain modes. These strain energy values can be obtained from finite element analysis (FEA) of the unit cell. Since the finite element method (FEM) is a numerical method, the effective elastic constants are generally obtained numerically.

1.2 Statement of the problem

Although computing the effective elastic constants of periodic cellular solids numerically using FEM is certainly useful, the effective elastic constants have to be numerically obtained for each solid, one by one. As a result, investigation of how topologies and shapes of unit cells affect the effective elastic constants of the resulting periodic cellular solids can be difficult to perform. It will be quite beneficial if the closed-form effective elastic constants of periodic cellular solids can be found.

It is apparent that there exist no general closed-form effective elastic constants for periodic cellular solids of arbitrary shapes. However, many useful periodic cellular solids are generated by connecting slender strut members and, therefore, resemble frame structures. These frame-like periodic cellular solids can be modelled accurately as frame structures using beam elements. For frame-like periodic cellular solids, it is sometimes possible to analytically determine their closed-form effective elastic constants using, for example, manual calculations (Zhu, Knott, & Mills, 1997; Gibson & Ashby, 1999; Wang & McDowell, 2004) or symbolic FE programs. The problems are that manual calculations are tedious and prone to errors and symbolic FE programs are not commonly available. Another possible alternative is to determine the exact forms of the effective elastic constants for arbitrary frame-like periodic cellular solids. Unlike periodic cellular solids that are not frame-like, it is quite possible that frame-like periodic cellular solids share certain basic forms of their effective elastic constants. This is because the effective elastic constants are derived from strain energy values of unit cells under prescribed strain modes and strain energy of different beams can be written in the same form. The exact forms of the effective elastic constants for arbitrary frame-like periodic cellular solids will allow the closed-form effective elastic constants of frame-like periodic cellular solids having different unit-cell topologies to be determined via exact curve fitting.

If the closed-form effective elastic constants of periodic cellular solids having a certain unit-cell topology is known, it will be possible to determine the degrees of homogeneity of periodic solids with different numbers of unit cells. As aforementioned, if the number of unit cells in a periodic cellular solid is continuously increased, the behavior of the solid will converge to that of a homogeneous material and the apparent elastic constants of the solid will converge to its effective elastic constants. Knowing the limiting values of the apparent elastic constants from the closed-form solutions allows the degrees of homogeneity to be determined.

In addition to the degrees of homogeneity, the closed-form effective elastic constants of frame-like periodic cellular solids having a certain unit-cell topology also allow the effect of relative unit-cell strut sizes to be investigated. One of the most important effects of relative

unit-cell strut sizes is the degree of isotropic symmetry. Changing relative strut sizes within unit cells can change the degree of isotropic symmetry of the resulting periodic solid. The closed-form effective elastic constants permit design of frame-like periodic cellular solids for isotropic symmetry by appropriate sizing of unit-cell struts to be performed.

1.3 Objectives

The objectives of this study are as follows:

1) To study the applicability of Euler beam elements in the determination of the effective elastic constants of frame-like periodic cellular solids.
2) To derive the exact forms of the effective elastic constants of arbitrary frame-like periodic cellular solids using the homogenization method based on equivalent strain energy.
3) To investigate the degrees of homogeneity of frame-like periodic cellular solids with respect to the relative sizes between unit cells and solids.
4) To develop a methodology to design frame-like periodic solids for isotropic symmetry by appropriate sizing of unit-cell struts.

1.4 Scope of study

The scope of this study is as follows:

1) Materials are assumed to be linear elastic.
2) Periodic cellular solids are frame-like and their struts can be accurately modelled as Euler beams.
3) Homogenization based on equivalent strain energy is used to determine the effective elastic properties.

Chapter 2
Literature Review

There are many useful periodic cellular solids whose structures are frame-like (Gibson & Ashby, 1999; Wallach & Gibson, 2001; Luxner, Stampfl, & Pettermann, 2005; Jang et al., 2013). For this type of periodic structure, using beam theories via beam elements can be a good alternative. The suitability of beam elements for modeling periodic cellular solids depends on how much their structures are frame-like. A periodic cellular solid is more frame-like if its structure consists only of struts whose cross-sectional dimensions are much smaller than their longitudinal dimensions. In other words, a periodic cellular solid is more frame-like if its elements are slenderer. Beam elements have been used to successfully model such frame-like periodic cellular solids by many researchers (Zhu, Knott, & Mills, 1997; Grenestedt, 1998; Onck, Andrews, & Gibson, 2001; Kwon, Cooke, & Park, 2003; Luxner, Stampfl, & Pettermann, 2005; Doyoyo & Hu, 2006; Lipperman, Ryvkin, & Fuchs, 2008; Luxner, Stampfl, & Pettermann, 2009; Thiyagasundaram, Sankar, & Arakere, 2010).

Beam elements are used in the determination of the effective elastic constants of open-cell foams represented by equisided and elongated tetrakaidecahedral unit cells by Thiyagasundaram, Sankar, and Arakere (2010). The maximum relative density considered in their work is 3.45%. The relative density is defined as the ratio between the mass densities of the cellular solid and its base material. The effective elastic constants are obtained from FEA of each unit cell. The unit cells are modeled by both Euler and Timoshenko beam elements and are subject to periodic displacement boundary conditions. The obtained results from the finite element (FE) models employing Euler beam elements match well with the results from the analytical models by Zhu, Knott, and Mills (1997), Sullivan, Ghosn, and Lerch (2008), and Sullivan and Ghosn (2009). These analytical models employ the Euler beam theory and, therefore, do not consider shear deformation in beams. The results from the FE models using Euler and Timoshenko beam elements are found to be comparable in most cases. The models using Euler beam elements yield larger Young's moduli than the ones using Timoshenko beam elements when the struts have smaller slenderness ratios. This is clearly due to the omission of shear deformation in the Euler beam elements. Beam elements are also used by Kwon, Cooke, and Park (2003) in the determination of the effective Young's moduli and the failure strengths of open-cell metal foams represented by tetrakaidecahedral unit cells. The relative densities under consideration range approximately from 6% to 8%. The effective Young's moduli are obtained directly from the deformation of unit cells under appropriate loading without the use

of a homogenization method. The results from Kwon, Cooke, and Park (2003) compare quite satisfactorily with experimental results.

Table 1 Closed forms for the effective elastic constants by Wang and McDowell (2004).

Unit cell		$\dfrac{E_i^*}{E}$	v_{ij}^*	$\dfrac{G_{ij}^*}{E}$
Square		$\dfrac{W}{L}$	$v\left(\dfrac{W}{L}\right)$	$\dfrac{1}{2}\left(\dfrac{W}{L}\right)^3$
Mixed cell		$\left(\dfrac{2\sqrt{2}+2}{2\sqrt{2}+1}\right)\left(\dfrac{W}{L}\right)$	$\dfrac{1}{2\sqrt{2}+1}$	$\dfrac{1}{2\sqrt{2}}\left(\dfrac{W}{L}\right)$
Triangle		$\dfrac{2}{\sqrt{3}}\left(\dfrac{W}{L}\right)$	$\dfrac{1}{3}$	$\dfrac{\sqrt{3}}{4}\left(\dfrac{W}{L}\right)$
Hexagon		$\dfrac{4\sqrt{3}}{3}\left(\dfrac{W}{L}\right)^3$	1	$\dfrac{1}{\sqrt{3}}\left(\dfrac{W}{L}\right)^3$
Diamond		$\dfrac{1}{\sqrt{3}}\left(\dfrac{W}{L}\right)$	$\dfrac{1}{3}$	$\dfrac{\sqrt{3}}{4}\left(\dfrac{W}{L}\right)$
Kagome		$\dfrac{1}{\sqrt{3}}\left(\dfrac{W}{L}\right)$	$\dfrac{1}{3}$	$\dfrac{\sqrt{3}}{8}\left(\dfrac{W}{L}\right)$
Rectangle		$\dfrac{W_1}{L_1}$ for $\dfrac{E_1^*}{E}$ $\dfrac{W_2}{L_2}$ for $\dfrac{E_2^*}{E}$	$v\left(\dfrac{W_1}{L_1}\right)$ for v_{12}^* $v\left(\dfrac{W_2}{L_2}\right)$ for v_{21}^*	$\dfrac{W_1{}^3\,W_2{}^3}{L_1 L_2\left(L_1 W_1{}^3 + L_2 W_2{}^3\right)}$
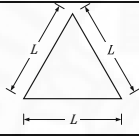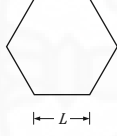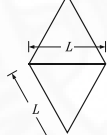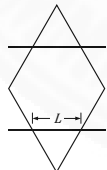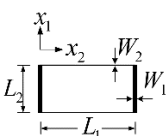
Timoshenko beam elements are used by Luxner, Stampfl, and Pettermann (2005) to obtain the effective Young's moduli of 3D periodic cellular solids having relative densities ranging from 10% to 20%. In their work, four different unit-cell structures are considered. The relation between the effective Young's modulus and the relative density for each cellular solid and in each orthotropic direction is empirically written from the FE results of its unit cell as an

exponential regression function. To compensate for the lack of joint dimensions when beam elements are used, models with increased element rigidity in the vicinity of joints are also employed. The results obtained from the models using beam elements are compared with those using solid elements as well as experiments. It is found that the mechanical behavior of the considered periodic cellular structures is represented well by the models using beam elements. It is also found that the increase of the rigidity of elements in the vicinity of joints does not guarantee better results.

When periodic cellular solids are frame-like and can be modelled accurately using beam elements, it is sometimes possible to analytically derive their effective elastic constants. By considering each unit-cell strut as a beam or a rod, analytical forms of the effective Young's moduli E_i^*, shear moduli G_{ij}^*, and Poisson's ratios v_{ij}^* for 2D periodic cellular solids are derived by Wang and McDowell (2004). In their study, seven different unit-cell structures are considered. The effective elastic constants are written in terms of the characteristic length L of the unit cell, the widths W of the rectangular unit-cell struts, and Young's modulus of the base material E. The closed forms for the effective elastic constants from their study are shown in Table 1. After that, the effective elastic constants are further derived in terms of the relative density. A multiscale procedure is proposed by Vigliotti and Pasini (2012) to analytically determine the effective constitutive matrices of arbitrary 2D periodic cellular solids. In the analysis, Euler beam elements are used and the unit cells are assumed to have unit thickness. The procedure is applied to three unit-cell structures, namely the triangle, hexagon, and kagome unit cells. The effective constitutive matrices $[c_{ij}^*]$ are written as functions of Young's modulus of the base material, the characteristic length of the unit cell, the area A and the moment of inertia I of the struts. Their results are shown as follows:

For a triangle periodic cellular solid,

$$[c_{ij}^*] = \frac{3E}{4\sqrt{3}L^3} \begin{bmatrix} 3(AL^2 + 4I) & AL^2 - 12I & 0 \\ & 3(AL^2 + 4I) & 0 \\ Sym & & AL^2 + 12I \end{bmatrix}, \tag{1}$$

For a hexagon periodic cellular solid,

$$[c_{ij}^*] = \frac{EA}{2\sqrt{3}L(AL^2 + 12I)} \begin{bmatrix} AL^2 + 36I & AL^2 - 12I & 0 \\ & AL^2 + 36I & 0 \\ Sym & & 24I \end{bmatrix}, \tag{2}$$

For a kagome periodic cellular solid,

7

$$[c_{ij}^*] = \frac{\sqrt{3}E}{8L^3}\begin{bmatrix} 3(AL^2 + 2I) & AL^2 - 6I & 0 \\ & 3(AL^2 + 2I) & 0 \\ Sym & & AL^2 + 6I \end{bmatrix}. \tag{3}$$

Analytical forms of the effective Young's moduli, Poisson's ratios, and shear moduli for several periodic cellular solids are given by Gibson and Ashby (1999). The analytical forms are derived from the unit cells of the solids that are modelled as frames. Analytical forms of the effective Young's moduli, shear moduli, and Poisson's ratios for open-cell foams represented by tetrakaidecahedral unit cells are derived by Zhu, Knott, and Mills (1997) by applying the Euler beam theory to the unit-cell struts. In their work, the bending, axial, and torsional rigidities are considered. The equations of the effective elastic constants are obtained by direct consideration of the stiffness of the unit cell without the use of a homogenization method. The consideration of the stiffness of the unit cell is done via the principle of stationary potential energy. The obtained equations of the effective elastic constants are written in terms of the characteristic length of the unit cell, the sectional properties of the unit-cell struts, and the elastic constants of the base material. Because torsional rigidity is considered, the polar moment of inertia J is also included in the equations, i.e.

$$E_i^* = \frac{6\sqrt{2}EI}{L^4\left(1 + \frac{12I}{AL^2}\right)}, \tag{4}$$

$$v_{ij}^* = \frac{1}{2}\left(\frac{AL^2 - 12I}{AL^2 + 12I}\right), \tag{5}$$

$$G_{ij}^* = \frac{6EAI}{12\sqrt{2}IL^2 + \sqrt{2}AL^4\left(\frac{8EI + GJ}{5EI + GJ}\right)}. \tag{6}$$

The approach employed by Zhu, Knott, and Mills (1997) is also used by Sullivan, Ghosn, and Lerch (2008) and Sullivan and Ghosn (2009) to obtain analytical forms of the effective Young's moduli, shear moduli, and Poisson's ratios of open-cell foams represented by elongated tetrakaidecahedral unit cells.

Homogenization methods are based on the assumption that the sizes of unit cells are infinitely small compared to the sizes of solids. Hence, the obtained effective elastic properties from homogenization methods are valid for solids that are composed of sufficient large numbers of unit cells. The effects of the relative sizes between solids and their unit cells on the apparent elastic properties are investigated by some researchers. For example, the effects of the relative sizes between 2D hexagon periodic cellular solids and their unit cells on Young's modulus, shear modulus, and hardness are numerically investigated by Onck, Andrews, and

Gibson (2001). In the study, the solids subject to uniaxial compression, simple shear, and indentation are simulated. For the uniaxial compression and simple shear, the hexagon periodic cellular solids have infinite numbers of unit cells in the dimension along the applied loads and have finite numbers of unit cells in the other dimension. For indentation, the solids are set to be large enough so that there is no influence from the boundaries. The obtained results show that all elastic properties are affected by the relative sizes. At low relative sizes between the solid and its unit cell, the apparent elastic properties are much different from the effective elastic properties. However, the apparent elastic properties will approach to the effective elastic properties when the relative size increases. The experimental results from their companion paper (Andrews et al., 2001) also show the same convergence behavior. In the experiments, open-cell and closed-cell aluminum foams at various relative sizes of solids and their unit cells are investigated. Wallach and Gibson (2001) employed FEM to find Young's moduli of triangulated aluminum alloy modeled by truss elements. The solids are composed of unit cells aligned only in one plane. The number of unit cells in the solid plane is varied and Young's modulus in each axis is determined. The result shows that when the number of unit cells increases, Young's modulus converges to a constant. Dai and Zhang (2008) numerically determined flexural rigidities and deflections of sandwich cantilever beams that have periodic cellular cores. The numbers of the unit cells in the cores are varied. The convergences of the results confirm the effect of the relative sizes between solids and its unit cells on the apparent mechanical properties of the solids.

Many attempts are devoted to achieve frame-like periodic solids that have isotropic symmetry. Arranging unit-cell struts to obtain isotropic symmetry intuitively is not easy. It is however possible to create algorithms to find unit-cell topologies that give isotropic symmetry. Quite often, isotropic symmetry is considered as a constraint in topology optimization of unit cells. In the work by Neves et al. (2000), mathematical programming techniques are used to obtain optimal designs of 2D periodic solids under design constraints on material volume fractions and material symmetries. In their study, 2D periodic solids are treated as 2D continuums. Orthotropic, square, and isotropic symmetries are considered as design constraints. In the work by Challis et al. (2008), the level-set method of topology optimization is used to design 3D isotropic two-phase periodic multifunctional composites, and isotropic symmetry is considered as a design constraint. Isotropic symmetry is also considered as a constraint in topology optimization of 2D periodic trusses by Guth et al. (2012) and of 3D periodic trusses by Guth et al. (2015).

Chapter 3
Strain-Energy-Based Homogenization

When periodic cellular solids are used as load-bearing structures, the effective elastic properties of periodic cellular solids are of significant interest and are among the main considerations of cellular solid design. A periodic cellular solid behaves like a homogeneous material when there are a significantly large number of unit cells in the solid. The apparent mechanical elastic properties of a periodic cellular solid depend the number of unit cells in the solid. However, the properties will converge to constants called effective properties when the number of unit cells is sufficiently large. The desired effective elastic properties of a periodic cellular solid can be obtained by appropriate selection of the base material and the architecture of its unit cell. A homogenization method can be used to calculate the effective elastic properties of a periodic cellular solid from its unit-cell structure (Suquet, 1987; Sigmund, 1995; Fang, Starly, & Sun, 2005; Luxner, Stampfl, & Pettermann, 2005; Liu, Deng, & Lu, 2006; Drago & Pindera, 2007; Dai & Zhang, 2009; Huang, Radman, & Xie, 2011; Guinovart-Díaz et al., 2012). In general, homogenization methods define the effective constitutive material law of a material as a relationship between some average stress and some average strain. The effective elastic constants can be obtained by analyzing the material under appropriate boundary conditions at far-field. For a periodic cellular solid, periodic boundary conditions can be used and the average stress and average strain can be computed directly from the solid's unit cell due to the periodicity.

3.1 Definition of the effective material properties

The main concept of homogenization methods is to replace a material with inhomogeneity in a small scale with an equivalent homogeneous material in a large scale. The concept is depicted in Fig. 2. In the small scale, the material properties are not uniform due to inhomogeneity. However, in the large scale, the average material properties can become uniform if the inhomogeneity is perfectly random or perfectly periodic. Thus, if the material properties are defined in the large scale using the concept of averaging, then the material can be modelled as a homogeneous material. As aforementioned, generally, homogenization methods define the effective constitutive material law of a material as a relationship between some average stress and some average strain. Here, the definitions of the average stress, average strain, and effective material properties used in this study are shown.
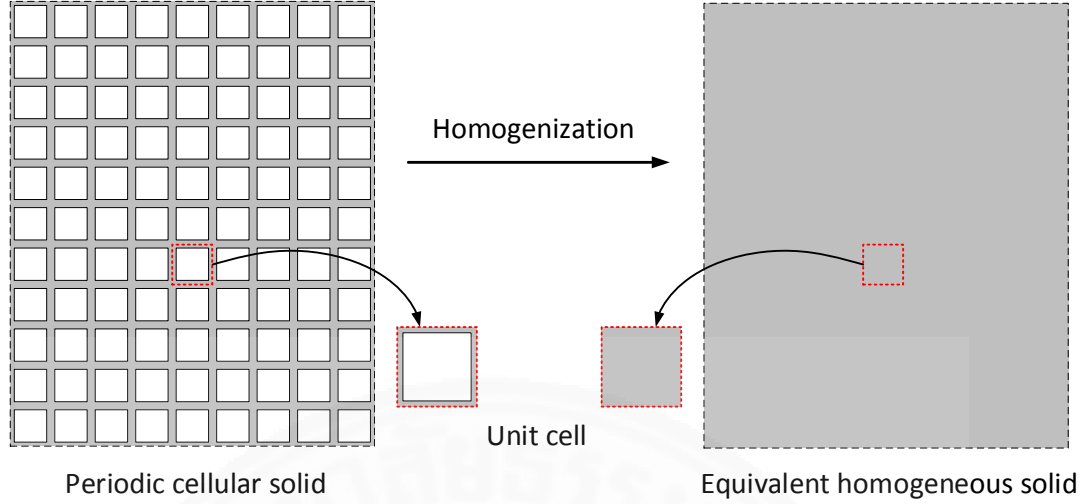
Fig. 2   Concept of homogenization.

Consider a domain V of a periodic elastic solid in a coordinate system x_i that is composed of a significantly large number of unit cells. Let S be the boundary of V. Define the average of any quantity Q in V (Suquet, 1987; Michel, Moulinec, & Suquet, 1999; Nemat-Nasser & Hori, 1999; Drago & Pindera, 2007; Pindera et al., 2009) as

$$\langle Q \rangle = \frac{1}{V} \int_V Q \, dV. \tag{7}$$

A set of kinematic boundary conditions is applied to the domain V such that it results in the following displacement field u_i, i.e.

$$u_i = \epsilon_{ij}^o x_j + u_i^p. \tag{8}$$

Here, ϵ_{ij}^o is a constant symmetric tensor. In addition, u_i^p is a periodic displacement vector. Eq. (8) implies that the applied kinematic boundary conditions are periodic. The displacement field in Eq. (8) is extended everywhere in the domain V, including the inside of voids (Suquet, 1987). This can be reasoned by considering voids as the limit cases of infinitely soft inclusions (Suquet, 1987). The displacement u_i in Eq. (8) yields the following strain, i.e.

$$\epsilon_{ij} = \epsilon_{ij}^o + \frac{1}{2}\left(u_{i,j}^p + u_{j,i}^p\right) = \epsilon_{ij}^o + \epsilon_{ij}^p. \tag{9}$$

Since u_i^p is periodic, ϵ_{ij}^p is periodic. Subsequently, since ϵ_{ij}^o is constant and ϵ_{ij}^p is periodic, the resulting strain ϵ_{ij} is periodic. The average of ϵ_{ij}^p can be shown to be equal to zero (Suquet, 1987). An average of a periodic quantity over the whole domain V is the same as an average over one unit cell V_C. This gives

9

$$\langle \epsilon_{ij}^p \rangle = \frac{1}{V} \int_V \epsilon_{ij}^p dV = \frac{1}{V_C} \int_{V_C} \epsilon_{ij}^p dV = \frac{1}{2V_C} \int_{V_C} \left(u_{i,j}^p + u_{j,i}^p \right) dV$$

$$= \frac{1}{2V_C} \int_{S_C} \left(u_i^p n_j + u_j^p n_i \right) dS = 0. \tag{10}$$

Here, S_C denotes the boundary surface of the unit cell. On S_C, n_i takes opposite values on positions that are periodically opposite to each other while u_i^p takes identical values. It therefore follows that the integral on S_C in the above equation vanishes. Note that $u_{i,j}^p$ may not be continuous everywhere in V_C because of the presence of inclusions. When inclusions are present, the divergence theorem has to be applied to each inclusion. However, the surface integral terms on the boundary surfaces of the inclusions inside V_C from the divergence theorem cancel out and do not appear in Eq. (10).

The relationship between the stress σ_{ij} and the strain ϵ_{ij} is written as

$$\sigma_{ij} = C_{ijkl} \epsilon_{kl}, \tag{11}$$

where C_{ijkl} is the material constitutive tensor, which is periodic. As the strain ϵ_{ij} is also periodic, the stress σ_{ij} is periodic. Without loss of generality, write the stress as

$$\sigma_{ij} = \sigma_{ij}^o + \sigma_{ij}^p, \tag{12}$$

where σ_{ij}^o is constant and σ_{ij}^p is periodic, whose average $\langle \sigma_{ij}^p \rangle$ is zero. Define the effective material constitutive tensor C_{ijkl}^* for an equivalent homogeneous continuum of the periodic solid as

$$\langle \sigma_{ij} \rangle = C_{ijkl}^* \langle \epsilon_{kl} \rangle, \tag{13}$$

which can be written as

$$\sigma_{ij}^o = C_{ijkl}^* \epsilon_{kl}^o. \tag{14}$$

3.2 Homogenization based on equivalent strain energy

The homogenization method based on equivalent strain energy is an efficient and convenient method for the determination of the effective elastic properties of frame-like periodic cellular solids. It has been successfully used by many researchers (Zhang et al., 2007; Wang et al., 2008; Dai & Zhang, 2009; Xu & Zhang, 2011) in various applications. In this

method, the effective elastic properties are calculated from the strain energy of unit cells under some prescribed periodic boundary conditions.

3.2.1 Strain energy equation

Consider the average strain energy density $\bar{U}$ of the domain V written as

$$\bar{U} = \frac{1}{2V}\int_V \sigma_{ij}\epsilon_{ij}dV = \frac{1}{2V_C}\int_{V_C} \sigma_{ij}\epsilon_{ij}dV = \frac{1}{2V}\int_V \left(\sigma_{ij}^o + \sigma_{ij}^p\right)\epsilon_{ij}^o dV + \frac{1}{2V}\int_V \sigma_{ij}\epsilon_{ij}^p dV$$

$$= \frac{1}{2}\sigma_{ij}^o\epsilon_{ij}^o + \frac{1}{2}\langle\sigma_{ij}^p\rangle\epsilon_{ij}^o + \frac{1}{2V}\int_V \sigma_{ij}\epsilon_{ij}^p dV = \frac{1}{2}\sigma_{ij}^o\epsilon_{ij}^o + \frac{1}{2V}\int_V \sigma_{ij}u_{i,j}^p dV \tag{15}$$

$$= \frac{1}{2}\sigma_{ij}^o\epsilon_{ij}^o + \frac{1}{2V_C}\int_{V_C} \sigma_{ij}u_{i,j}^p dV.$$

The last integral in the above equation can be rewritten as

$$\frac{1}{2V_C}\int_{V_C} \sigma_{ij}u_{i,j}^p dV = \frac{1}{2V_C}\int_{V_{CS}} \sigma_{ij}u_{i,j}^p dV = \frac{1}{2V_C}\int_{S_{CS}} \sigma_{ij}u_i^p n_j dS = \frac{1}{2V_C}\int_{S_{CS}} T_i u_i^p dS$$

$$= \frac{1}{2V_C}\int_{S_{CSV}} T_i u_i^p dS + \frac{1}{2V_C}\int_{S_{CSS}} T_i u_i^p dS = 0. \tag{16}$$

Here, V_{CS} denotes the solid part of the unit cell and S_{CS} denotes its boundary surface. In addition, T_i denotes the surface traction on S_{CS}. Note that the equilibrium equation $\sigma_{ji,j} = 0$ is used in Eq. (16). When inclusions are present in V_{CS}, $\sigma_{ij}u_{i,j}^p$ may not be continuous everywhere in V_{CS} and the divergence theorem has to be applied to each inclusion. Fortunately, similar to Eq. (10), the surface integral terms on the boundary surfaces of the inclusions inside V_{CS} from the divergence theorem cancel out. In the above equation, the surface S_{CS} is divided into two parts. The two parts are the surface S_{CSV} between the solid part and any existing voids, and the boundary surface S_{CSS} between the solid part of the unit cell and the solid part of its adjacent cells. Fig. 3 shows an example of a 2D unit cell with its S_{CSV} and S_{CSS}. On S_{CSV}, T_i is zero. On S_{CSS}, T_i takes opposite values on positions that are periodically opposite to each other while u_i^p takes identical values. It therefore follows that both integrals on S_{CSV} and S_{CSS} in Eq. (16) vanish. The strain energy of the unit cell U_C can then be obtained as

$$U_C = \frac{1}{2}\int_{V_C} \sigma_{ij}\epsilon_{ij}dV = \bar{U}V_C = \frac{1}{2}\sigma_{ij}^o\epsilon_{ij}^o V_C = \frac{1}{2}C_{ijkl}^*\epsilon_{kl}^o\epsilon_{ij}^o V_C. \tag{17}$$
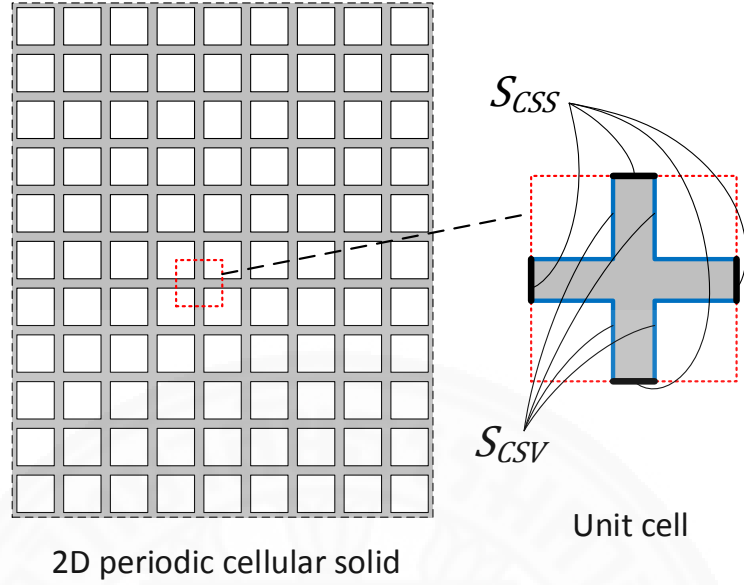
Fig. 3   Boundary of a unit cell.

By prescribing different modes of ϵ_{ij}^o to the unit cell with the help of Eq. (8) and computing the corresponding strain energy values by structural analysis, Eq. (17) allows C_{ijkl}^* to be computed (Sigmund, 1994; Sigmund, 1995; Zhang et al., 2007; Zhang et al., 2007). For example, for two-dimensional cases, using $\epsilon_{11}^o = 1$, $\epsilon_{22}^o = 0$, and $\epsilon_{12}^o = \epsilon_{21}^o = 0$ gives

$$U_C = \frac{1}{2} C_{1111}^* V_C. \tag{18}$$

This strain energy U_C in Eq. (18) can be computed by FEM, and C_{1111}^* can be easily obtained from Eq. (18).

The derivation of the homogenization method based on equivalent strain energy shown here utilizes periodic kinematic boundary conditions. Note that a variant of the method that employs periodic natural boundary conditions also exists (Mohsen Karimian & Straatman, 2007; Huang et al., 2009).

3.2.2 Effective elastic properties computed from strain energy

For a 3D orthotropic period cellular solid, Eq. (14) can be written in matrix form as

$$\boldsymbol{\sigma}^o = \begin{Bmatrix} \sigma_{11}^o \\ \sigma_{22}^o \\ \sigma_{33}^o \\ \sigma_{12}^o \\ \sigma_{23}^o \\ \sigma_{13}^o \end{Bmatrix} = \begin{bmatrix} c_{11}^* & c_{12}^* & c_{13}^* & 0 & 0 & 0 \\ & c_{22}^* & c_{23}^* & 0 & 0 & 0 \\ & & c_{33}^* & 0 & 0 & 0 \\ & & & c_{44}^* & 0 & 0 \\ & Sym & & & c_{55}^* & 0 \\ & & & & & c_{66}^* \end{bmatrix} \begin{Bmatrix} \epsilon_{11}^o \\ \epsilon_{22}^o \\ \epsilon_{33}^o \\ \gamma_{12}^o \\ \gamma_{23}^o \\ \gamma_{13}^o \end{Bmatrix} = \boldsymbol{c}^* \boldsymbol{\epsilon}^o. \tag{19}$$

The effective Young's moduli E_i^*, Poisson's ratios ν_{ij}^*, and shear moduli G_{ij}^* for the material can be expressed in terms of c_{ij}^* as (Bower, 2010)

$$E_1^* = \frac{c_{11}^* c_{22}^* c_{33}^* + 2c_{23}^* c_{12}^* c_{13}^* - c_{11}^* (c_{23}^*)^2 - c_{22}^* (c_{13}^*)^2 - c_{33}^* (c_{12}^*)^2}{c_{22}^* c_{33}^* - (c_{23}^*)^2},$$

$$E_2^* = \frac{c_{11}^* c_{22}^* c_{33}^* + 2c_{23}^* c_{12}^* c_{13}^* - c_{11}^* (c_{23}^*)^2 - c_{22}^* (c_{13}^*)^2 - c_{33}^* (c_{12}^*)^2}{c_{11}^* c_{33}^* - (c_{13}^*)^2},$$

$$E_3^* = \frac{c_{11}^* c_{22}^* c_{33}^* + 2c_{23}^* c_{12}^* c_{13}^* - c_{11}^* (c_{23}^*)^2 - c_{22}^* (c_{13}^*)^2 - c_{33}^* (c_{12}^*)^2}{c_{11}^* c_{22}^* - (c_{12}^*)^2},$$

$$\nu_{12}^* = \frac{c_{12}^* c_{33}^* - c_{13}^* c_{23}^*}{c_{22}^* c_{33}^* - (c_{23}^*)^2}, \quad \nu_{21}^* = \frac{c_{12}^* c_{33}^* - c_{13}^* c_{23}^*}{c_{11}^* c_{33}^* - (c_{13}^*)^2}, \tag{20}$$

$$\nu_{23}^* = \frac{c_{11}^* c_{23}^* - c_{12}^* c_{13}^*}{c_{11}^* c_{33}^* - (c_{13}^*)^2}, \quad \nu_{32}^* = \frac{c_{11}^* c_{23}^* - c_{12}^* c_{13}^*}{c_{11}^* c_{22}^* - (c_{12}^*)^2},$$

$$\nu_{13}^* = \frac{c_{13}^* c_{22}^* - c_{12}^* c_{23}^*}{c_{22}^* c_{33}^* - (c_{23}^*)^2}, \quad \nu_{31}^* = \frac{c_{13}^* c_{22}^* - c_{12}^* c_{23}^*}{c_{11}^* c_{22}^* - (c_{12}^*)^2},$$

$$G_{12}^* = c_{44}^*, \quad G_{23}^* = c_{55}^*, \quad G_{13}^* = c_{66}^*.$$

Since there are nine independent effective material constants, nine different modes of ϵ_{ij}^o in Eq. (17) are required. Define these strain modes as

$$\boldsymbol{\epsilon}^{o(1)} = [1 \quad 0 \quad 0 \quad 0 \quad 0 \quad 0]^T, \quad \boldsymbol{\epsilon}^{o(2)} = [0 \quad 1 \quad 0 \quad 0 \quad 0 \quad 0]^T,$$

$$\boldsymbol{\epsilon}^{o(3)} = [0 \quad 0 \quad 1 \quad 0 \quad 0 \quad 0]^T, \quad \boldsymbol{\epsilon}^{o(4)} = [1 \quad 1 \quad 0 \quad 0 \quad 0 \quad 0]^T,$$

$$\boldsymbol{\epsilon}^{o(5)} = [0 \quad 1 \quad 1 \quad 0 \quad 0 \quad 0]^T, \quad \boldsymbol{\epsilon}^{o(6)} = [1 \quad 0 \quad 1 \quad 0 \quad 0 \quad 0]^T, \tag{21}$$

$$\boldsymbol{\epsilon}^{o(7)} = [0 \quad 0 \quad 0 \quad 1 \quad 0 \quad 0]^T, \quad \boldsymbol{\epsilon}^{o(8)} = [0 \quad 0 \quad 0 \quad 0 \quad 1 \quad 0]^T,$$

$$\boldsymbol{\epsilon}^{o(9)} = [0 \quad 0 \quad 0 \quad 0 \quad 0 \quad 1]^T.$$

Let $U_C^{(i)}$ denote the strain energy of the unit cell to which $\boldsymbol{\epsilon}^o = \boldsymbol{\epsilon}^{o(i)}$ is applied. From Eq. (17), the coefficients in Eq. (19) can be obtained in terms of $U_C^{(i)}$ as

$$c_{11}^* = \frac{2U_C^{(1)}}{V_C}, \qquad c_{22}^* = \frac{2U_C^{(2)}}{V_C}, \qquad c_{33}^* = \frac{2U_C^{(3)}}{V_C},$$

$$c_{44}^* = \frac{2U_C^{(7)}}{V_C}, \qquad c_{55}^* = \frac{2U_C^{(8)}}{V_C}, \qquad c_{66}^* = \frac{2U_C^{(9)}}{V_C},$$

$$c_{12}^* = \frac{U_C^{(4)} - U_C^{(1)} - U_C^{(2)}}{V_C}, \qquad c_{13}^* = \frac{U_C^{(6)} - U_C^{(1)} - U_C^{(3)}}{V_C},$$
(22)

$$c_{23}^* = \frac{U_C^{(5)} - U_C^{(2)} - U_C^{(3)}}{V_C}.$$

By using Eq. (22) in Eq. (20), the effective material constants can be obtained from $U_C^{(i)}$.

For an orthotropic periodic cellular solid under the plane stress condition, Eq. (14) can be written as

$$\boldsymbol{\sigma}^o = \begin{Bmatrix} \sigma_{11}^o \\ \sigma_{22}^o \\ \sigma_{12}^o \end{Bmatrix} = \begin{bmatrix} c_{11}^* & c_{12}^* & 0 \\ & c_{22}^* & 0 \\ Sym & & c_{33}^* \end{bmatrix} \begin{Bmatrix} \epsilon_{11}^o \\ \epsilon_{22}^o \\ \gamma_{12}^o \end{Bmatrix} = \boldsymbol{c}^* \boldsymbol{\epsilon}^o.$$
(23)

The effective material constants can be expressed in terms of C_{ij}^* as

$$E_1^* = \frac{c_{11}^* c_{22}^* - (c_{12}^*)^2}{c_{22}^*}, \qquad E_2^* = \frac{c_{11}^* c_{22}^* - (c_{12}^*)^2}{c_{11}^*},$$

$$v_{12}^* = \frac{c_{12}^*}{c_{22}^*}, \qquad v_{21}^* = \frac{c_{12}^*}{c_{11}^*},$$
(24)

$$G_{12}^* = c_{33}^*.$$

Since there are four independent effective material constants, four different modes of ϵ_{ij}^o are required. Set these four modes of ϵ_{ij}^o to be (Zhang et al., 2007; Zhang et al., 2007)

$$\boldsymbol{\epsilon}^{o(1)} = \begin{bmatrix} 1 & 0 & 0 \end{bmatrix}^T, \quad \boldsymbol{\epsilon}^{o(2)} = \begin{bmatrix} 0 & 1 & 0 \end{bmatrix}^T,$$

$$\boldsymbol{\epsilon}^{o(3)} = \begin{bmatrix} 1 & 1 & 0 \end{bmatrix}^T, \quad \boldsymbol{\epsilon}^{o(4)} = \begin{bmatrix} 0 & 0 & 1 \end{bmatrix}^T.$$
(25)

Consequently, Eq. (17) yields

$$c_{11}^* = \frac{2U_C^{(1)}}{V_C}, \qquad c_{22}^* = \frac{2U_C^{(2)}}{V_C}, \qquad c_{33}^* = \frac{2U_C^{(4)}}{V_C}, \qquad c_{12}^* = \frac{U_C^{(3)} - U_C^{(1)} - U_C^{(2)}}{V_C}. \tag{26}$$

Using Eq. (26) in Eq. (24) gives

$$E_1^* = \frac{2U_C^{(1)}}{V_C} \left[1 - \frac{\left(U_C^{(3)} - U_C^{(1)} - U_C^{(2)} \right)^2}{4U_C^{(1)} U_C^{(2)}} \right], \tag{27}$$

$$E_2^* = \frac{2U_C^{(2)}}{V_C} \left[1 - \frac{\left(U_C^{(3)} - U_C^{(1)} - U_C^{(2)} \right)^2}{4U_C^{(1)} U_C^{(2)}} \right], \tag{28}$$

$$v_{12}^* = \frac{U_C^{(3)} - U_C^{(1)} - U_C^{(2)}}{2U_C^{(2)}}, \tag{29}$$

$$v_{21}^* = \frac{U_C^{(3)} - U_C^{(1)} - U_C^{(2)}}{2U_C^{(1)}}, \tag{30}$$

$$G_{12}^* = \frac{2U_C^{(4)}}{V_C}. \tag{31}$$

Chapter 4
Applicability of Euler Beam Elements

In the determination of effective elastic properties, homogenization methods can employ FEM to analyze unit cells (Luxner, Stampfl, & Pettermann, 2005; Drago & Pindera, 2007; Dai & Zhang, 2009). FEA using solid elements is extensively used in the determination of the effective elastic properties of periodic cellular solids (Lin et al., 2007; Xia, Ju, & Sasaki, 2007; Jean & Engelmayr Jr, 2010). Solid elements are accepted as the most reliable elements since they offer the most accurate results with more details. However, creating FE models for analysis of unit cells using solid elements can be cumbersome. Besides the difficulty in creating meshes using solid elements, the most difficult task is probably the application of periodic boundary conditions to these 3D meshes. Some periodic cellular solids resemble frame structures. Their structures are composed of connecting slender struts (Wallach & Gibson, 2001; Yan et al., 2006; Yeong et al., 2010). For such frame-like periodic cellular solids, unit-cell struts can be represented by beam elements. When shear deformation in beams is negligible, the classical beam theory, on which the Euler beam element is based, is accurate. Subsequently, the Euler beam element can be effectively used. If there is no distributed load applied along the lengths of unit-cell struts, each strut can be represented by one Euler beam element.

4.1 Beam element models

In analysis of a frame-like periodic cellular solid, a unit cell has to be selected from the solid. Depending on individual judgment, various unit-cell configurations are possible. The boundary of the selected configuration may cut through the struts transversely or longitudinally. If solid elements are used, correct modeling and correct periodic boundary conditions can be quite evident although their implementation can be rather involved. Oppositely, if beam elements are used, correct modeling and correct periodic boundary conditions can be quite obscure but their implementation can be quite simple. Especially when there are struts that are cut longitudinally in the unit cell, FE modeling by beam elements requires careful consideration of beam elements' sectional properties.
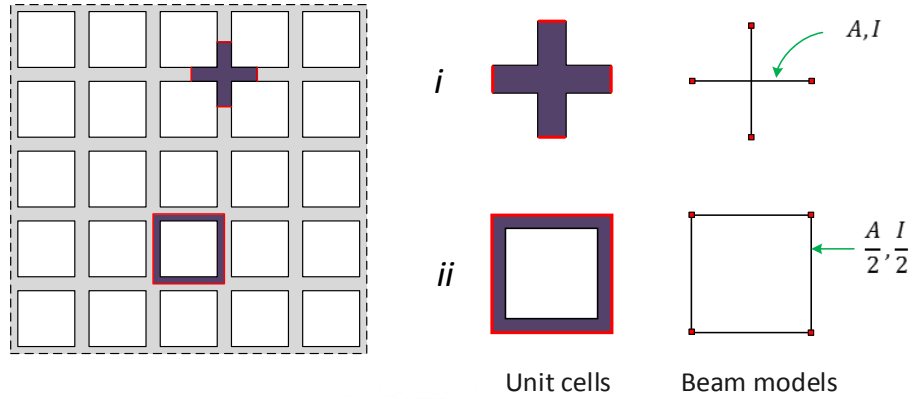
Fig. 4   A periodic cellular solid and two different unit cells.

Fig. 4 shows an example 2D periodic cellular solid, which is composed of square unit cells. The figure also shows two different unit-cell configurations. All struts of the unit cell in configuration *i* are cut transversely and all struts of the unit cell in configuration *ii* are cut longitudinally. When solid elements are used, the two configurations simply have different domains but the two domains do not require any special treatment. However, when beam elements are used, the axial and bending rigidities of struts in configuration *ii* must be only half of those in configuration *i*. If the unit cells of configuration *ii* are reassembled back together, each beam element and its adjacent element must together provide the original axial and bending rigidities. The half axial and bending rigidities can be obtained by simply reducing the values of the sectional area and moment of inertia by half.

4.2 Periodic boundary conditions for beam element models

In the determination of the effective properties of a frame-like periodic cellular solid from its unit cell, periodic boundary conditions have to be used. Periodic boundary conditions must satisfy the periodicity of the displacement field given by Eq. (8). Prescribing periodic boundary conditions requires two types of boundary prescription. The first type is the ordinary prescription of exact values of some degrees of freedom. The second type is the prescription of relative values between some degrees of freedom. The first type of boundary condition is required to prevent rigid body displacements. The second type of boundary condition comes from the periodic displacement field u_i^p in Eq. (8).

$u_i^p(x,0) = u_i^p(x,2L)$ $u_i^p(-L,y) = u_i^p(L,y)$ $\theta(0,0) = \theta(0,2L)$ $\theta(-L,L) = \theta(L,L)$
$u_i^p(0,0) = u_i^p(0,2L)$ $u_i^p(-L,L) = u_i^p(L,L)$

$u_i = 0$ $u_i = 0$

$u_i^p(x,0) = u_i^p(x,2L)$ $u_i^p(0,y) = u_i^p(2L,y)$ $\theta(0,0) = \theta(0,2L) = \theta(2L,2L) = \theta(2L,0)$
$u_i^p(0,0) = u_i^p(0,2L) = u_i^p(2L,2L) = u_i^p(2L,0)$

$u_i = 0$ $u_i = 0$

Unit cells   Beam models
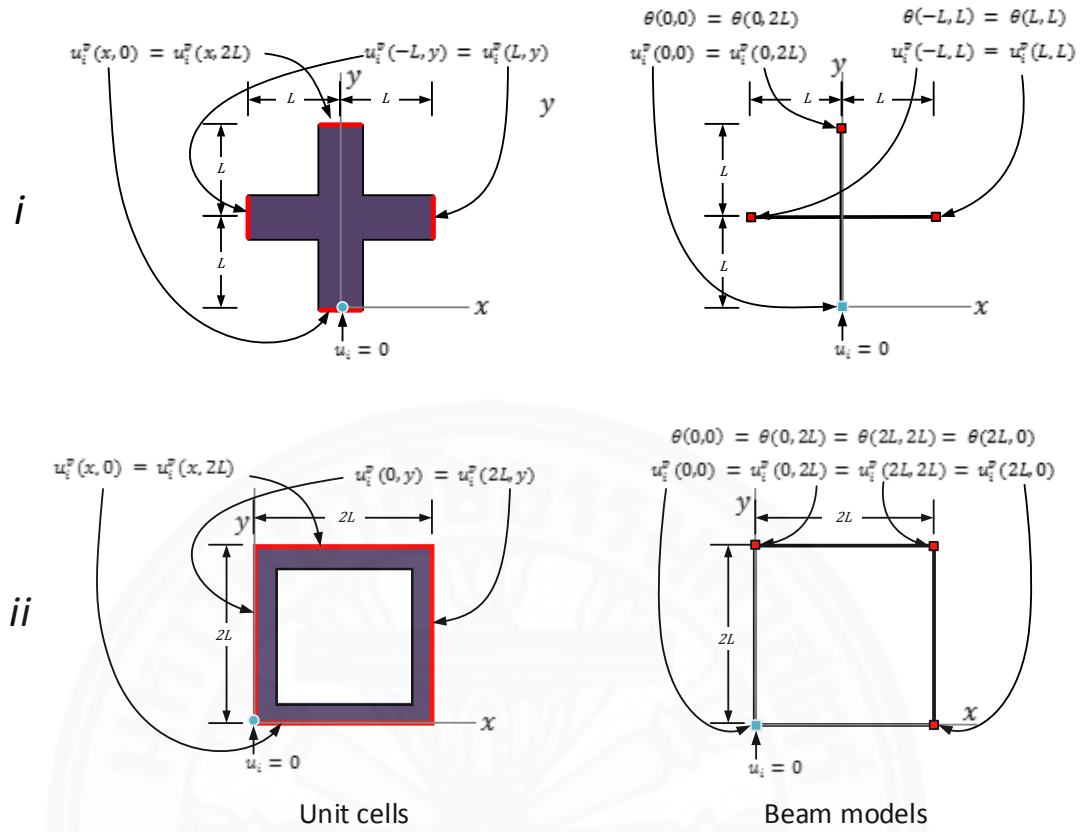
Fig. 5   Periodic boundary conditions of unit cells.

Fig. 5 shows the periodic boundary conditions of the example unit cells from the previous section. The figure shows the locations on the boundary where u_i^p must be the same due to the periodicity. If any two nodal points on the boundary have the same u_i^p, the relative displacements between the two points can be obtained from Eq. (8) for each prescribed strain mode. Then, the obtained relative displacement conditions have to be prescribed on the two nodal points. For models that use beam elements, when u_i^p of two nodal points are the same, their rotational degrees of freedom θ must also be the same.

To elucidate the prescription of periodic boundary conditions for beam element models, the determination of the periodic boundary conditions for the periodic cellular solid which is composed of hexagon unit cells is shown as an example. The periodic cellular solid and the unit cell are shown in Fig. 6. The distance between the opposing struts of a hexagonal unit cell is 1 mm. There are many possible unit-cell configurations, some of which are shown in Fig. 6. Between the three unit-cell configurations in Fig. 6, the H3 configuration has the smallest cut boundary surfaces. Consequently, the H3 configuration has the smallest number of relative displacement conditions.

18
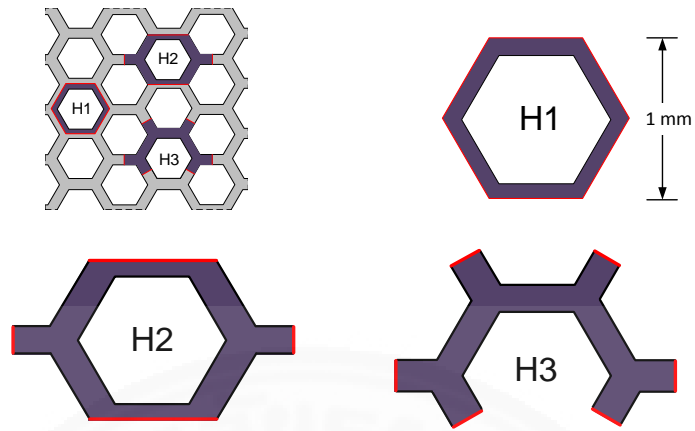
Fig. 6   The periodic cellular solid and hexagon unit cells.

The H3 configuration is selected as the example model. The H3 unit cell is modeled by 4-noded quadrilateral plane stress elements and Euler beam elements. Fig. 7 shows the periodic boundary conditions of the H3 unit cell both for the models using solid elements and beam elements. All translational displacements of a selected node in each model are fixed to prevent rigid body displacements. For this unit-cell configuration, there are three pairs of boundaries where relative displacement conditions must be considered as shown in Fig. 7.
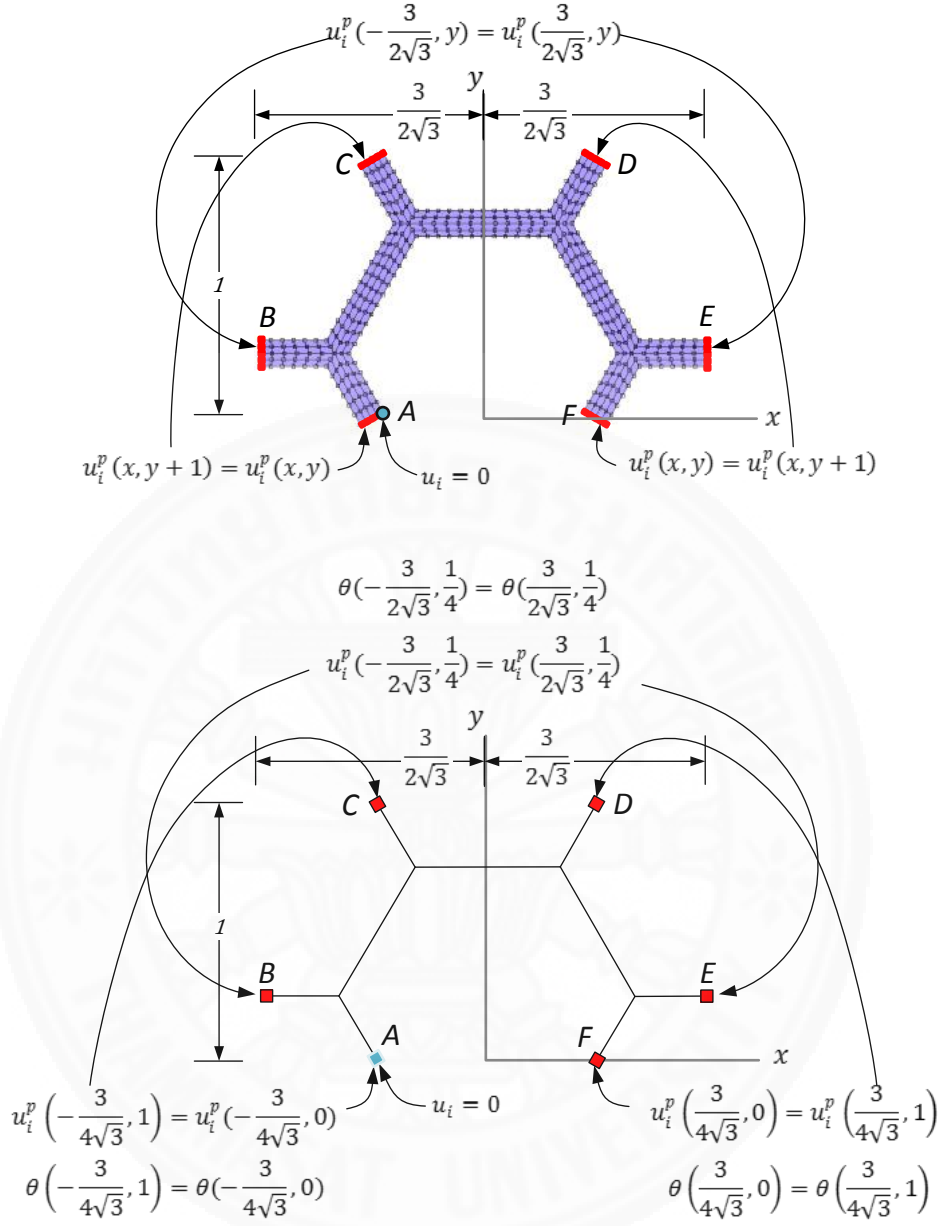
Fig. 7   Periodic boundary conditions of the H3 unit cell.

The periodic displacement boundary conditions for the unit shear strain mode $(\epsilon_{11}^o = \epsilon_{22}^o = 0, \ 2\epsilon_{12}^o = 1)$ for the H3 unit cell modeled by beam elements are shown as follows. The displacements u_1 of points A and C in the figure are written as

$$u_1\left(-\frac{3}{4\sqrt{3}}, 0\right) = \epsilon_{11}^o x_1 + \epsilon_{12}^o x_2 + u_1^p\left(-\frac{3}{4\sqrt{3}}, 0\right)$$

$$= (0)\left(-\frac{3}{4\sqrt{3}}\right) + \left(\frac{1}{2}\right)(0) + u_1^p\left(-\frac{3}{4\sqrt{3}}, 0\right) = u_1^p\left(-\frac{3}{4\sqrt{3}}, 0\right),$$

(32)

$$u_1\left(-\frac{3}{4\sqrt{3}},1\right) = \epsilon_{11}^o x_1 + \epsilon_{12}^o x_2 + u_1^p\left(-\frac{3}{4\sqrt{3}},1\right)$$

$$= (0)\left(-\frac{3}{4\sqrt{3}}\right) + \left(\frac{1}{2}\right)(1) + u_1^p\left(-\frac{3}{4\sqrt{3}},1\right) \tag{33}$$

$$= \frac{1}{2} + u_1^p\left(-\frac{3}{4\sqrt{3}},1\right).$$

Since $u_i = 0$ at $\left(-\frac{3}{4\sqrt{3}},0\right)$, Eq. (32) yields

$$u_1^p\left(-\frac{3}{4\sqrt{3}},0\right) = u_1\left(-\frac{3}{4\sqrt{3}},0\right) = 0. \tag{34}$$

Since $u_1^p\left(-\frac{3}{4\sqrt{3}},1\right) = u_1^p\left(-\frac{3}{4\sqrt{3}},0\right) = 0$, Eq. (33) yields

$$u_1\left(-\frac{3}{4\sqrt{3}},1\right) = \frac{1}{2}. \tag{35}$$

For u_1 of points F and D, they can be written as

$$u_1\left(\frac{3}{4\sqrt{3}},0\right) = (0)\left(\frac{3}{4\sqrt{3}}\right) + \left(\frac{1}{2}\right)(0) + u_1^p\left(\frac{3}{4\sqrt{3}},0\right) = u_1^p\left(\frac{3}{4\sqrt{3}},0\right), \tag{36}$$

$$u_1\left(\frac{3}{4\sqrt{3}},1\right) = (0)\left(\frac{3}{4\sqrt{3}}\right) + \left(\frac{1}{2}\right)(1) + u_1^p\left(\frac{3}{4\sqrt{3}},1\right) = \frac{1}{2} + u_1^p\left(\frac{3}{4\sqrt{3}},1\right). \tag{37}$$

Since $u_1^p\left(\frac{3}{4\sqrt{3}},0\right) = u_1^p\left(\frac{3}{4\sqrt{3}},1\right)$, Eqs. (36) and (37) give

$$u_1\left(\frac{3}{4\sqrt{3}},1\right) = u_1\left(\frac{3}{4\sqrt{3}},0\right) + \frac{1}{2}. \tag{38}$$

For u_1 of points B and E, they can be written as

$$u_1\left(-\frac{3}{2\sqrt{3}},\frac{1}{4}\right) = (0)\left(-\frac{3}{2\sqrt{3}}\right) + \left(\frac{1}{2}\right)\left(\frac{1}{4}\right) + u_1^p\left(-\frac{3}{2\sqrt{3}},\frac{1}{4}\right)$$

$$= \frac{1}{8} + u_1^p\left(-\frac{3}{2\sqrt{3}},\frac{1}{4}\right). \tag{39}$$

$$u_1\left(\frac{3}{2\sqrt{3}},\frac{1}{4}\right) = (0)\left(\frac{3}{2\sqrt{3}}\right) + \left(\frac{1}{2}\right)\left(\frac{1}{4}\right) + u_1^p\left(\frac{3}{2\sqrt{3}},\frac{1}{4}\right) = \frac{1}{8} + u_1^p\left(\frac{3}{2\sqrt{3}},\frac{1}{4}\right). \tag{40}$$

Since $u_1^p\left(-\frac{3}{2\sqrt{3}},\frac{1}{4}\right) = u_1^p\left(\frac{3}{2\sqrt{3}},\frac{1}{4}\right)$, Eqs. (39) and (40) yield

$$u_1\left(\frac{3}{2\sqrt{3}},\frac{1}{4}\right) = u_1\left(-\frac{3}{2\sqrt{3}},\frac{1}{4}\right). \tag{41}$$

Similarly, the following conditions can be obtained for u_2, i.e.

$$u_2\left(-\frac{3}{4\sqrt{3}},1\right) = u_2\left(-\frac{3}{4\sqrt{3}},0\right), \tag{42}$$

$$u_2\left(\frac{3}{4\sqrt{3}}, 1\right) = u_2\left(\frac{3}{4\sqrt{3}}, 0\right), \tag{43}$$

$$u_2\left(\frac{3}{2\sqrt{3}}, \frac{1}{4}\right) = u_2\left(-\frac{3}{2\sqrt{3}}, \frac{1}{4}\right) + \frac{3}{2\sqrt{3}}. \tag{44}$$

Note that the unit of length in the above equation is mm. The periodic boundary conditions for the other strain modes can be calculated in the same manner.

4.3 Validity of the results from beam element models

Models of periodic cellular solids that use Euler beam elements assume that their struts can be modelled accurately as Euler beams. Generally, if a strut is sufficiently slender, it can be modelled accurately as an Euler beam. In this section, the effect of beam slenderness on the accuracy of beam element models in the determination of the effective elastic constants of frame-like periodic solids is investigated. The accuracy is measured against the solutions obtained from models that use solid elements. The investigation is done with 2D periodic cellular solids.

4.3.1 Investigation

The applicability of the Euler beam element to the determination of the effective elastic properties of 2D periodic cellular solids is numerically investigated. The investigation is performed by comparing the effective elastic properties of various 2D periodic cellular structures obtained from FE models that employ 2D solid elements and beam elements. The investigated periodic cellular solids are shown in Fig. 8. Their unit-cell configurations are shown in the dashed frames.

I) Square   II) Body-centered square

III) Triangle   IV) Hexagon   V) Square Z_e3
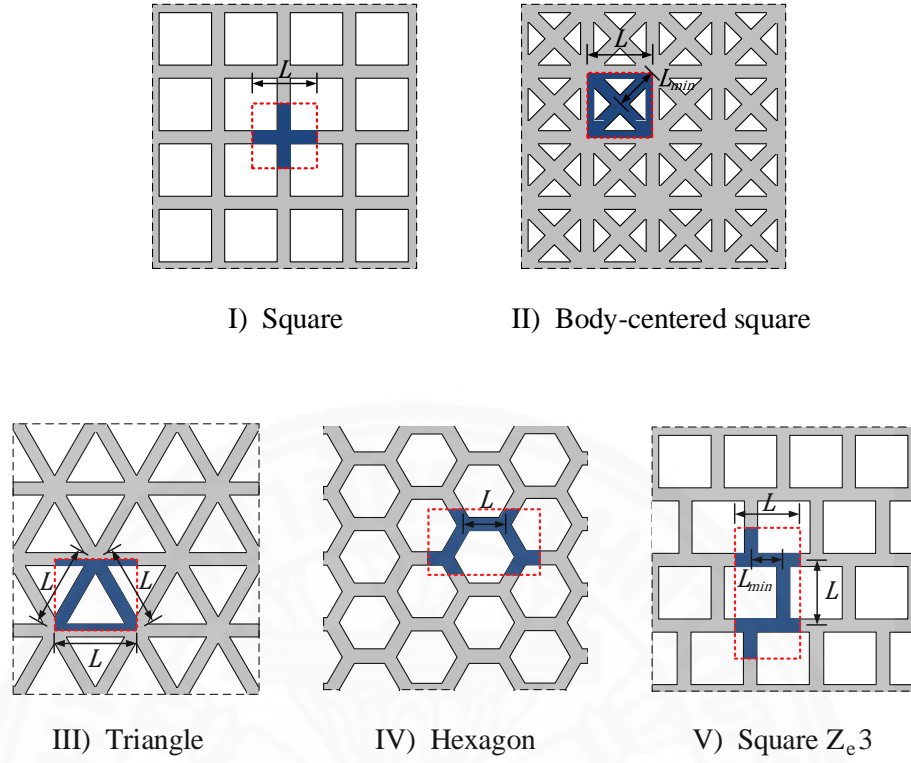
Fig. 8   Periodic cellular solids and their unit cells.

The characteristic length L of each unit cell as shown in Fig. 8 is set to 1 mm. The unit cells are composed of struts with square cross sections. The widths W of the sections are varied in order to vary the slenderness of the struts. The slenderness variation is performed to yield approximately $0.1 - 0.3$ material volume fractions, mvf. Materials with such range of material volume fractions are commonly classified as cellular solids (Gibson & Ashby, 1999). The slenderness s of a strut is defined as its length divided by the radius of gyration, i.e.

$$s = \frac{L}{\sqrt{I/A}}. \tag{45}$$

For the body-centered square unit cell and the square Z_e3 unit cell, there are two groups of struts which have different lengths. In such case, their slenderness values are determined from the lengths of the shortest struts L_{min} and are denoted as the minimum slenderness s_{min}. The constitutive material is assumed to be linear elastic isotropic with Young's modulus E equal to 1 MPa and Poisson's ratio v equal to zero.

The unit cells with different slenderness are model using solid and Euler beam elements. The effective elastic properties computed from the FE results using both types of element are compared. For solid element models, 4-noded quadrilateral plane stress elements are used. The homogenization method based on equivalent strain energy is used to calculate the

23

effective elastic properties of each periodic cellular solid from its unit cell. The determined properties include the effective Young's moduli, effective Poisson's ratios, and effective shear moduli. FEA is performed using MSC.Marc Mentat software. Examples of solid and beam element models are shown in Fig. 9.
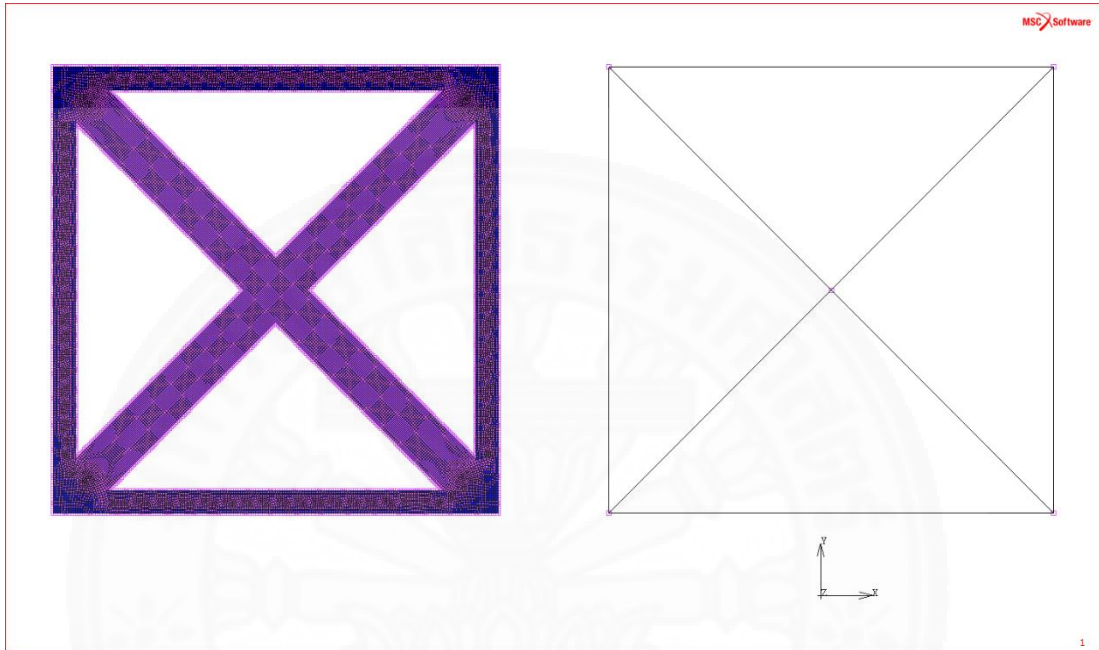
Fig. 9   Solid (left) and beam (right) element models of the body-centered square unit cell.

For the comparison to be meaningful, only converged FE solutions with respect to FE discretization will be used. The accuracies of the results obtained from a model with solid elements depend on the number of elements used in the model. In this study, the number of solid elements in each solid model is quadrupled until the model gives converged results. Since, in the determination of the effective elastic constants, FEA is used to determine strain energy of unit cells under prescribed strain modes, the convergence is defined based on strain energy values. Define the tolerance for convergence as

$$tolerance = \frac{|U_C'' - U_C'|}{U_C''}. \tag{46}$$

Here, U_C' is the strain energy from the previous rougher mesh, and U_C'' is the strain energy from the latest finer mesh. The result is considered converged when the tolerance is less than 0.001.

As aforementioned, the considered effective constants include the effective Young' modulus, effective Poisson's ratio, and effective shear modulus. The difference between an effective elastic constant obtained from a solid element model X_{solid}^* and from a beam element model X_{beam}^* is calculated in percentage as

24

$$difference = \frac{X^*_{beam} - X^*_{solid}}{X^*_{solid}} \times 100. \tag{47}$$

4.3.2 Results

The computational times for Euler beam models compared to solid models are significantly different. The computational time for a beam model is generally in a few seconds whereas the computational time for a solid element model is in several minutes. The results of the investigation are shown in Table 2, Table 3, Table 4, Table 5, and Table 6, respectively, for the square, body-centered square, triangle, hexagon, and square Z_e3 periodic cellular solids. All investigated periodic cellular solids have square symmetry except the square Z_e3 solids. According to the results, the effective Young's moduli and effective shear moduli obtained from the beam element models are lower than those obtained from the solid element models for all investigated solids and all strut slenderness values. As expected, the differences between the results are higher in the solids with lower strut slenderness.

Within the considered range of material volume fractions (approximately $0.1 - 0.3$), the highest differences between the results from the solid and beam element models are found in the square Z_e3 solids, whose effective elastic properties in the two axes are unequal. For the square Z_e3 solids, the highest differences are -9.36% and -21.01%, respectively, for the effective Young's modulus E_2^* in the vertical direction and the effective shear modulus.

Among the periodic cellular solids with square symmetry, the differences of the effective Young's moduli between the solid and beam element models are quite small. The differences are less than 5% and the highest difference of -4.84% is found in the hexagon periodic cellular solid with slenderness of 17.32. For the differences of the effective shear moduli, the highest difference of -18.49% is found in the square periodic cellular solid with slenderness of 17.32.

For the square periodic cellular solids, there are only struts aligned in the two orthogonal directions. Euler beams do not consider Poisson's effect on beam sections. Since Poisson's effect in square unit cells comes from Poisson's effect on beam sections, using Euler beam elements for square unit cells implies no Poisson's effect in square unit cells. On the contrary, the solid element models will be able to capture Poisson's effect in square unit cells even when the effect is very small. In fact, the effective Poisson's ratios of the square periodic cellular solids are so small and can be considered as zero. Hence, the effective Poisson's ratios of the square periodic cellular solids from the solid element models and those from the beam

element models are approximately similar. Likewise, this phenomenon is also found in the square Z_e3 periodic cellular solids and can be discussed in the same way.

For the body-centered square, triangle, hexagon periodic cellular solids, the effective Poisson's ratios obtained from the beam element models are higher than those obtained from the solid element models for all strut slenderness values. The differences between the results are higher in the solids with lower strut slenderness. The highest difference of -7.96% is found in the triangle periodic cellular solid with slenderness of 34.64.

When beam element models are used, the stiffness in the planes of beam cross sections is not considered. If this stiffness is considered, it will be more difficult to deform a beam inside a join volume because of the contribution of this stiffness from the other beams. When solid element models are used, the stiffness in the planes of beam cross sections is intrinsically considered. Therefore, the results from solid element models for E_i^* and G_{ij}^* are more accurate and stiffer. For Poisson's ratios, the same kind of stiffness will reduce the transverse deformation of the solid. As a result, smaller Poisson's ratios are observed when solid element models are used. According to the results from the investigated unit cells, when the ratios W/L_{min} of the unit cell struts are 0.1, beam element models will offer highly accurate results which are different from the solid element models' results less than 10%.

Table 2 Results from solid and beam element models of square unit cells.

$\dfrac{W}{L}$	S	mvf	X^*	Solid elements	Beam elements	Differences (%)
0.05	69.28	0.0975	E_i^* (MPa)	5.0360×10^{-2}	5.0000×10^{-2}	-0.72
			v_{ij}^*	3.0222×10^{-3}	0.0000×10^{0}	-100.00
			G_{ij}^* (MPa)	6.5212×10^{-5}	6.2500×10^{-5}	-4.16
0.10	34.64	0.1900	E_i^* (MPa)	1.0144×10^{-1}	1.0000×10^{-1}	-1.42
			v_{ij}^*	6.0268×10^{-3}	0.0000×10^{0}	-100.00
			G_{ij}^* (MPa)	5.4694×10^{-4}	5.0000×10^{-4}	-8.58
0.20	17.32	0.3600	E_i^* (MPa)	2.0598×10^{-1}	2.0000×10^{-1}	-2.90
			v_{ij}^*	1.2592×10^{-2}	0.0000×10^{0}	-100.00
			G_{ij}^* (MPa)	4.9071×10^{-3}	4.0000×10^{-3}	-18.49

Table 3 Results from solid and beam element models of body-centered square unit cells.

$\dfrac{W}{L_{min}}$	S_{min}	mvf	X^*	Solid elements	Beam elements	Differences (%)
0.025	138.56	0.0835	E_i^* (MPa)	2.5247×10^{-2}	2.5016×10^{-2}	-0.92
			v_{ij}^*	4.1112×10^{-1}	4.1385×10^{-1}	0.66
			G_{ij}^* (MPa)	2.5224×10^{-2}	2.5006×10^{-2}	-0.87
0.05	69.28	0.1634	E_i^* (MPa)	5.1172×10^{-2}	5.0125×10^{-2}	-2.05
			v_{ij}^*	4.0588×10^{-1}	4.1275×10^{-1}	1.69
			G_{ij}^* (MPa)	5.1017×10^{-2}	5.0044×10^{-2}	-1.91
0.10	34.64	0.3123	E_i^* (MPa)	1.0633×10^{-1}	1.0100×10^{-1}	-5.01
			v_{ij}^*	3.8831×10^{-1}	4.0839×10^{-1}	5.17
			G_{ij}^* (MPa)	1.0517×10^{-1}	1.0035×10^{-1}	-4.58

Table 4 Results from solid and beam element models of triangle unit cells.

$\dfrac{W}{L}$	S	mvf	X^*	Solid elements	Beam elements	Differences (%)
0.025	138.56	0.0847	E_i^* (MPa)	2.9208×10^{-2}	2.8880×10^{-2}	-1.12
			v_{ij}^*	3.2906×10^{-1}	3.3305×10^{-1}	1.21
			G_{ij}^* (MPa)	1.0988×10^{-2}	1.0839×10^{-2}	-1.36
0.05	69.28	0.1657	E_i^* (MPa)	5.9259×10^{-2}	5.7831×10^{-2}	-2.41
			v_{ij}^*	3.2286×10^{-1}	3.3222×10^{-1}	2.90
			G_{ij}^* (MPa)	2.2398×10^{-2}	2.1705×10^{-2}	-3.10
0.10	34.64	0.3164	E_i^* (MPa)	1.2301×10^{-1}	1.1624×10^{-1}	-5.51
			v_{ij}^*	3.0466×10^{-1}	3.2890×10^{-1}	7.96
			G_{ij}^* (MPa)	4.7144×10^{-2}	4.3734×10^{-2}	-7.23

Table 5 Results from solid and beam element models of hexagon unit cells.

$\dfrac{W}{L}$	S	mvf	X^*	Solid elements	Beam elements	Differences (%)
0.05	69.28	0.0847	E_i^* (MPa)	2.9137×10^{-4}	2.8648×10^{-4}	-1.68
			v_{ij}^*	9.8999×10^{-1}	9.9008×10^{-1}	0.01
			G_{ij}^* (MPa)	7.3212×10^{-5}	7.1989×10^{-5}	-1.67
0.10	34.64	0.1657	E_i^* (MPa)	2.3128×10^{-3}	2.2421×10^{-3}	-3.06
			v_{ij}^*	9.6063×10^{-1}	9.6117×10^{-1}	0.06
			G_{ij}^* (MPa)	5.8975×10^{-4}	5.7163×10^{-4}	-3.07
0.20	17.32	0.3164	E_i^* (MPa)	1.7335×10^{-2}	1.6496×10^{-2}	-4.84
			v_{ij}^*	8.5502×10^{-1}	8.5714×10^{-1}	0.25
			G_{ij}^* (MPa)	4.6725×10^{-3}	4.4412×10^{-3}	-4.95

Table 6 Results from solid and beam element models of square $Z_e 3$ unit cells.

$\dfrac{W}{L_{min}}$	S_{min}	mvf	X^*	Solid elements	Beam elements	Differences (%)
0.10	34.64	0.0975	E_1^* (MPa)	5.0360×10^{-2}	5.0000×10^{-2}	-0.67
			E_2^* (MPa)	2.0602×10^{-3}	1.9231×10^{-3}	-6.65
			v_{12}^*	4.3374×10^{-3}	0.0000×10^{0}	-100.00
			v_{21}^*	1.0598×10^{-1}	0.0000×10^{0}	-100.00
			G_{ij}^* (MPa)	1.0576×10^{-4}	9.9950×10^{-5}	-5.50
0.20	17.32	0.1900	E_1^* (MPa)	1.0124×10^{-1}	1.0000×10^{-1}	-1.23
			E_2^* (MPa)	1.4997×10^{-2}	1.3793×10^{-2}	-8.03
			v_{12}^*	1.3874×10^{-2}	0.0000×10^{0}	-100.00
			v_{21}^*	9.3659×10^{-2}	0.0000×10^{0}	-100.00
			G_{ij}^* (MPa)	8.9584×10^{-4}	7.9840×10^{-4}	-10.88
0.40	8.66	0.3600	E_1^* (MPa)	2.0507×10^{-1}	2.0000×10^{-1}	-2.47
			E_2^* (MPa)	8.6106×10^{-2}	7.8049×10^{-2}	-9.36
			v_{12}^*	3.8280×10^{-2}	0.0000×10^{0}	-100.00
			v_{21}^*	9.1170×10^{-2}	0.0000×10^{0}	-100.00
			G_{ij}^* (MPa)	8.0384×10^{-3}	6.3492×10^{-3}	-21.01

Chapter 5
Exact Forms of the Effective Elastic Constants

The equations of the effective elastic constants of periodic cellular solids that can be modelled accurately as frame structures can be obtained from elaborate analytical structural analysis of their unit cells. These equations for periodic cellular solids with different unit-cell architectures are naturally not the same. Thus, new analytical structural analysis has to be performed every time a new topology is considered. These equations, in fact, share certain basic forms. This study aims to derive the exact forms of the effective elastic constants of arbitrary frame-like periodic cellular solids that can be modelled accurately using Euler beams. The forms are derived analytically by using the homogenization method based on equivalent strain energy.

In the derivation, the Euler beam theory is employed. The cross sections of all struts in a periodic cellular solid with an arbitrary topology are set to be the same, and are also set to have the same moment of inertia in all directions. The exact forms of the effective elastic constants are obtained in terms of some dimensionless factors, the characteristic length and volume of the unit cell, the area and moment of inertia of the struts, and Young's modulus of the base material. The dimensionless factors are different for different topologies of solids. In general, these factors can be functions of the area and moment of inertia of the struts. However, if these factors are constant, the forms can be used as exact parametric forms. The constant factors for periodic cellular solids with a particular topology can be determined by exact curve fitting using FE results with different areas and moments of inertia. After that, the obtained equations can be tested using additional FE results with areas and moments of inertia that are different from the fitting data. If exact fitting is achieved with the additional FE results, the obtained equations are valid and elaborate analytical structural analysis can be avoided. On the contrary, if exact fitting cannot be achieved with the additional FE results, it means that some of the dimensionless factors are not constant and the results of the curve fitting should not be used. The exact forms of the effective elastic constants proposed in this study are checked by using them with several topologies of 2D and 3D periodic cellular solids. The obtained effective elastic constants are compared with exact solutions from symbolic FE computations and/or the literature.

5.1 Exact forms

Using Eqs. (9) and (11) in the equilibrium equation gives

$$\sigma_{ji,j} = \left(C_{jikl}\epsilon_{kl}\right)_{,j} = \left[C_{jikl}\left(\epsilon_{kl}^o + \epsilon_{kl}^p\right)\right]_{,j} = 0, \tag{48}$$

which subsequently yields

$$\left(C_{jikl}\epsilon_{kl}^p\right)_{,j} = -\left(C_{jikl}\epsilon_{kl}^o\right)_{,j} = -C_{jikl,j}\epsilon_{kl}^o. \tag{49}$$

The unknown of Eq. (49) is ϵ_{kl}^p. It is shown by Suquet (1987) that Eq. (49) gives ϵ_{kl}^p that is directly proportional to ϵ_{kl}^o, i.e.

$$\epsilon_{ij}^p(x_m) = \epsilon_{kl}^o H_{ijkl}(x_m), \tag{50}$$

where the components of H_{ijkl} are periodic functions of position. Consequently, u_i^p can be written as

$$u_i^p(x_m) = \epsilon_{kl}^o Q_{ikl}(x_m) + c_i, \tag{51}$$

where the components of Q_{ikl} are periodic functions of position and c_i is a constant tensor.

A difference between u_i's of any two points x_m^a and x_m^b can be written as

$$u_i(x_m^b) - u_i(x_m^a) = \left[\epsilon_{il}^o x_l^b + \epsilon_{kl}^o Q_{ikl}(x_m^b) + c_i\right] - \left[\epsilon_{il}^o x_l^a + \epsilon_{kl}^o Q_{ikl}(x_m^a) + c_i\right]$$

$$= \epsilon_{il}^o(x_l^b - x_l^a) + \epsilon_{kl}^o\left[Q_{ikl}(x_m^b) - Q_{ikl}(x_m^a)\right] \tag{52}$$

$$= \epsilon_{kl}^o\left\{\delta_{ki}(x_l^b - x_l^a) + \left[Q_{ikl}(x_m^b) - Q_{ikl}(x_m^a)\right]\right\} = \epsilon_{kl}^o S_{ikl}(x_m^a, x_m^b).$$

In addition, the derivative of u_i with respect to x_j is equal to

$$u_{i,j}(x_m) = \epsilon_{il}^o x_{l,j} + \epsilon_{kl}^o Q_{ikl,j}(x_m) = \epsilon_{ij}^o + \epsilon_{kl}^o Q_{ikl,j}(x_m)$$

$$= \epsilon_{kl}^o\left\{\delta_{ki}\delta_{lj} + Q_{ikl,j}(x_m)\right\} = \epsilon_{kl}^o Z_{ijkl}(x_m). \tag{53}$$

Consider a beam element J that belongs to a unit cell shown in Fig. 10. Let L_J be the length of the beam element and L be the characteristic length of the unit cell. L_J and L are related through $L_J = h_J L$. Without loss of generality, the coordinate x_1 is set along the longitudinal axis of the element. The strain energy of the element from axial deformation is given by

$$U_{aJ} = \frac{E\zeta_J A}{2L_J} \left(u_1^b - u_1^a\right)^2. \tag{54}$$

Here, E denotes Young's modulus of the base material while A denotes the sectional area of the struts in the periodic solid. Note that all elements in the periodic solid have the same material and sectional properties. In the above equation, ζ_J is a constant used for adjusting the rigidity of the beam element. If the beam element is used to model a beam of the unit cell that is a result of cutting longitudinally a strut of the periodic solid shared by N adjacent unit cells, then ζ_J is equal to $1/N$. If the beam element represents a whole strut of the solid, then ζ_J is equal to 1.
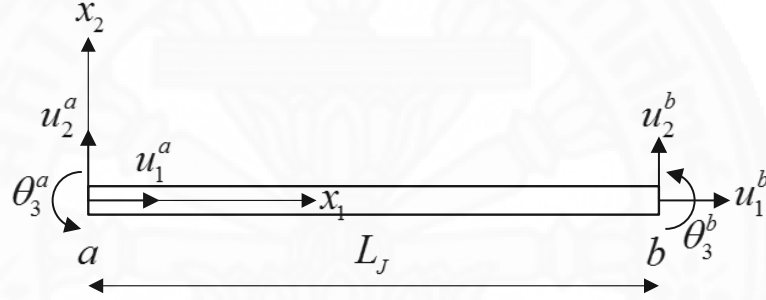
Fig. 10 A general beam element in a unit cell.

Eq. (52) gives

$$u_1^b - u_1^a = \left[\frac{\epsilon_{kl}^o S_{1kl}\left(x_1^a, x_1^b\right)}{L}\right] L = \psi_{1J}L,$$

$$u_2^b - u_2^a = \left[\frac{\epsilon_{kl}^o S_{2kl}\left(x_1^a, x_1^b\right)}{L}\right] L = \psi_{2J}L, \tag{55}$$

where ψ_{1J} and ψ_{2J} are dimensionless functions of ϵ_{ij}^o. Consequently, U_{aJ} can be expressed as

$$U_{aJ} = \frac{E\zeta_J A}{2L_J}\psi_{1J}^2 L^2 = \frac{E\zeta_J A}{2h_J}\psi_{1J}^2 L = \alpha_J EAL, \tag{56}$$

where α_J is a dimensionless function of ϵ_{ij}^o.

Next, consider the strain energy from bending deformation in the $x_1 - x_2$ plane, which is expressed as

$$U_{b3J} = \frac{E\zeta_J I}{2L_J} \left[4\left((\theta_3^a)^2 + \theta_3^a \theta_3^b + (\theta_3^b)^2 \right) - \frac{12}{L_J}(u_2^b - u_2^a)(\theta_3^a + \theta_3^b) \right.$$

$$\left. + \frac{12}{L_J^2}(u_2^b - u_2^a)^2 \right].$$

(57)

Here, I denotes the moment of inertia of the struts in the periodic solid.

Eq. (52) gives

$$\theta_3^a = u_{2,1}^a = \epsilon_{kl}^o Z_{21kl}(x_1^a) = \hat{\psi}_{3J}^a,$$

$$\theta_3^b = u_{2,1}^b = \epsilon_{kl}^o Z_{21kl}(x_1^b) = \hat{\psi}_{3J}^b,$$

(58)

where $\hat{\psi}_{3J}^a$ and $\hat{\psi}_{3J}^b$ are dimensionless functions of ϵ_{ij}^o. Consequently, U_{b3J} becomes

$$U_{b3J} = \frac{E\zeta_J I}{2h_J L} \left[4\left((\hat{\psi}_{3J}^a)^2 + \hat{\psi}_{3J}^a \hat{\psi}_{3J}^b + (\hat{\psi}_{3J}^b)^2 \right) - \frac{12}{h_J}\psi_{2J}(\hat{\psi}_{3J}^a + \hat{\psi}_{3J}^b) + \frac{12}{h_J^2}\psi_{2J}^2 \right]$$

$$= \beta_{3J} \frac{EI}{L},$$

(59)

where β_{3J} is a dimensionless function of ϵ_{ij}^o. Similarly, the strain energy due to bending deformation in the $x_1 - x_3$ plane can be written as $U_{b2J} = \beta_{2J} EI/L$.

It follows that the strain energy of the element is equal to

$$U_J = \alpha_J EAL + \beta_{2J} \frac{EI}{L} + \beta_{3J} \frac{EI}{L} = \alpha_J EAL + \beta_J \frac{EI}{L}.$$

(60)

Similar to α_J, β_J is also a dimensionless function of ϵ_{ij}^o.

The strain energy of a unit cell is the sum of the strain energy from all strut members. For 3D periodic cellular solids, Eqs. (20), (22), and (60) give

$$E_i^* = \frac{E}{V_C} \left[\frac{\phi_{i1}(AL)^3 + \phi_{i2}(A^2 IL) + \phi_{i3}\left(\frac{AI^2}{L}\right) + \phi_{i4}\left(\frac{I}{L}\right)^3}{(AL)^2 + \phi_{i5}(AI) + \phi_{i6}\left(\frac{I}{L}\right)^2} \right],$$

(61)

$$v_{ij}^* = \frac{\varphi_{ij1}(AL)^2 + \varphi_{ij2}(AI) + \varphi_{ij3}\left(\frac{I}{L}\right)^2}{(AL)^2 + \varphi_{ij4}(AI) + \varphi_{ij5}\left(\frac{I}{L}\right)^2},$$

(62)

$$G_{ij}^* = \frac{E}{V_C} \left[\eta_{ij1}(AL) + \eta_{ij2} \left(\frac{I}{L} \right) \right], \tag{63}$$

where ϕ_{ik}, φ_{ijk}, and η_{ijk} are dimensionless factors.

For 2D periodic cellular solids, Eqs. (27)−(31), and (60) give

$$E_i^* = \frac{E}{V_C} \left[\frac{\phi_{i1}(AL)^2 + \phi_{i2}(AI) + \phi_{i3} \left(\frac{I}{L} \right)^2}{AL + \phi_{i4} \left(\frac{I}{L} \right)} \right], \tag{64}$$

$$v_{ij}^* = \frac{\varphi_{ij1}(AL) + \varphi_{ij2} \left(\frac{I}{L} \right)}{AL + \varphi_{ij3} \left(\frac{I}{L} \right)}, \tag{65}$$

$$G_{12}^* = \frac{E}{V_C} \left[\eta_1(AL) + \eta_2 \left(\frac{I}{L} \right) \right], \tag{66}$$

where ϕ_{ik}, φ_{ijk}, and η_k are dimensionless factors.

For periodic cellular solids with a particular topology, whose dimensionless factors in the exact forms in Eqs. (61)−(66) are constants, these constant factors can be obtained by exact curve fitting using FE results. As an example, consider E_1^* given by Eq. (64). This equation can be rearranged as

$$(AL)^2 \phi_{11} + (AI) \phi_{12} + \left(\frac{I}{L} \right)^2 \phi_{13} - \left(\frac{E_1^* V_C}{E} \right) \left(\frac{I}{L} \right) \phi_{14} = \left(\frac{E_1^* V_C}{E} \right) (AL). \tag{67}$$

By using a unit cell with a fixed set of E, V_C, and L, Eq. (27) can be used to compute E_1^* for four different combinations of A and I. The strain energy required by Eq. (27) can be obtained from FEA of the considered unit cell under the relevant strain modes. The four sets of E_1^*, A and I are then substituted into Eq. (67) to create four simultaneous linear equations as shown in the following equation:

$$
\begin{bmatrix}
(A_1L)^2 & A_1I_1 & \left(\dfrac{I_1}{L}\right)^2 & -\left(\dfrac{E^*_{1(1)}V_C}{E}\right)\left(\dfrac{I_1}{L}\right) \\[2mm]
(A_2L)^2 & A_2I_2 & \left(\dfrac{I_2}{L}\right)^2 & -\left(\dfrac{E^*_{1(2)}V_C}{E}\right)\left(\dfrac{I_2}{L}\right) \\[2mm]
(A_3L)^2 & A_3I_3 & \left(\dfrac{I_3}{L}\right)^2 & -\left(\dfrac{E^*_{1(3)}V_C}{E}\right)\left(\dfrac{I_3}{L}\right) \\[2mm]
(A_4L)^2 & A_4I_4 & \left(\dfrac{I_4}{L}\right)^2 & -\left(\dfrac{E^*_{1(4)}V_C}{E}\right)\left(\dfrac{I_4}{L}\right)
\end{bmatrix}
\begin{Bmatrix}
\phi_{11} \\ \phi_{12} \\ \phi_{13} \\ \phi_{14}
\end{Bmatrix}
=
\begin{Bmatrix}
\left(\dfrac{E^*_{1(1)}V_C}{E}\right)(A_1L) \\[2mm]
\left(\dfrac{E^*_{1(2)}V_C}{E}\right)(A_2L) \\[2mm]
\left(\dfrac{E^*_{1(3)}V_C}{E}\right)(A_3L) \\[2mm]
\left(\dfrac{E^*_{1(4)}V_C}{E}\right)(A_4L)
\end{Bmatrix}.
\tag{68}
$$

Solving the obtained system of linear equations yields ϕ_{11}, ϕ_{12}, ϕ_{13}, and ϕ_{14}, and the expression of E^*_1 in Eq. (64) is obtained. Since ϕ_{11}, ϕ_{12}, ϕ_{13}, and ϕ_{14} may not be constants as assumed, the obtained expression of E^*_1 must be tested by other combinations of A and I that are different from the ones used in the exact curve fitting.

5.2 Reduced exact forms

Some of the exact forms for 3D periodic cellular solids can be reduced into the forms for 2D periodic cellular solids when symmetry of unit cells is available. If a 3D periodic cellular solid has $U_C^{(1)} = U_C^{(2)}$, $U_C^{(5)} = U_C^{(6)}$, and $U_C^{(8)} = U_C^{(9)}$, it has tetragonal symmetry with x_3 as the axis of rotational symmetry. It follows that $E^*_1 = E^*_2$, $v^*_{12} = v^*_{21}$, $v^*_{13} = v^*_{23}$, $v^*_{31} = v^*_{32}$, and $G^*_{23} = G^*_{13}$. By taking the conditions of $U_C^{(1)} = U_C^{(2)}$, and $U_C^{(5)} = U_C^{(6)}$ into account when considering Eqs. (20), (22), and (60), the exact forms of E^*_3, v^*_{31}, and v^*_{32} can be reduced into those for 2D periodic cellular solids in Eqs. (64) and (65).

If a 3D periodic cellular solid has $U_C^{(1)} = U_C^{(2)} = U_C^{(3)}$, $U_C^{(4)} = U_C^{(5)} = U_C^{(6)}$, and $U_C^{(7)} = U_C^{(8)} = U_C^{(9)}$, it has cubic symmetry. It follows that $E^*_1 = E^*_2 = E^*_3$, $v^*_{12} = v^*_{13} = v^*_{21} = v^*_{23} = v^*_{31} = v^*_{32}$, and $G^*_{12} = G^*_{23} = G^*_{13}$. The conditions of $U_C^{(1)} = U_C^{(2)} = U_C^{(3)}$, and $U_C^{(4)} = U_C^{(5)} = U_C^{(6)}$ can be used with Eqs. (20), (22), and (60) to reduce the exact forms of all Young's moduli and Poisson's ratios into the forms for 2D periodic cellular solids in Eqs. (64) and (65).

5.3 Results

In order to check the validity of the proposed exact forms of the effective elastic constants, the forms are used with 2D and 3D periodic cellular solids of various topologies shown in Fig. 11 and Fig. 12. The dash lines show the boundary edges of the selected unit cells. It is assumed that the dimensionless factors in all exact forms are constant, and these constants are then obtained from exact curve fitting using FE results. For any 3D unit-cell topology, whose geometry clearly show tetragonal or cubic symmetry, the reduced exact forms of effective Young's moduli and Poisson's ratios, if they exist, are used instead of the original forms. After the factors in the exact forms are obtained from the exact curve fitting, the obtained expressions are tested using additional FE results with the areas and moments of inertia outside the fitting data in order to determine whether the obtained expressions are valid or not. Finally, the obtained expressions are also compared with the exact solutions from symbolic FEA in MATLAB and/or the literature. The symbolic FEA by MATLAB is described in a master's degree thesis by Sam (2015).

Table 7 shows the volumes V_C of the unit cells in Fig. 11 and Fig. 12. Here, L represents the characteristic length of each unit cell as defined in Fig. 11 and Fig. 12 while T denotes the thickness of a 2D unit cell. In the exact curve fitting, the base Young's modulus E and the characteristic length L for every case are both set to 1. For the 2D cases, the unit thickness is assumed, i.e. $T = 1$. The combinations of A and I used in the exact curve fitting are arbitrarily selected based on convenience and do not physically represent real sections. Mathematically, it is not necessary to use physically real sections to perform exact curve fitting. The employed combinations of A and I are shown in Table 8. The effective elastic constants for these combinations of A and I are directly obtained from Eqs. (20), (22), and Eqs. (27)−(31) using strain energy from FEA of the unit cells under the required strain modes. Subsequently, the obtained effective elastic constants are used for the exact curve fitting.

Table 7 Volume of unit cells.

Unit cell		Volume V_C
2D	Square	L^2T
	Body-centered square	L^2T
	Diamond square	L^2T
	Triangle	$\dfrac{\sqrt{3}}{2}L^2T$
	Hexagon	$\dfrac{3\sqrt{3}}{2}L^2T$
	Diamond	L^2T
	Elongated diamond	$\dfrac{\sqrt{3}}{2}L^2T$
3D	Cubic	L^3
	Body-centered cubic	L^3
	Face-centered cubic	L^3
	Cuboctahedron	$2\sqrt{2}L^3$
	Tetrakaidecahedron	$16\sqrt{2}L^3$
	Octahedron	$2\sqrt{2}L^3$
	Tetragonal bipyramid	$\dfrac{\sqrt{14}}{4}L^3$

Table 8 Areas and moments of inertia for exact curve fitting.

No. of dimensionless factors	(A, I)	
	2D	3D
6	-	$(1, 6), (2, 5), (3, 4), (4, 3), (5, 2), (6, 1)$
5	-	$(1, 6), (2, 5), (3, 4), (4, 3), (5, 2)$
4	$(1, 4), (2, 3), (3, 2), (4, 1)$	$(1, 6), (2, 5), (3, 4), (4, 3)$
3	$(1, 4), (2, 3), (3, 2)$	$(1, 6), (2, 5), (3, 4)$
2	$(1, 4), (2, 3)$	$(1, 6), (2, 5)$
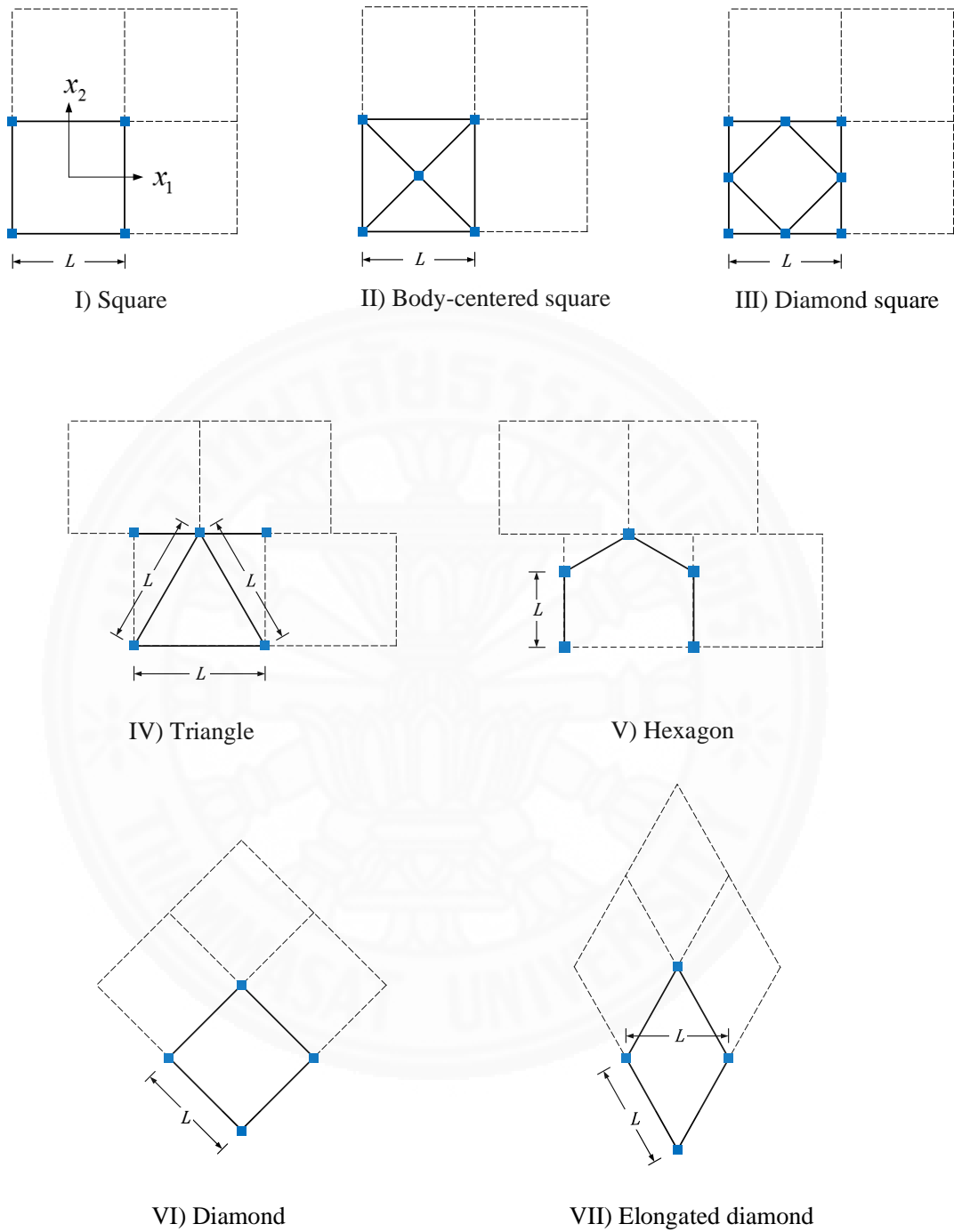
Fig. 11 Two-dimensional unit cells.
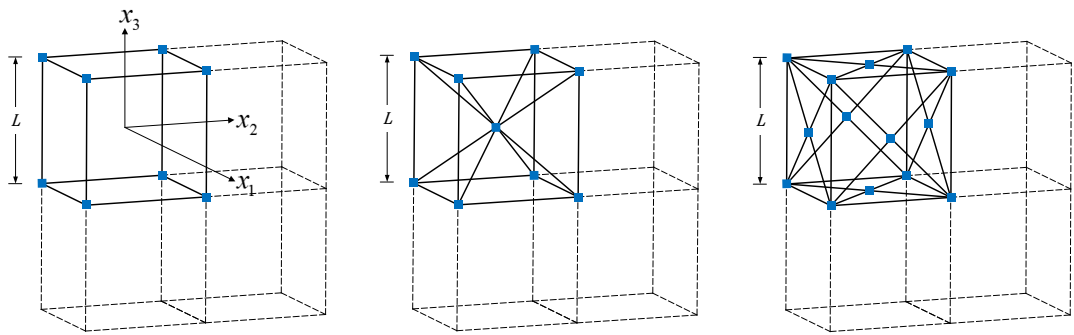
I) Simple cubic   II) Body-centered cubic   III) Face-centered cubic
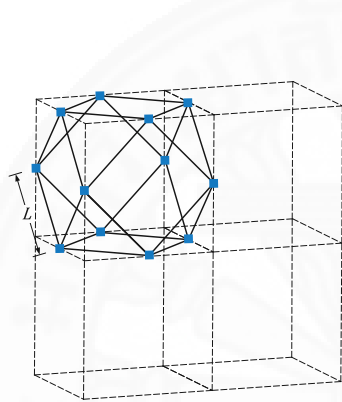
IV) Cuboctahedron
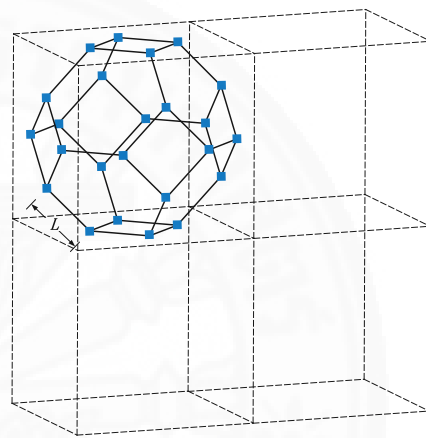
V) Tetrakaidecahedron
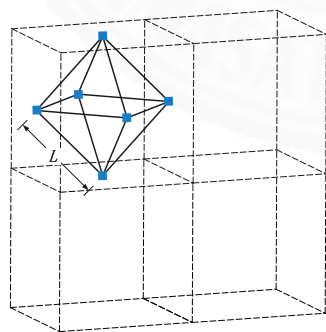
VI) Octahedron
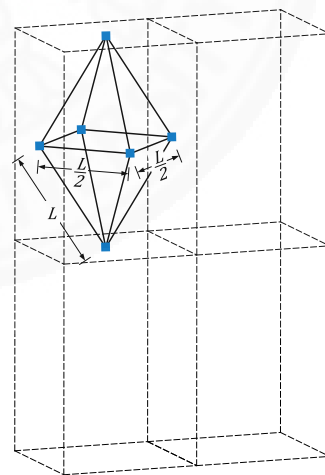
VII) Tetragonal bipyramid

Fig. 12 Three-dimensional unit cells.

Table 9-Table 14 show the expressions of effective Young's moduli, Poisson's ratios, and shear moduli obtained from the exact curve fitting. The volumes V_C in Table 9-Table 14 can be obtained from Table 7. It must be noted that, for the square and cubic unit cells, the obtained systems of linear equations for effective Young's moduli and Poisson's ratios have multiple solutions of the dimensionless factors. However, all of the solutions yield the same expressions shown in Table 9, Table 10, Table 12, and Table 13. The problems of multiple solutions with the square and cubic unit cells happen because effective Young's moduli are functions of A only, and the effective Poisson's ratios are not functions of A and I at all. As a result, the proposed exact forms become too generic, and permit multiple solutions of the dimensionless factors that can, in fact, represent in the same final expressions. In fact, for 3D periodic cellular solids, whose reduced exact forms of effective Young's moduli and Poisson's ratios exist due to symmetry, the reduced exact forms must be used to avoid this kind of problem.

The expressions obtained from the exact curve fitting in Table 9-Table 14 are tested with two sets of A and I. For 2D unit cells, $T \times T$ square struts with $T = 0.1$ for the first set and 0.2 for the second set are used. Note that T is also the thickness of each 2D unit cell. For 3D unit cells, circular struts with diameter $D = 0.1$ and 0.2 are used. In testing, base Young's modulus E and the characteristic length L are still set to 1. First, the effective elastic constants for the test sets of A and I are computed from the expressions from the exact curve fitting. Then, the effective elastic constants are directly determined from Eqs. (20), (22), and Eqs. (27)−(31) using strain energy from FEA of the unit cells. The effective elastic constants from the expressions from the exact curve fitting and from the FE results are compared in Table 15 and Table 16. Note that, when there are distinct effective elastic constants for different directions, the values in Table 15 and Table 16 are ordered in the same way as in Table 9-Table 14. It is found that all of the effective elastic constants from the expressions obtained from the exact curve fitting and from the FE results are identical except for effective shear moduli of the hexagonal and tetrakaidecahedral solids. The large differences in the cases of effective shear moduli of the hexagonal and tetrakaidecahedral solids imply that the real exact solutions of effective shear moduli of these two solids have some dimensionless factors that are not constants as assumed. Therefore, effective shear moduli of the hexagonal and tetrakaidecahedral solids from the curve fitting are not correct and should not be used.

Table 9-Table 14, the exact solutions of the effective elastic constants from elaborate symbolic FE computations are also given. Symbolic FEA is performed in MATLAB to symbolically determine strain energy under different strain modes. The symbolic expressions of strain energy are then used to symbolically compute the effective elastic constants. It can be

seen from the comparison with the exact solutions in Table 9-Table 14 that, except for effective shear moduli of the hexagonal and tetrakaidecahedral solids, the effective elastic constants obtained from this study are the same as the exact solutions. This confirms the comparison results reported in Table 15 and Table 16, where effective shear moduli of the hexagonal and tetrakaidecahedral solids yield large errors with the test data. It must be noted that the exact solutions of effective shear moduli of the hexagonal and tetrakaidecahedral solids can still be written in the exact forms proposed in this study. However, some of their dimensionless factors are not constant.

Table 9 Effective Young's moduli for 2D periodic cellular solids.

Unit cell	Effective Young's moduli	
	Present study	Exact solution[a]
Square	$E_i^* = \dfrac{E}{V_C}\left[\dfrac{1.00000(AL)^2 + 0.00000(AI) + 0.00000\left(\frac{I}{L}\right)^2}{AL + 0.00000\left(\frac{I}{L}\right)}\right]$	$E_i^* = \dfrac{E}{V_C}(AL)$
Body-centered square	$E_i^* = \dfrac{E}{V_C}\left[\dfrac{1.41421(AL)^2 + 48.00000(AI) + 0.00000\left(\frac{I}{L}\right)^2}{AL + 9.94113\left(\frac{I}{L}\right)}\right]$	$E_i^* = \dfrac{E}{V_C}\left[\dfrac{\sqrt{2}(AL)^2 + 48(AI)}{AL + \left(\frac{24\sqrt{2}}{2+\sqrt{2}}\right)\left(\frac{I}{L}\right)}\right] = \dfrac{E}{V_C}\left[\dfrac{1.41421(AL)^2 + 48(AI)}{AL + 9.94113\left(\frac{I}{L}\right)}\right]$
Diamond square	$E_i^* = \dfrac{E}{V_C}\left[\dfrac{1.41421(AL)^2 + 48.00000(AI) + 0.00000\left(\frac{I}{L}\right)^2}{AL + 9.94113\left(\frac{I}{L}\right)}\right]$	$E_i^* = \dfrac{E}{V_C}\left[\dfrac{\left(2 + 2\sqrt{2}\right)(AL)^2 + \left(96 + 48\sqrt{2}\right)AI}{\left(2 + \sqrt{2}\right)AL + 24\sqrt{2}\left(\frac{I}{L}\right)}\right]$ $= \dfrac{E}{V_C}\left[\dfrac{1.41421(AL)^2 + 48(AI)}{AL + 9.94113\left(\frac{I}{L}\right)}\right]$
Triangle	$E_i^* = \dfrac{E}{V_C}\left[\dfrac{1.00000(AL)^2 + 12.00000(AI) + 0.00000\left(\frac{I}{L}\right)^2}{AL + 4.00000\left(\frac{I}{L}\right)}\right]$	$E_i^* = \dfrac{E}{V_C}\left[\dfrac{(AL)^2 + 12(AI)}{AL + 4\left(\frac{I}{L}\right)}\right]$

44

Table 9 (Continued) Effective Young's moduli for 2D periodic cellular solids.

| Unit cell | Effective Young's moduli | |
	Present study	Exact solution[a]
Hexagon	$E_i^* = \dfrac{E}{V_C}\left[\dfrac{0.00000(AL)^2 + 72.00000(AI) + 0.00000\left(\frac{I}{L}\right)^2}{AL + 36.00000\left(\frac{I}{L}\right)}\right]$	$E_i^* = \dfrac{E}{V_C}\left[\dfrac{72(AI)}{AL + 36\left(\frac{I}{L}\right)}\right]$
Diamond	$E_i^* = \dfrac{E}{V_C}\left[\dfrac{0.00000(AL)^2 + 24.00000(AI) + 0.00000\left(\frac{I}{L}\right)^2}{AL + 12.00000\left(\frac{I}{L}\right)}\right]$	$E_i^* = \dfrac{E}{V_C}\left[\dfrac{24(AI)}{AL + 12\left(\frac{I}{L}\right)}\right]$
Elongated diamond	$E_1^* = \dfrac{E}{V_C}\left[\dfrac{0.00000(AL)^2 + 8.00000(AI) + 0.00000\left(\frac{I}{L}\right)^2}{AL + 4.00000\left(\frac{I}{L}\right)}\right]$	$E_1^* = \dfrac{E}{V_C}\left[\dfrac{8(AI)}{AL + 4\left(\frac{I}{L}\right)}\right]$
	$E_2^* = \dfrac{E}{V_C}\left[\dfrac{0.00000(AL)^2 + 72.00000(AI) + 0.00000\left(\frac{I}{L}\right)^2}{AL + 36.00000\left(\frac{I}{L}\right)}\right]$	$E_2^* = \dfrac{E}{V_C}\left[\dfrac{72(AI)}{AL + 36\left(\frac{I}{L}\right)}\right]$

a) All exact solutions are from symbolic computations in MATLAB.

Table 10 Effective Poisson's ratios for 2D periodic cellular solids.

Unit cell	Effective Poisson's ratios	
	Present study	Exact solution[a]
Square	$v_{ij}^* = 0.00000$	$v_{ij}^* = 0$
Body-centered square	$v_{ij}^* = \dfrac{0.41421(AL) - 9.94113\left(\frac{I}{L}\right)}{AL + 9.94113\left(\frac{I}{L}\right)}$	$v_{ij}^* = \dfrac{(\sqrt{2}-1)(AL) - (24\sqrt{2}-24)\left(\frac{I}{L}\right)}{AL + (24\sqrt{2}-24)\left(\frac{I}{L}\right)}$ $= \dfrac{0.41421(AL) - 9.94113\left(\frac{I}{L}\right)}{AL + 9.94113\left(\frac{I}{L}\right)}$
Diamond square	$v_{ij}^* = \dfrac{0.41421(AL) - 9.94113\left(\frac{I}{L}\right)}{AL + 9.94113\left(\frac{I}{L}\right)}$	$v_{ij}^* = \dfrac{(\sqrt{2}-1)(AL) - (24\sqrt{2}-24)\left(\frac{I}{L}\right)}{AL + (24\sqrt{2}-24)\left(\frac{I}{L}\right)}$ $= \dfrac{0.41421(AL) - 9.94113\left(\frac{I}{L}\right)}{AL + 9.94113\left(\frac{I}{L}\right)}$
Triangle	$v_{ij}^* = \dfrac{0.33333(AL) - 4.00000\left(\frac{I}{L}\right)}{AL + 4.00000\left(\frac{I}{L}\right)}$	$v_{ij}^* = \dfrac{\left(\frac{1}{3}\right)(AL) - 4\left(\frac{I}{L}\right)}{AL + 4\left(\frac{I}{L}\right)}$
Hexagon	$v_{ij}^* = \dfrac{1.00000(AL) - 12.00000\left(\frac{I}{L}\right)}{AL + 36.00000\left(\frac{I}{L}\right)}$	$v_{ij}^* = \dfrac{AL - 12\left(\frac{I}{L}\right)}{AL + 36\left(\frac{I}{L}\right)}$
Diamond	$v_{ij}^* = \dfrac{1.00000(AL) - 12.00000\left(\frac{I}{L}\right)}{AL + 12.00000\left(\frac{I}{L}\right)}$	$v_{ij}^* = \dfrac{AL - 12\left(\frac{I}{L}\right)}{AL + 12\left(\frac{I}{L}\right)}$
Elongated diamond	$v_{12}^* = \dfrac{0.33333(AL) - 4.00000\left(\frac{I}{L}\right)}{AL + 4.00000\left(\frac{I}{L}\right)}$ $v_{21}^* = \dfrac{3.00000(AL) - 36.00000\left(\frac{I}{L}\right)}{AL + 36.00000\left(\frac{I}{L}\right)}$	$v_{12}^* = \dfrac{\left(\frac{1}{3}\right)(AL) - 4\left(\frac{I}{L}\right)}{AL + 4\left(\frac{I}{L}\right)}$ $v_{21}^* = \dfrac{3(AL) - 36\left(\frac{I}{L}\right)}{AL + 36\left(\frac{I}{L}\right)}$

a) All exact solutions are from symbolic computations in MATLAB.

Table 11 Effective shear moduli for 2D periodic cellular solids.

Unit cell	Effective shear modulus	
	Present study	Exact solution[a]
Square	$G_{12}^* = \dfrac{E}{V_C}\left[0.00000(AL) + 6.00000\left(\dfrac{I}{L}\right)\right]$	$G_{12}^* = \dfrac{E}{V_C}\left[6\left(\dfrac{I}{L}\right)\right]$
Body-centered square	$G_{12}^* = \dfrac{E}{V_C}\left[0.70711(AL) + 6.00000\left(\dfrac{I}{L}\right)\right]$	$G_{12}^* = \dfrac{E}{V_C}\left[\left(\dfrac{\sqrt{2}}{2}\right)(AL) + 6\left(\dfrac{I}{L}\right)\right]$ $= \dfrac{E}{V_C}\left[0.70711(AL) + 6\left(\dfrac{I}{L}\right)\right]$
Diamond square	$G_{12}^* = \dfrac{E}{V_C}\left[0.70711(AL) + 13.45584\left(\dfrac{I}{L}\right)\right]$	$G_{12}^* = \dfrac{E}{V_C}\left[\left(\dfrac{\sqrt{2}}{2}\right)(AL) + (18\sqrt{2} - 12)\left(\dfrac{I}{L}\right)\right]$ $= \dfrac{E}{V_C}\left[0.70711(AL) + 13.45584\left(\dfrac{I}{L}\right)\right]$
Triangle	$G_{12}^* = \dfrac{E}{V_C}\left[0.37500(AL) + 4.50000\left(\dfrac{I}{L}\right)\right]$	$G_{12}^* = \dfrac{E}{V_C}\left[\left(\dfrac{3}{8}\right)(AL) + \left(\dfrac{9}{2}\right)\left(\dfrac{I}{L}\right)\right]$ $G_{12}^* = \dfrac{E}{V_C}\left[0.375(AL) + 4.5\left(\dfrac{I}{L}\right)\right]$
Hexagon	$G_{12}^* = \dfrac{E}{V_C}\left[1.39205(AL) + 0.01933\left(\dfrac{I}{L}\right)\right]$	$G_{12}^* = \dfrac{E}{V_C}\left[\left(\dfrac{18I}{AL^2 + 12I}\right)(AL)\right]$
Diamond	$G_{12}^* = \dfrac{E}{V_C}\left[0.50000(AL) + 0.00000\left(\dfrac{I}{L}\right)\right]$	$G_{12}^* = \dfrac{E}{V_C}\left[\left(\dfrac{1}{2}\right)(AL)\right]$
Elongated diamond	$G_{12}^* = \dfrac{E}{V_C}\left[0.37500(AL) + 0.00000\left(\dfrac{I}{L}\right)\right]$	$G_{12}^* = \dfrac{E}{V_C}\left[\left(\dfrac{3}{8}\right)(AL)\right]$ $= \dfrac{E}{V_C}\left[0.375(AL)\right]$

a) All exact solutions are from symbolic computations in MATLAB.

Table 12 Effective Young's moduli for 3D periodic cellular solids.

Unit cell	Effective Young's moduli	
	Present study	Exact solution[a]
Cubic	$E_i^* = \dfrac{E}{V_C}\left[\dfrac{1.00000(AL)^2 + 0.00000(AI) + 0.00000\left(\frac{I}{L}\right)^2}{AL + 0.00000\left(\frac{I}{L}\right)}\right]$	$E_i^* = \dfrac{E}{V_C}(AL)$
Body-centered cubic	$E_i^* = \dfrac{E}{V_C}\left[\dfrac{1.30312(AL)^2 + 48.15078(AI) + 0.00000\left(\frac{I}{L}\right)^2}{AL + 4.84990\left(\frac{I}{L}\right)}\right]$	$E_i^* = \dfrac{E}{V_C}\left[\dfrac{\left[\left(\frac{12\sqrt{3}+9}{8\sqrt{3}+9}\right)(AL)^2 + \left(\frac{192\sqrt{3}+768}{8\sqrt{3}+9}\right)(AI)\right]}{AL + \left(\frac{64\sqrt{3}}{8\sqrt{3}+9}\right)\left(\frac{I}{L}\right)}\right]$ $= \dfrac{E}{V_C}\left[\dfrac{1.30312(AL)^2 + 48.15078(AI)}{AL + 4.84990\left(\frac{I}{L}\right)}\right]$
Face-centered cubic	$E_i^* = \dfrac{E}{V_C}\left[\dfrac{2.09384(AL)^2 + 57.94113(AI) + 369.07458\left(\frac{I}{L}\right)^2}{AL + 16.31095\left(\frac{I}{L}\right)}\right]$	$E_i^* = \dfrac{E}{V_C}\left[\dfrac{\left[\left(\frac{9+4\sqrt{2}}{7}\right)(AL)^2 + \left(24\sqrt{2}+24\right)AI + \left(\frac{3456\sqrt{2}-2304}{7}\right)\left(\frac{I}{L}\right)^2\right]}{AL + \left(\frac{216-72\sqrt{2}}{7}\right)\left(\frac{I}{L}\right)}\right]$ $= \dfrac{E}{V_C}\left[\dfrac{2.09384(AL)^2 + 57.94113(AI) + 369.07458\left(\frac{I}{L}\right)^2}{AL + 16.31095\left(\frac{I}{L}\right)}\right]$
Cuboctahedron	$E_i^* = \dfrac{E}{V_C}\left[\dfrac{1.33333(AL)^2 + 48.00000(AI) + 0.00000\left(\frac{I}{L}\right)^2}{AL + 4.00000\left(\frac{I}{L}\right)}\right]$	$E_i^* = \dfrac{E}{V_C}\left[\dfrac{\left(\frac{4}{3}\right)(AL)^2 + 48(AI)}{AL + 4\left(\frac{I}{L}\right)}\right] = \dfrac{E}{V_C}\left[\dfrac{1.33333(AL)^2 + 48(AI)}{AL + 4\left(\frac{I}{L}\right)}\right]$

Table 12 (Continued) Effective Young's moduli for 3D periodic cellular solids.

Unit cell	Effective Young's moduli	
	Present study	Exact solution[a]
Tetrakai-decahedron	$E_i^* = \dfrac{E}{V_C}\left[\dfrac{0.00000(AL)^2 + 192.00000(AI) + 0.00000\left(\frac{I}{L}\right)^2}{AL + 12.00000\left(\frac{I}{L}\right)}\right]$	$E_i^* = \dfrac{E}{V_C}\left[\dfrac{192(AI)}{AL + 12\left(\frac{I}{L}\right)}\right]$
Octahedron	$E_i^* = \dfrac{E}{V_C}\left[\dfrac{1.33333(AL)^2 + 48.00000(AI) + 0.00000\left(\frac{I}{L}\right)^2}{AL + 4.00000\left(\frac{I}{L}\right)}\right]$	$E_i^* = \dfrac{E}{V_C}\left[\dfrac{\left(\frac{4}{3}\right)(AL)^2 + 48(AI)}{AL + 4\left(\frac{I}{L}\right)}\right] = \dfrac{E}{V_C}\left[\dfrac{1.33333(AL)^2 + 48(AI)}{AL + 4\left(\frac{I}{L}\right)}\right]$
Tetragonal bipyramid	$\begin{aligned}E_1^* &= E_2^* \\ &= \dfrac{E}{V_C}\left[\dfrac{0.11765(AL)^3 + 101.24370(A^2 IL) + 859.15966\left(\frac{AI^2}{L}\right) + 0.00000\left(\frac{I}{L}\right)^3}{(AL)^2 + 58.28571(AI) + 85.91597\left(\frac{I}{L}\right)^2}\right]\end{aligned}$	$\begin{aligned}E_1^* = E_2^* &= \dfrac{E}{V_C}\left[\dfrac{\left(\frac{2}{17}\right)(AL)^3 + \left(\frac{12,048}{119}\right)(A^2 IL) + \left(\frac{102,240}{119}\right)\left(\frac{AI^2}{L}\right)}{(AL)^2 + \left(\frac{408}{7}\right)(AI) + \left(\frac{10,224}{119}\right)\left(\frac{I}{L}\right)^2}\right] \\ &= \dfrac{E}{V_C}\left[\dfrac{0.11765(AL)^3 + 101.24370(A^2 IL) + 859.15966\left(\frac{AI^2}{L}\right)}{(AL)^2 + 58.28571(AI) + 85.91597\left(\frac{I}{L}\right)^2}\right]\end{aligned}$
	$E_3^* = \dfrac{E}{V_C}\left[\dfrac{5.76471(AL)^2 + 49.41176(AI) + 0.00000\left(\frac{I}{L}\right)^2}{AL + 4.94118\left(\frac{I}{L}\right)}\right]$	$\begin{aligned}E_3^* &= \dfrac{E}{V_C}\left[\dfrac{\left(\frac{98}{17}\right)(AL)^2 + \left(\frac{840}{17}\right)(AI)}{AL + \left(\frac{84}{17}\right)\left(\frac{I}{L}\right)}\right] \\ &= \dfrac{E}{V_C}\left[\dfrac{5.76471(AL)^2 + 49.41176(AI)}{AL + 4.94118\left(\frac{I}{L}\right)}\right]\end{aligned}$

a) All exact solutions are from symbolic computations in MATLAB. The same exact solution for the tetrakaidecahedral cell is also obtained by Zhu, Knott, and Mills (1997)

Table 13 Effective Poisson's ratios for 3D periodic cellular solids.

Unit cell	Effective Poisson's ratios	
	Present study	Exact solution[a]
Cubic	$v_{ij}^* = 0.00000$	$v_{ij}^* = 0$
Body-centered cubic	$v_{ij}^* = \dfrac{0.30312(AL) - 4.84990\left(\frac{I}{L}\right)}{AL + 4.84990\left(\frac{I}{L}\right)}$	$v_{ij}^* = \dfrac{\left(\frac{4\sqrt{3}}{8\sqrt{3}+9}\right)(AL) - \left(\frac{64\sqrt{3}}{8\sqrt{3}+9}\right)\left(\frac{I}{L}\right)}{AL + \left(\frac{64\sqrt{3}}{8\sqrt{3}+9}\right)\left(\frac{I}{L}\right)} = \dfrac{0.30312(AL) - 4.84990\left(\frac{I}{L}\right)}{AL + 4.84990\left(\frac{I}{L}\right)}$
Face-centered cubic	$v_{ij}^* = \dfrac{0.22654(AL) - 5.43698\left(\frac{I}{L}\right)}{AL + 16.31095\left(\frac{I}{L}\right)}$	$v_{ij}^* = \dfrac{\left(\frac{3-\sqrt{2}}{7}\right)(AL) + \left(\frac{72-24\sqrt{2}}{7}\right)\left(\frac{I}{L}\right)}{(AL) + \left(\frac{216-72\sqrt{2}}{7}\right)\left(\frac{I}{L}\right)} = \dfrac{0.22654(AL) - 5.43698\left(\frac{I}{L}\right)}{AL + 16.31095\left(\frac{I}{L}\right)}$
Cuboctahedron	$v_{ij}^* = \dfrac{0.33333(AL) - 4.00000\left(\frac{I}{L}\right)}{AL + 4.00000\left(\frac{I}{L}\right)}$	$v_{ij}^* = \dfrac{\left(\frac{1}{3}\right)(AL) - 4\left(\frac{I}{L}\right)}{AL + 4\left(\frac{I}{L}\right)}$
Tetrakai-decahedron	$v_{ij}^* = \dfrac{0.50000(AL) - 6.00000\left(\frac{I}{L}\right)}{AL + 12.00000\left(\frac{I}{L}\right)}$	$v_{ij}^* = \dfrac{\left(\frac{1}{2}\right)(AL) - 6\left(\frac{I}{L}\right)}{AL + 12\left(\frac{I}{L}\right)}$
Octahedron	$v_{ij}^* = \dfrac{0.33333(AL) - 4.00000\left(\frac{I}{L}\right)}{AL + 4.00000\left(\frac{I}{L}\right)}$	$v_{ij}^* = \dfrac{\left(\frac{1}{3}\right)(AL) - 4\left(\frac{I}{L}\right)}{AL + 4\left(\frac{I}{L}\right)}$

Table 13 (Continued) Effective Poisson's ratios for 3D periodic cellular solids.

Unit cell	Effective Poisson's ratios	
	Present study	Exact solution[a]
Tetragonal bipyramid	$v_{13}^* = v_{23}^* = \dfrac{0.00840(AL)^2 + 7.05882(AI) - 85.91597\left(\frac{I}{L}\right)^2}{(AL)^2 + 58.28571(AI) + 85.91597\left(\frac{I}{L}\right)^2}$	$v_{13}^* = v_{23}^* = \dfrac{\left(\frac{1}{119}\right)(AL)^2 + \left(\frac{120}{17}\right)(AI) - \left(\frac{10{,}224}{119}\right)\left(\frac{I}{L}\right)^2}{(AL)^2 + \left(\frac{408}{7}\right)(AI) + \left(\frac{10{,}224}{119}\right)\left(\frac{I}{L}\right)^2}$ $= \dfrac{0.00840(AL)^2 + 7.05882(AI) - 85.91597\left(\frac{I}{L}\right)^2}{(AL)^2 + 58.28571(AI) + 85.91597\left(\frac{I}{L}\right)^2}$
	$v_{31}^* = v_{32}^* = \dfrac{0.41176(AL) - 4.94118\left(\frac{I}{L}\right)}{AL + 4.94118\left(\frac{I}{L}\right)}$	$v_{31}^* = v_{32}^* = \dfrac{\left(\frac{7}{17}\right)(AL) - \left(\frac{84}{17}\right)\left(\frac{I}{L}\right)}{AL + \left(\frac{84}{17}\right)\left(\frac{I}{L}\right)}$ $= \dfrac{0.41176(AL) - 4.94118\left(\frac{I}{L}\right)}{AL + 4.94118\left(\frac{I}{L}\right)}$
	$v_{12}^* = v_{21}^* = \dfrac{0.88235(AL)^2 - 42.15126(AI) - 85.91597\left(\frac{I}{L}\right)^2}{(AL)^2 + 58.28571(AI) + 85.91597\left(\frac{I}{L}\right)^2}$	$v_{12}^* = v_{21}^* = \dfrac{\left(\frac{15}{17}\right)(AL)^2 - \left(\frac{5{,}016}{119}\right)(AI) - \left(\frac{10{,}224}{119}\right)\left(\frac{I}{L}\right)^2}{(AL)^2 + \left(\frac{408}{7}\right)(AI) + \left(\frac{10{,}224}{119}\right)\left(\frac{I}{L}\right)^2}$ $= \dfrac{0.88235(AL)^2 - 42.15126(AI) - 85.91597\left(\frac{I}{L}\right)^2}{(AL)^2 + 58.28571(AI) + 85.91597\left(\frac{I}{L}\right)^2}$

a) All exact solutions are from symbolic computations in MATLAB. The same exact solution for the tetrakaidecahedral cell is also obtained by Zhu, Knott, and Mills (1997)

Table 14 Effective shear moduli for 3D periodic cellular solids.

Unit cell	Effective Shear moduli	
	Present study	Exact solution[a]
Cubic	$G_{ij}^* = \dfrac{E}{V_C}\left[0.00000(AL) + 6.00000\left(\dfrac{I}{L}\right)\right]$	$G_{ij}^* = \dfrac{E}{V_C}\left[6\left(\dfrac{I}{L}\right)\right]$
Body-centered cubic	$G_{ij}^* = \dfrac{E}{V_C}\left[0.76980(AL) + 12.15840\left(\dfrac{I}{L}\right)\right]$	$G_{ij}^* = \dfrac{E}{V_C}\left[\left(\dfrac{4\sqrt{3}}{9}\right)(AL) + \left(\dfrac{54 + 32\sqrt{3}}{9}\right)\left(\dfrac{I}{L}\right)\right]$ $= \dfrac{E}{V_C}\left[0.76980(AL) + 12.15840\left(\dfrac{I}{L}\right)\right]$
Face-centered cubic	$G_{ij}^* = \dfrac{E}{V_C}\left[0.70711(AL) + 10.24264\left(\dfrac{I}{L}\right)\right]$	$G_{ij}^* = \dfrac{E}{V_C}\left[\dfrac{\sqrt{2}}{2}(AL) + \left(6 + 3\sqrt{2}\right)\left(\dfrac{I}{L}\right)\right]$ $= \dfrac{E}{V_C}\left[0.70711(AL) + 10.24264\left(\dfrac{I}{L}\right)\right]$
Cuboctahedron	$G_{ij}^* = \dfrac{E}{V_C}\left[1.00000(AL) + 7.50000\left(\dfrac{I}{L}\right)\right]$	$G_{ij}^* = \dfrac{E}{V_C}\left[AL + \left(\dfrac{15}{2}\right)\left(\dfrac{I}{L}\right)\right]$
Tetrakai-decahedron	$G_{ij}^* = \dfrac{E}{V_C}\left[7.42983(AL) + 0.06604\left(\dfrac{I}{L}\right)\right]$	$G_{ij}^* = \dfrac{E}{V_C}\left[\dfrac{120I}{2AL^2 + 15I}\right](AL)$
Octahedron	$G_{ij}^* = \dfrac{E}{V_C}\left[1.00000(AL) + 7.50000\left(\dfrac{I}{L}\right)\right]$	$G_{ij}^* = \dfrac{E}{V_C}\left[AL + \left(\dfrac{15}{2}\right)\left(\dfrac{I}{L}\right)\right]$
Tetragonal bipyramid	$G_{13}^* = G_{23}^* = \dfrac{E}{V_C}\left[0.43750(AL) + 13.62043\left(\dfrac{I}{L}\right)\right]$	$G_{13}^* = G_{23}^* = \dfrac{E}{V_C}\left[\left(\dfrac{7}{16}\right)(AL) + \left(\dfrac{110{,}271}{8{,}096}\right)\left(\dfrac{I}{L}\right)\right]$ $= \dfrac{E}{V_C}\left[0.4375(AL) + 13.62043\left(\dfrac{I}{L}\right)\right]$
	$G_{12}^* = \dfrac{E}{V_C}\left[0.50000(AL) + 2.75000\left(\dfrac{I}{L}\right)\right]$	$G_{12}^* = \dfrac{E}{V_C}\left[\left(\dfrac{1}{2}\right)(AL) + \left(\dfrac{11}{4}\right)\left(\dfrac{I}{L}\right)\right]$ $= \dfrac{E}{V_C}\left[0.5(AL) + 2.75\left(\dfrac{I}{L}\right)\right]$

a) All exact solutions are from symbolic computations in MATLAB. The same exact solution for the tetrakaidecahedral cell is also obtained by Zhu, Knott, and Mills (1997)

Table 15 Testing of the expressions obtained by exact curve fitting for 2D periodic cellular solids.

Unit cell	E	L	T	Effective Young's modulus			Effective Poisson's ratio			Effective shear modulus		
				Present study, a	FEM, b	Difference, $(a-b)/b$	Present study, a	FEM, b	Difference, $(a-b)/b$	Present study, a	FEM, b	Difference, $(a-b)/b$
Square	1.0	1.0	0.1	1.000×10^{-1}	1.000×10^{-1}	0.000	0.000×10^{0}	0.000×10^{0}	No difference	5.000×10^{-4}	5.000×10^{-4}	0.000
	1.0	1.0	0.2	2.000×10^{-1}	2.000×10^{-1}	0.000	0.000×10^{0}	0.000×10^{0}	No difference	4.000×10^{-3}	4.000×10^{-3}	0.000
Body-centered square	1.0	1.0	0.1	1.442×10^{-1}	1.442×10^{-1}	0.000	4.026×10^{-1}	4.026×10^{-1}	0.000	7.121×10^{-2}	7.121×10^{-2}	0.000
	1.0	1.0	0.2	3.047×10^{-1}	3.047×10^{-1}	0.000	3.689×10^{-1}	3.689×10^{-1}	0.000	1.454×10^{-1}	1.454×10^{-1}	0.000
Diamond square	1.0	1.0	0.1	1.442×10^{-1}	1.442×10^{-1}	0.000	4.026×10^{-1}	4.026×10^{-1}	0.000	7.183×10^{-2}	7.183×10^{-2}	0.000
	1.0	1.0	0.2	3.047×10^{-1}	3.047×10^{-1}	0.000	3.689×10^{-1}	3.689×10^{-1}	0.000	1.504×10^{-1}	1.504×10^{-1}	0.000
Triangle	1.0	1.0	0.1	1.162×10^{-1}	1.162×10^{-1}	0.000	3.289×10^{-1}	3.289×10^{-1}	0.000	4.373×10^{-2}	4.373×10^{-2}	0.000
	1.0	1.0	0.2	2.370×10^{-1}	2.370×10^{-1}	0.000	3.158×10^{-1}	3.158×10^{-1}	0.000	9.007×10^{-2}	9.007×10^{-2}	0.000
Hexagon	1.0	1.0	0.1	2.242×10^{-3}	2.242×10^{-3}	0.000	9.612×10^{-1}	9.612×10^{-1}	0.000	5.358×10^{-2}	5.716×10^{-4}	9.274×10^{1}
	1.0	1.0	0.2	1.650×10^{-2}	1.650×10^{-2}	0.000	8.571×10^{-1}	8.571×10^{-1}	0.000	1.072×10^{-1}	4.441×10^{-3}	2.314×10^{1}
diamond	1.0	1.0	0.1	1.980×10^{-3}	1.980×10^{-3}	0.000	9.802×10^{-1}	9.802×10^{-1}	0.000	5.000×10^{-2}	5.000×10^{-2}	0.000
	1.0	1.0	0.2	1.538×10^{-2}	1.538×10^{-2}	0.000	9.231×10^{-1}	9.231×10^{-1}	0.000	1.000×10^{-1}	1.000×10^{-1}	0.000
Elongated diamond	1.0	1.0	0.1	7.672×10^{-4} 6.726×10^{-3}	7.672×10^{-4} 6.726×10^{-3}	0.000 0.000	3.289×10^{-1} 2.883×10^{0}	3.289×10^{-1} 2.883×10^{0}	0.000 0.000	4.330×10^{-2}	4.330×10^{-2}	0.000
	1.0	1.0	0.2	6.077×10^{-3} 4.949×10^{-2}	6.077×10^{-3} 4.949×10^{-2}	0.000 0.000	3.158×10^{-1} 2.571×10^{0}	3.158×10^{-1} 2.571×10^{0}	0.000 0.000	8.660×10^{-2}	8.660×10^{-2}	0.000

Table 16 Testing of the expressions obtained by exact curve fitting for 3D periodic cellular solids.

Unit cell	E	L	D	Effective Young's modulus			Effective Poisson's ratio			Effective shear modulus		
				Present study, a	FEM, b	Difference, $(a-b)/b$	Present study, a	FEM, b	Difference, $(a-b)/b$	Present study, a	FEM, b	Difference, $(a-b)/b$
Cubic	1.0	1.0	0.1	7.854×10^{-3}	7.854×10^{-3}	0.000	0.000×10^{0}	0.000×10^{0}	No difference	2.945×10^{-5}	2.945×10^{-5}	0.000
	1.0	1.0	0.2	3.142×10^{-2}	3.142×10^{-2}	0.000	0.000×10^{0}	0.000×10^{0}	No difference	4.712×10^{-4}	4.712×10^{-4}	0.000
Body-centered cubic	1.0	1.0	0.1	1.044×10^{-2}	1.044×10^{-2}	0.000	2.992×10^{-1}	2.992×10^{-1}	0.000	6.106×10^{-3}	6.106×10^{-3}	0.000
	1.0	1.0	0.2	4.418×10^{-2}	4.418×10^{-2}	0.000	2.875×10^{-1}	2.875×10^{-1}	0.000	2.514×10^{-2}	2.514×10^{-2}	0.000
Face-centered cubic	1.0	1.0	0.1	1.656×10^{-2}	1.656×10^{-2}	0.000	2.276×10^{-1}	2.276×10^{-1}	0.000	5.604×10^{-3}	5.604×10^{-3}	0.000
	1.0	1.0	0.2	6.764×10^{-2}	6.764×10^{-2}	0.000	2.307×10^{-1}	2.307×10^{-1}	0.000	2.302×10^{-2}	2.302×10^{-2}	0.000
Cubocta-hedron	1.0	1.0	0.1	3.776×10^{-3}	3.776×10^{-3}	0.000	3.300×10^{-1}	3.300×10^{-1}	0.000	2.790×10^{-3}	2.790×10^{-3}	0.000
	1.0	1.0	0.2	1.598×10^{-2}	1.598×10^{-2}	0.000	3.201×10^{-1}	3.201×10^{-1}	0.000	1.132×10^{-2}	1.132×10^{-2}	0.000
Tetrakai-decahedron	1.0	1.0	0.1	4.134×10^{-5}	4.134×10^{-5}	0.000	4.926×10^{-1}	4.926×10^{-1}	0.000	2.579×10^{-3}	1.296×10^{-5}	1.980×10^{2}
	1.0	1.0	0.2	6.470×10^{-4}	6.470×10^{-4}	0.000	4.709×10^{-1}	4.709×10^{-1}	0.000	1.032×10^{-2}	2.044×10^{-4}	4.949×10^{1}
Octahedron	1.0	1.0	0.1	3.776×10^{-3}	3.776×10^{-3}	0.000	3.300×10^{-1}	3.300×10^{-1}	0.000	2.790×10^{-3}	2.790×10^{-3}	0.000
	1.0	1.0	0.2	1.598×10^{-2}	1.598×10^{-2}	0.000	3.201×10^{-1}	3.201×10^{-1}	0.000	1.132×10^{-2}	1.132×10^{-2}	0.000
Tetragonal bipyramid	1.0	1.0	0.1	1.468×10^{-3} 4.851×10^{-2}	1.468×10^{-3} 4.851×10^{-2}	0.000 0.000	1.233×10^{-2} 4.074×10^{-1} 8.259×10^{-1}	1.233×10^{-2} 4.074×10^{-1} 8.259×10^{-1}	0.000 0.000 0.000	3.745×10^{-3} 4.213×10^{-3}	3.745×10^{-3} 4.213×10^{-3}	0.000
	1.0	1.0	0.2	1.102×10^{-2} 1.953×10^{-1}	1.102×10^{-2} 1.953×10^{-1}	0.000 0.000	2.226×10^{-2} 3.945×10^{-1} 6.774×10^{-1}	2.226×10^{-2} 3.945×10^{-1} 6.774×10^{-1}	0.000 0.000 0.000	1.584×10^{-2} 1.702×10^{-2}	1.584×10^{-2} 1.702×10^{-2}	0.000

Chapter 6
Degrees of Homogeneity

As aforementioned, if the sizes of unit cells in a frame-like periodic solid are sufficiently small when compared to the size of the whole solid, the solid behaves like a homogeneous material. Such a periodic cellular solid will exhibit the effective elastic properties and a homogenization method can be used to determine these effective properties. If the sizes of unit cells are not sufficiently small when compared to the size of the whole solid, its apparent elastic properties can be different from the effective elastic properties. It is advantageous to know how small is sufficiently small.

The degrees of homogeneity can be determined from the relative sizes between the solids and their unit cells, which can be defined as the ratio between the solid size and the unit-cell size. Periodic cellular solids with different unit-cell topologies require different numbers of unit cells to reach their effective elastic properties. The number of unit cells that is required for a periodic cellular solid to exhibit the effective elastic properties can also be used to determine the relative size between the solid and its unit cells required for homogenization. A periodic cellular solid that requires a low number of unit cells for its apparent elastic properties to converge to the effective elastic properties can be said to have a high degree of homogeneity. On the contrary, a periodic cellular solid that requires a large number of unit cells for its apparent elastic properties to converge to the effective elastic properties can be said to have a low degree of homogeneity.

6.1 Investigation of the degrees of homogeneity

Here, the degrees of homogeneity of some common frame-like periodic solids are investigated by determining, for each solid, the number of unit cells required for the apparent elastic properties to converge to the effective elastic properties. Both 2D and 3D frame-like periodic solids with various geometrical shapes are numerically investigated. The apparent effective properties of the considered periodic cellular solids with various numbers of unit cells are determined by FEA. The degrees of homogeneity are then obtained by comparing the obtained apparent elastic constants with the exact effective elastic constants calculated from the exact forms with exact curve fitting. If the dimensionless factors in the exact forms are not constant, the exact solutions from symbolic FEA will be used instead.
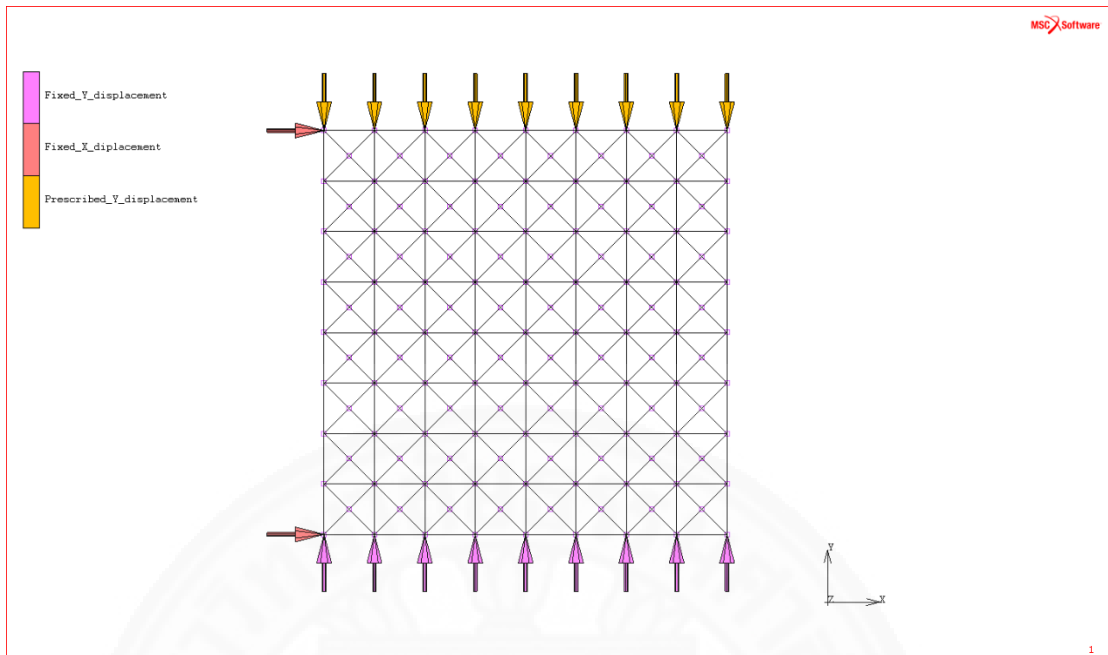
Fig. 13 2D solid and boundary conditions.
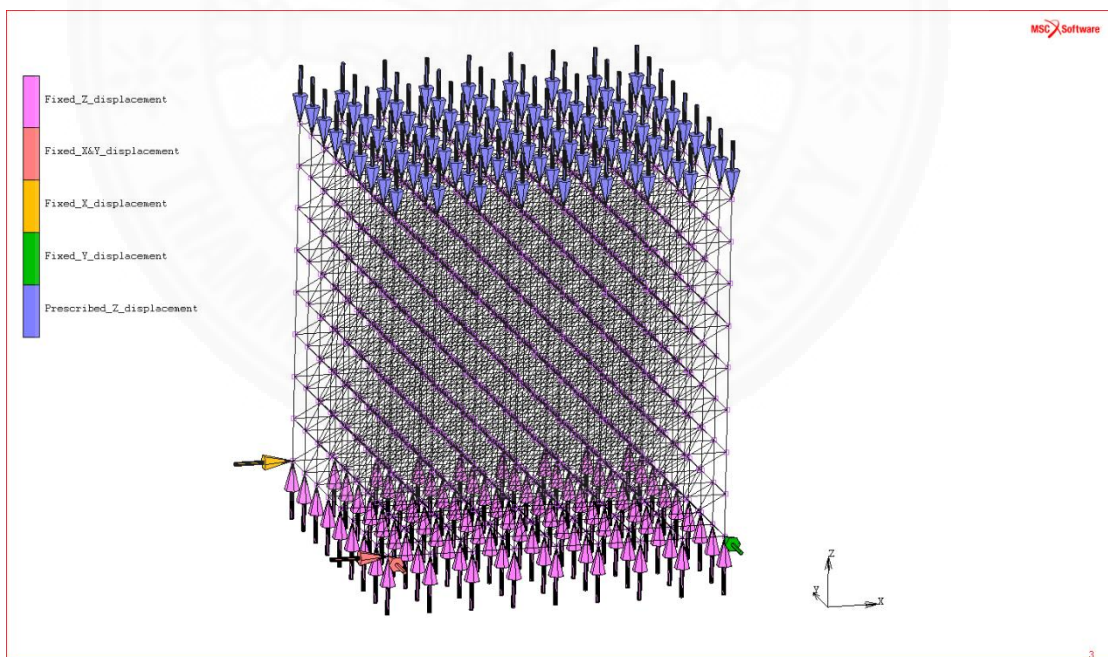
Fig. 14 3D solid and boundary conditions.

The investigated 2D periodic cellular solids include square, body-centered square, triangle, hexagon, diamond, and elongated diamond cellular solids. Their configurations can be seen in Fig. 11. The investigated 3D periodic cellular solids include cubic, body-centered cubic,

cuboctahedron, tetrakaidecahedron, octahedron, and tetragonal bipyramid cellular solids. Their configurations can be found in Fig. 12. The characteristic lengths L of unit cells are 1 mm. For 2D periodic cellular solids, the struts have 0.1×0.1 mm square cross sections. For 3D periodic cellular solids, the struts have circular cross sections with 0.1 mm diameter. The base material is assumed to be linear elastic isotropic with Young's modulus equal to 1 MPa and Poisson's ratio equal to zero.

The apparent elastic properties are determined from the periodic cellular solids under uniaxial compression and pure shear. The uniaxial compression is simulated by prescribing uniform vertical displacement boundary conditions while allowing free lateral displacements. FEA is performed using MSC.Marc Mentat software. Examples of FE models and the uniaxial boundary conditions are shown in Fig. 13 and Fig. 14 for 2D and 3D solids, respectively. Denote the number of unit cells in an orthogonal direction of a solid by n_C. The total number of unit cells in a 2D periodic cellular solid is therefore equal to $n_C \times n_C$ while that in a 3D solid is equal to $n_C \times n_C \times n_C$. In the investigation, n_C is increased and the apparent elastic constants are computed for different values of n_C. Define a relative elastic property as the ratio between the apparent elastic property of a solid and the effective elastic property of the equivalent homogeneous solid. A percentage difference is used to investigate the convergence of an apparent elastic property to its corresponding effective elastic property. This percentage difference is defined as

$$\text{Percentage difference} = \frac{\text{Apparent property} - \text{Effective property}}{\text{Effective property}} \times 100. \tag{69}$$

In this study, the convergence of an apparent elastic property to its corresponding effective elastic property is considered achieved when the percentage difference of less than 1% is obtained.

6.2 Results

The effective elastic properties of the investigated periodic cellular solids from the exact solutions are concluded in Table 17. The apparent elastic properties of the 2D periodic cellular solids for different values of n_C are shown in Table 18, Table 19, Table 20, Table 21, Table 22, and Table 23 for the square, body-center square, triangle, hexagon, diamond, and elongated diamond cellular solids, respectively. Note that the superscript n is used to represent apparent elastic properties. The values of n_C of the 2D cellular solids are increased to 512, which is sufficient for the apparent elastic properties of all considered 2D cellular solids to

57

converge to the effective elastic properties. It is found that the square, diamond, and elongated diamond solids need only one unit cell to exhibit the effective elastic properties. Therefore, the square, diamond, and elongated diamond solids can be regarded as 2D cellular solids that have the highest degrees of homogeneity. For the body-centered square solid, the apparent Young's modulus and Poisson's ratio converge when n_C is equal to 2 while the apparent shear modulus converges when n_C is equal to 1. For the triangle solid, the apparent Young's modulus, Poisson's ratio, and shear modulus converge when the values of n_C are equal to 32, 256, and 1, respectively. For the hexagon solid, the apparent Young's modulus, Poisson's ratio, and shear modulus converge when the values of n_C are equal to 128, 8, and 512, respectively. Consequently, the degrees of homogeneity are the highest in the square, diamond, and elongated diamond cellular solids, followed by the body-centered square, triangle, and hexagon cellular solids, respectively.

Table 17 Effective elastic properties of the investigated periodic cellular solids.

Unit cell		E_i^* (MPa)	v_{ij}^*	G_{ij}^* (MPa)
2D	Square	1.000×10^{-1}	0.000×10^{0}	5.000×10^{-4}
	Body-centered square	1.442×10^{-1}	4.026×10^{-1}	7.121×10^{-2}
	Triangle	1.162×10^{-1}	3.289×10^{-1}	4.373×10^{-2}
	Hexagon	2.242×10^{-3}	9.612×10^{-1}	5.716×10^{-4}
	Diamond	1.980×10^{-3}	9.802×10^{-1}	5.000×10^{-2}
	Elongated diamond	7.672×10^{-4} 6.077×10^{-3}	3.289×10^{-1} 2.883×10^{0}	4.330×10^{-2}
3D	Cubic	7.854×10^{-3}	0.000×10^{0}	2.945×10^{-5}
	Body-centered cubic	1.044×10^{-2}	2.992×10^{-1}	6.106×10^{-3}
	Cuboctahedron	3.776×10^{-3}	3.300×10^{-1}	2.790×10^{-3}
	Tetrakaidecahedron	4.134×10^{-5}	4.926×10^{-1}	1.296×10^{-5}
	Octahedron	3.776×10^{-3}	3.300×10^{-1}	2.790×10^{-3}
	Tetragonal bipyramid	1.468×10^{-3} 4.851×10^{-2}	8.259×10^{-1} 1.233×10^{-2} 4.074×10^{-1}	4.213×10^{-3} 3.745×10^{-3}

The apparent elastic properties of the 3D periodic cellular solids for different values of n_C are shown in Table 24, Table 25, Table 26, Table 27, Table 28, and Table 29 for the cubic, body-centered cubic, cuboctahedron, tetrakaidecahedron, octahedron, and tetragonal bipyramid cellular solids, respectively. The values of n_C of the 3D cellular solids are increased to 64, which is sufficient for the convergence of most of the considered 3D cellular solids. When n_C is equal to 64, the apparent Young's modulus and Poisson's ratio of the cuboctahedron solid

still do not converge to its effective properties under the employed convergence criterion. Nevertheless, one cuboctahedron unit cell can exhibit the effective shear modulus. When n_c is equal to 64, the tetrakaidecahedron solid has 3,194,880 nodes and the FE mesh becomes too large to be solved by the computers used in this study. Thus, there is no result for the tetrakaidecahedron solid when n_c is equal to 64. When n_c is equal to 32, only the apparent shear modulus of the tetrakaidecahedron solid converges to the effective shear modulus while the other apparent elastic properties still do not converge to their effective values under the employed convergence criterion. For the body-centered cubic solid, the apparent Young's modulus, Poisson's ratio, and shear modulus converge when the values of n_c are equal to 2, 4, and 8, respectively. It is found that the cubic, octahedron, and tetragonal bipyramid solids need only one unit cell to exhibit the effective elastic properties. Therefore, the cubic, octahedron, and tetragonal bipyramid solids can be regarded as 3D cellular solids that have the highest degrees of homogeneity.

The convergences of the apparent Young's moduli, Poisson's ratios, and shear moduli of 2D periodic cellular solids are shown in Fig. 15,

Fig. **16**, and Fig. 17, respectively. In the figures, the elastic constants are shown as the relative constants which are the ratios between the apparent elastic constants of the solids and the effective elastic constants. For the elongated diamond cellular solids, Young's moduli for the two axes are different but the relative Young's moduli are found to be the same. As a result, the convergences of the apparent Young's moduli for the two axes are the same, and they are shown in the same figure. For the 3D periodic cellular solids, the convergences of the apparent Young's moduli, Poisson's ratios, and shear moduli are shown in Fig. 18, Fig. 19, and Fig. 20, respectively. For the tetragonal bipyramid cellular solids, the convergences of the apparent elastic constants in different directions are found to be the same. Therefore, these results are only shown in one figure.

Table 18 Apparent elastic properties of the square periodic cellular solids.

n_C	E_i^n (MPa)	$\frac{E_i^n - E_i^*}{E_i^*} \times 100$	v_{ij}^n	$\frac{v_{ij}^n - v_{ij}^*}{v_{ij}^*} \times 100$	G_{ij}^n (MPa)	$\frac{G_{ij}^n - G_{ij}^*}{G_{ij}^*} \times 100$
1	1.000×10^{-1}	0.000	0.000×10^0	-	5.000×10^{-4}	0.000
2	1.000×10^{-1}	0.000	0.000×10^0	-	5.000×10^{-4}	0.000
4	1.000×10^{-1}	0.000	0.000×10^0	-	5.000×10^{-4}	0.000
8	1.000×10^{-1}	0.000	0.000×10^0	-	5.000×10^{-4}	0.000
16	1.000×10^{-1}	0.000	0.000×10^0	-	5.000×10^{-4}	0.000
32	1.000×10^{-1}	0.000	0.000×10^0	-	5.000×10^{-4}	0.000
64	1.000×10^{-1}	0.000	0.000×10^0	-	5.000×10^{-4}	0.000
128	1.000×10^{-1}	0.000	0.000×10^0	-	5.000×10^{-4}	0.000
256	1.000×10^{-1}	0.000	0.000×10^0	-	5.000×10^{-4}	0.000
512	1.000×10^{-1}	0.000	0.000×10^0	-	5.000×10^{-4}	0.000

Table 19 Apparent elastic properties of the body-centered square periodic cellular solids.

n_C	E_i^n (MPa)	$\frac{E_i^n - E_i^*}{E_i^*} \times 100$	v_{ij}^n	$\frac{v_{ij}^n - v_{ij}^*}{v_{ij}^*} \times 100$	G_{ij}^n (MPa)	$\frac{G_{ij}^n - G_{ij}^*}{G_{ij}^*} \times 100$
1	1.427×10^{-1}	-1.074	4.100×10^{-1}	-1.837	7.096×10^{-2}	-0.350
2	1.439×10^{-1}	-0.224	3.991×10^{-1}	-0.873	7.107×10^{-2}	-0.190
4	1.441×10^{-1}	-0.072	4.026×10^{-1}	-0.014	7.114×10^{-2}	-0.099
8	1.442×10^{-1}	-0.018	4.026×10^{-1}	-0.019	7.117×10^{-2}	-0.050
16	1.442×10^{-1}	-0.005	4.026×10^{-1}	-0.008	7.119×10^{-2}	-0.250
32	1.442×10^{-1}	-0.001	4.026×10^{-1}	-0.005	7.120×10^{-2}	-0.012
64	1.442×10^{-1}	0.000	4.026×10^{-1}	-0.004	7.121×10^{-2}	-0.006
128	1.442×10^{-1}	0.000	4.026×10^{-1}	-0.003	7.121×10^{-2}	-0.002
256	1.442×10^{-1}	0.000	4.026×10^{-1}	-0.003	7.121×10^{-2}	-0.001
512	1.442×10^{-1}	0.000	4.026×10^{-1}	0.000	7.121×10^{-2}	0.000

Table 20 Apparent elastic properties of the triangle periodic cellular solids.

n_C	E_i^n (MPa)	$\dfrac{E_i^n - E_i^*}{E_i^*} \times 100$	v_{ij}^n	$\dfrac{v_{ij}^n - v_{ij}^*}{v_{ij}^*} \times 100$	G_{ij}^n (MPa)	$\dfrac{G_{ij}^n - G_{ij}^*}{G_{ij}^*} \times 100$
1	1.074×10^{-1}	-7.603	3.070×10^{-1}	-6.663	4.373×10^{-2}	0.000
2	1.077×10^{-1}	-7.381	8.678×10^{-2}	-73.614	4.373×10^{-2}	0.000
4	1.115×10^{-1}	-4.045	4.356×10^{-1}	-32.448	4.373×10^{-2}	0.000
8	1.139×10^{-1}	-2.015	3.829×10^{-1}	-16.407	4.373×10^{-2}	0.000
16	1.151×10^{-1}	-1.003	3.559×10^{-1}	-8.205	4.373×10^{-2}	0.000
32	1.157×10^{-1}	-0.501	3.424×10^{-1}	-4.101	4.373×10^{-2}	0.000
64	1.160×10^{-1}	-0.251	3.356×10^{-1}	-2.050	4.373×10^{-2}	0.000
128	1.161×10^{-1}	-0.127	3.323×10^{-1}	-1.025	4.373×10^{-2}	0.000
256	1.162×10^{-1}	-0.065	3.306×10^{-1}	-0.512	4.373×10^{-2}	0.000
512	1.162×10^{-1}	-0.034	3.306×10^{-1}	-0.256	4.373×10^{-2}	0.000

Table 21 Apparent elastic properties of the hexagon periodic cellular solids.

n_C	E_i^n (MPa)	$\dfrac{E_i^n - E_i^*}{E_i^*} \times 100$	v_{ij}^n	$\dfrac{v_{ij}^n - v_{ij}^*}{v_{ij}^*} \times 100$	G_{ij}^n (MPa)	$\dfrac{G_{ij}^n - G_{ij}^*}{G_{ij}^*} \times 100$
1	1.036×10^{-3}	-53.811	1.734×10^{0}	-80.457	1.440×10^{-4}	-74.811
2	1.073×10^{-3}	-52.131	4.849×10^{-1}	-49.546	2.486×10^{-4}	-56.516
4	1.699×10^{-3}	-24.207	9.466×10^{-1}	-1.519	3.454×10^{-4}	-39.574
8	1.998×10^{-3}	-10.896	9.618×10^{-1}	-0.063	4.306×10^{-4}	-24.667
16	2.132×10^{-3}	-4.924	9.624×10^{-1}	-0.125	4.912×10^{-4}	-14.067
32	2.191×10^{-3}	-2.278	9.619×10^{-1}	-0.076	5.284×10^{-4}	-7.563
64	2.218×10^{-3}	-1.081	9.616×10^{-1}	-0.040	5.492×10^{-4}	-3.927
128	2.230×10^{-3}	-0.523	9.614×10^{-1}	-0.020	5.602×10^{-4}	-2.000
256	2.236×10^{-3}	-0.256	9.613×10^{-1}	-0.017	5.658×10^{-4}	-1.007
512	2.236×10^{-3}	-0.126	9.613×10^{-1}	-0.006	5.658×10^{-4}	-0.503

Table 22 Apparent elastic properties of the diamond periodic cellular solids.

n_C	E_i^n (MPa)	$\frac{E_i^n - E_i^*}{E_i^*} \times 100$	v_{ij}^n	$\frac{v_{ij}^n - v_{ij}^*}{v_{ij}^*} \times 100$	G_{ij}^n (MPa)	$\frac{G_{ij}^n - G_{ij}^*}{G_{ij}^*} \times 100$
1	1.980×10^{-3}	0.000	9.802×10^{-1}	0.000	5.000×10^{-2}	0.000
2	1.980×10^{-3}	0.000	9.802×10^{-1}	0.000	5.000×10^{-2}	0.000
4	1.980×10^{-3}	0.000	9.802×10^{-1}	0.000	5.000×10^{-2}	0.000
8	1.980×10^{-3}	0.000	9.802×10^{-1}	0.000	5.000×10^{-2}	0.000
16	1.980×10^{-3}	0.000	9.802×10^{-1}	0.000	5.000×10^{-2}	0.000
32	1.980×10^{-3}	0.000	9.802×10^{-1}	0.000	5.000×10^{-2}	0.000
64	1.980×10^{-3}	0.000	9.802×10^{-1}	0.000	5.000×10^{-2}	0.000
128	1.980×10^{-3}	0.000	9.802×10^{-1}	0.000	5.000×10^{-2}	0.000
256	1.980×10^{-3}	0.000	9.802×10^{-1}	0.000	5.000×10^{-2}	0.000
512	1.980×10^{-3}	0.000	9.802×10^{-1}	0.000	5.000×10^{-2}	0.000

Table 23 Apparent elastic properties of the elongated diamond periodic cellular solids.

n_C	E_i^n (MPa)	$\frac{E_i^n - E_i^*}{E_i^*} \times 100$	v_{ij}^n	$\frac{v_{ij}^n - v_{ij}^*}{v_{ij}^*} \times 100$	G_{ij}^n (MPa)	$\frac{G_{ij}^n - G_{ij}^*}{G_{ij}^*} \times 100$
1	7.672×10^{-4}	0.000	3.289×10^{-1}	0.000	4.330×10^{-2}	0.000
	6.726×10^{-3}	0.000	2.884×10^{0}	0.000		
2	7.672×10^{-4}	0.000	3.289×10^{-1}	0.000	4.330×10^{-2}	0.000
	6.726×10^{-3}	0.000	2.883×10^{0}	0.000		
4	7.672×10^{-4}	0.000	3.289×10^{-1}	0.000	4.330×10^{-2}	0.000
	6.726×10^{-3}	0.000	2.883×10^{0}	0.000		
8	7.672×10^{-4}	0.000	3.289×10^{-1}	0.000	4.330×10^{-2}	0.000
	6.726×10^{-3}	0.000	2.883×10^{0}	0.000		
16	7.672×10^{-4}	0.000	3.289×10^{-1}	0.000	4.330×10^{-2}	0.000
	6.726×10^{-3}	0.000	2.883×10^{0}	0.000		
32	7.672×10^{-4}	0.000	3.289×10^{-1}	0.000	4.330×10^{-2}	0.000
	6.726×10^{-3}	0.000	2.883×10^{0}	0.000		
64	7.672×10^{-4}	0.000	3.289×10^{-1}	0.000	4.330×10^{-2}	0.000
	6.726×10^{-3}	0.000	2.883×10^{0}	0.000		
128	7.672×10^{-4}	0.000	3.289×10^{-1}	0.000	4.330×10^{-2}	0.000
	6.726×10^{-3}	0.000	2.883×10^{0}	0.000		
256	7.672×10^{-4}	0.000	3.289×10^{-1}	0.000	4.330×10^{-2}	0.000
	6.726×10^{-3}	0.000	2.883×10^{0}	0.000		
512	7.672×10^{-4}	0.000	3.289×10^{-1}	0.000	4.330×10^{-2}	0.000
	6.726×10^{-3}	0.000	2.883×10^{0}	0.000		
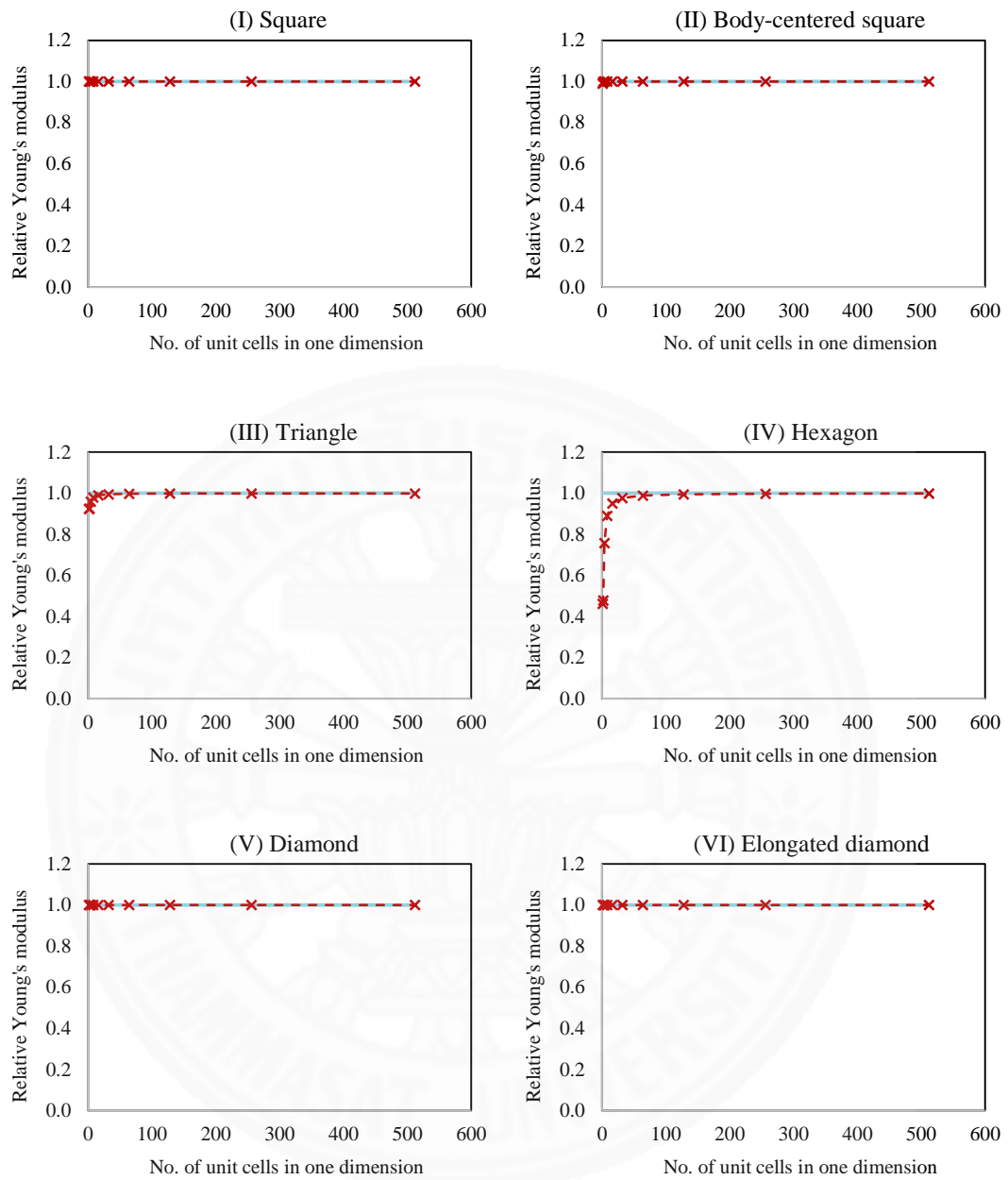
Fig. 15 Convergences of the relative Young's moduli of the 2D periodic cellular solids.
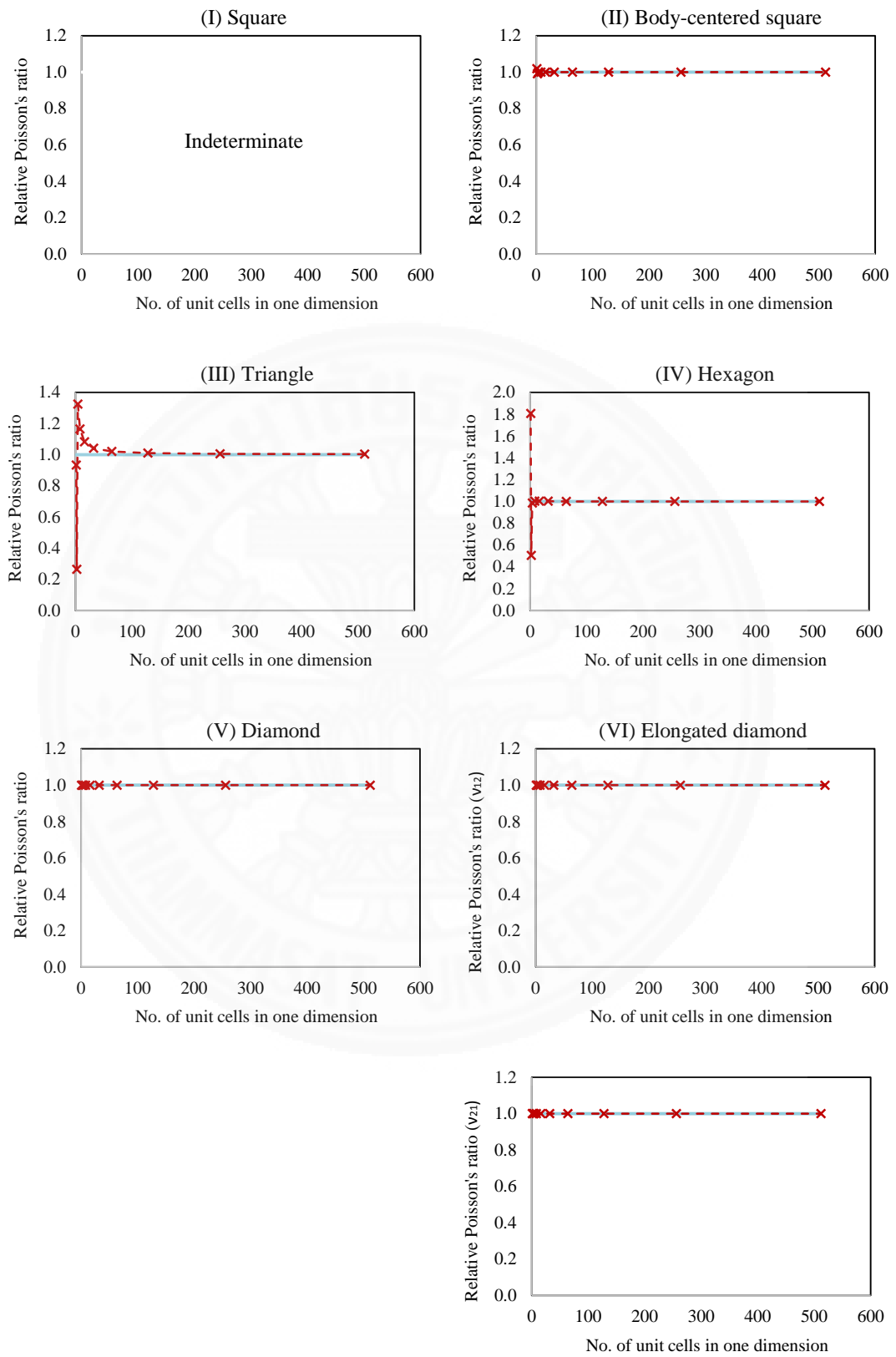
Fig. 16 Convergences of the relative Poisson's ratios of the 2D periodic cellular solids.
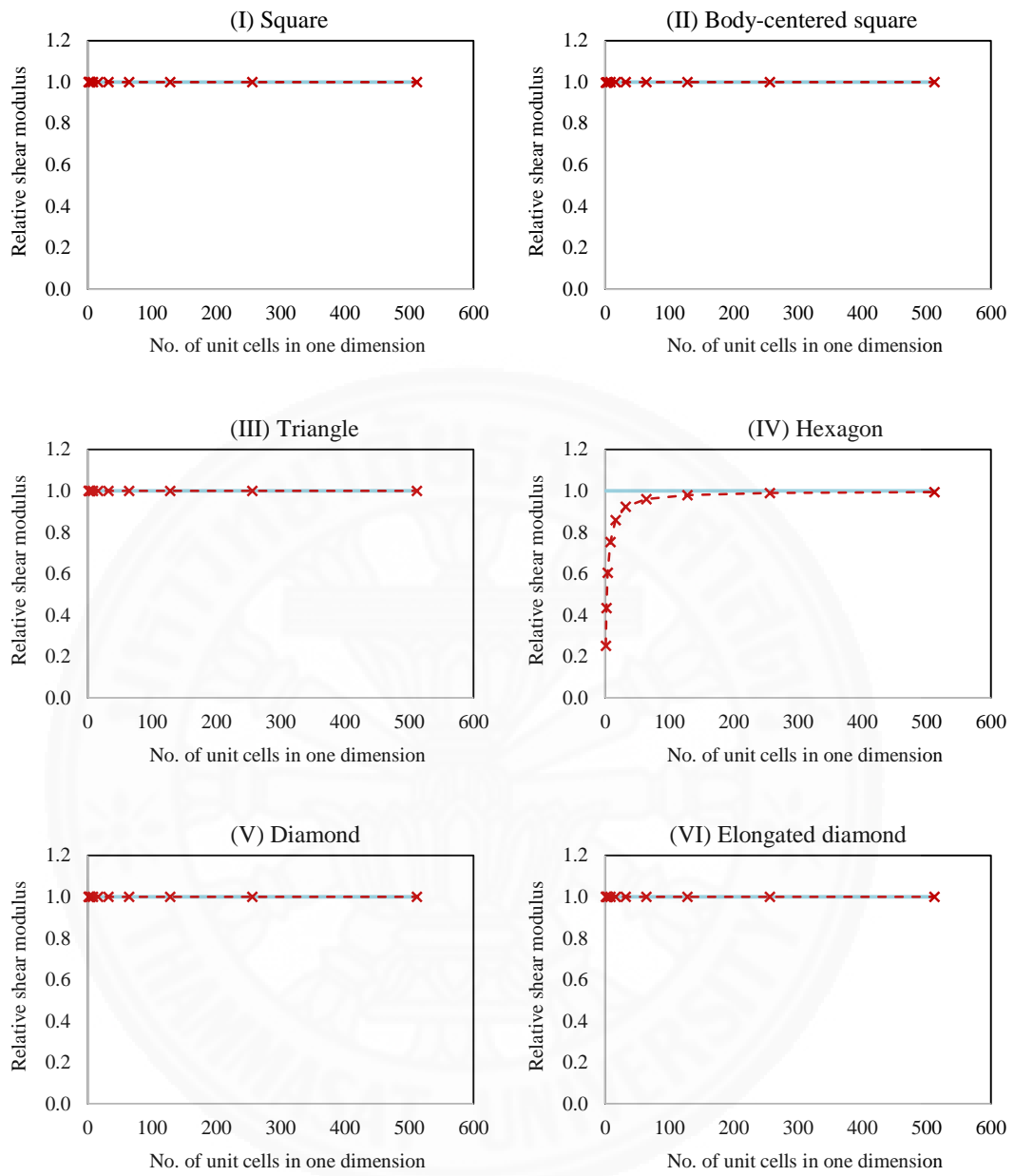
Fig. 17 Convergences of the relative shear moduli of the 2D periodic cellular solids.

Table 24 Apparent elastic properties of the cubic periodic cellular solids.

n_C	E_i^n (MPa)	$\frac{E_i^n - E_i^*}{E_i^*} \times 100$	v_{ij}^n	$\frac{v_{ij}^n - v_{ij}^*}{v_{ij}^*} \times 100$	G_{ij}^n (MPa)	$\frac{G_{ij}^n - G_{ij}^*}{G_{ij}^*} \times 100$
1	7.854×10^{-3}	0.000	0.000×10^0	-	2.945×10^{-5}	0.000
2	7.854×10^{-3}	0.000	0.000×10^0	-	2.945×10^{-5}	0.000
4	7.854×10^{-3}	0.000	0.000×10^0	-	2.945×10^{-5}	0.000
8	7.854×10^{-3}	0.000	0.000×10^0	-	2.945×10^{-5}	0.000
16	7.854×10^{-3}	0.000	0.000×10^0	-	2.945×10^{-5}	0.000
32	7.854×10^{-3}	0.000	0.000×10^0	-	2.945×10^{-5}	0.000
64	7.854×10^{-3}	0.000	0.000×10^0	-	2.945×10^{-5}	0.000

Table 25 Apparent elastic properties of the body-centered cubic periodic cellular solids.

n_C	E_i^n (MPa)	$\frac{E_i^n - E_i^*}{E_i^*} \times 100$	v_{ij}^n	$\frac{v_{ij}^n - v_{ij}^*}{v_{ij}^*} \times 100$	G_{ij}^n (MPa)	$\frac{G_{ij}^n - G_{ij}^*}{G_{ij}^*} \times 100$
1	1.031×10^{-2}	-1.206	3.016×10^{-1}	0.817	3.480×10^{-3}	-43.008
2	1.041×10^{-3}	-0.309	2.957×10^{-1}	-1.152	5.515×10^{-3}	-9.670
4	1.043×10^{-3}	-0.082	2.991×10^{-1}	-0.014	6.015×10^{-3}	-1.480
8	1.044×10^{-2}	-0.020	2.992×10^{-1}	0.014	6.094×10^{-3}	-0.199
16	1.044×10^{-2}	-0.004	2.992×10^{-1}	0.008	6.104×10^{-3}	-0.026
32	1.044×10^{-2}	0.000	2.992×10^{-1}	0.007	6.106×10^{-3}	0.000
64	1.044×10^{-2}	0.000	2.992×10^{-1}	0.000	6.106×10^{-3}	0.000

Table 26 Apparent elastic properties of the cuboctahedron periodic cellular solids.

n_C	E_i^n (MPa)	$\frac{E_i^n - E_i^*}{E_i^*} \times 100$	v_{ij}^n	$\frac{v_{ij}^n - v_{ij}^*}{v_{ij}^*} \times 100$	G_{ij}^n (MPa)	$\frac{G_{ij}^n - G_{ij}^*}{G_{ij}^*} \times 100$
1	2.053×10^{-4}	-94.562	9.779×10^{-1}	196.343	2.790×10^{-3}	0.000
2	1.754×10^{-3}	-53.545	6.976×10^{-1}	-55.632	2.790×10^{-3}	0.000
4	2.650×10^{-3}	-29.819	5.019×10^{-1}	-47.176	2.790×10^{-3}	0.000
8	3.193×10^{-3}	-1.539	4.130×10^{-1}	-23.857	2.790×10^{-3}	0.000
16	3.482×10^{-3}	-7.782	3.712×10^{-1}	-11.866	2.790×10^{-3}	0.000
32	3.629×10^{-3}	-3.889	3.504×10^{-1}	-5.904	2.790×10^{-3}	0.000
64	3.703×10^{-3}	-1.939	3.399×10^{-1}	-2.939	2.790×10^{-3}	0.000

Table 27 Apparent elastic properties of the tetrakaidecahedron periodic cellular solids

n_C	E_i^n (MPa)	$\frac{E_i^n - E_i^*}{E_i^*} \times 100$	v_{ij}^n	$\frac{v_{ij}^n - v_{ij}^*}{v_{ij}^*} \times 100$	G_{ij}^n (MPa)	$\frac{G_{ij}^n - G_{ij}^*}{G_{ij}^*} \times 100$
1	2.824×10^{-5}	-31.694	2.104×10^{-1}	-57.281	1.176×10^{-5}	-9.246
2	2.979×10^{-5}	-27.938	1.687×10^{-1}	-65.749	1.108×10^{-5}	-14.482
4	3.506×10^{-5}	-15.198	3.201×10^{-1}	-35.022	1.198×10^{-5}	-7.497
8	3.813×10^{-5}	-7.756	4.065×10^{-1}	-17.470	1.246×10^{-5}	-3.816
16	3.974×10^{-5}	-3.867	4.500×10^{-1}	-8.640	1.271×10^{-5}	-1.925
32	4.055×10^{-5}	-1.916	4.714×10^{-1}	-4.292	1.283×10^{-5}	-0.967

Table 28 Apparent elastic properties of the octahedron periodic cellular solids

n_C	E_i^n (MPa)	$\frac{E_i^n - E_i^*}{E_i^*} \times 100$	v_{ij}^n	$\frac{v_{ij}^n - v_{ij}^*}{v_{ij}^*} \times 100$	G_{ij}^n (MPa)	$\frac{G_{ij}^n - G_{ij}^*}{G_{ij}^*} \times 100$
1	3.776×10^{-3}	0.000	3.301×10^{-1}	0.030	2.790×10^{-3}	0.000
2	3.776×10^{-3}	0.000	3.300×10^{-1}	0.000	2.790×10^{-3}	0.000
4	3.776×10^{-3}	0.000	3.300×10^{-1}	0.000	2.790×10^{-3}	0.000
8	3.776×10^{-3}	0.000	3.300×10^{-1}	0.000	2.790×10^{-3}	0.000
16	3.776×10^{-3}	0.000	3.300×10^{-1}	0.000	2.790×10^{-3}	0.000
32	3.776×10^{-3}	0.000	3.300×10^{-1}	0.000	2.790×10^{-3}	0.000
64	3.776×10^{-3}	0.000	3.300×10^{-1}	0.000	2.790×10^{-3}	0.000

Table 29 Apparent elastic properties of the tetragonal bipyramid periodic cellular solids

n_C	E_i^n (MPa)	$\frac{E_i^n - E_i^*}{E_i^*} \times 100$	v_{ij}^n	$\frac{v_{ij}^n - v_{ij}^*}{v_{ij}^*} \times 100$	G_{ij}^n (MPa)	$\frac{G_{ij}^n - G_{ij}^*}{G_{ij}^*} \times 100$
1	1.468×10^{-3} 4.851×10^{-2}	0.000 0.000	8.259×10^{-1} 1.233×10^{-2} 4.074×10^{-1}	0.000 0.000 0.000	4.213×10^{-3} 3.745×10^{-3}	0.000 0.000
2	1.468×10^{-3} 4.851×10^{-2}	0.000 0.000	8.259×10^{-1} 1.233×10^{-2} 4.074×10^{-1}	0.000 0.000 0.000	4.213×10^{-3} 3.745×10^{-3}	0.000 0.000
4	1.468×10^{-3} 4.851×10^{-2}	0.000 0.000	8.259×10^{-1} 1.233×10^{-2} 4.074×10^{-1}	0.000 0.000 0.000	4.213×10^{-3} 3.745×10^{-3}	0.000 0.000
8	1.468×10^{-3} 4.851×10^{-2}	0.000 0.000	8.259×10^{-1} 1.233×10^{-2} 4.074×10^{-1}	0.000 0.000 0.000	4.213×10^{-3} 3.745×10^{-3}	0.000 0.000
16	1.468×10^{-3} 4.851×10^{-2}	0.000 0.000	8.259×10^{-1} 1.233×10^{-2} 4.074×10^{-1}	0.000 0.000 0.000	4.213×10^{-3} 3.745×10^{-3}	0.000 0.000
32	1.468×10^{-3} 4.851×10^{-2}	0.000 0.000	8.259×10^{-1} 1.233×10^{-2} 4.074×10^{-1}	0.000 0.000 0.000	4.213×10^{-3} 3.745×10^{-3}	0.000 0.000
64	1.468×10^{-3} 4.851×10^{-2}	0.000 0.000	8.259×10^{-1} 1.233×10^{-2} 4.074×10^{-1}	0.000 0.000 0.000	4.213×10^{-3} 3.745×10^{-3}	0.000 0.000

Fig. 18 Convergences of the relative Young's moduli of the 3D periodic cellular solids.
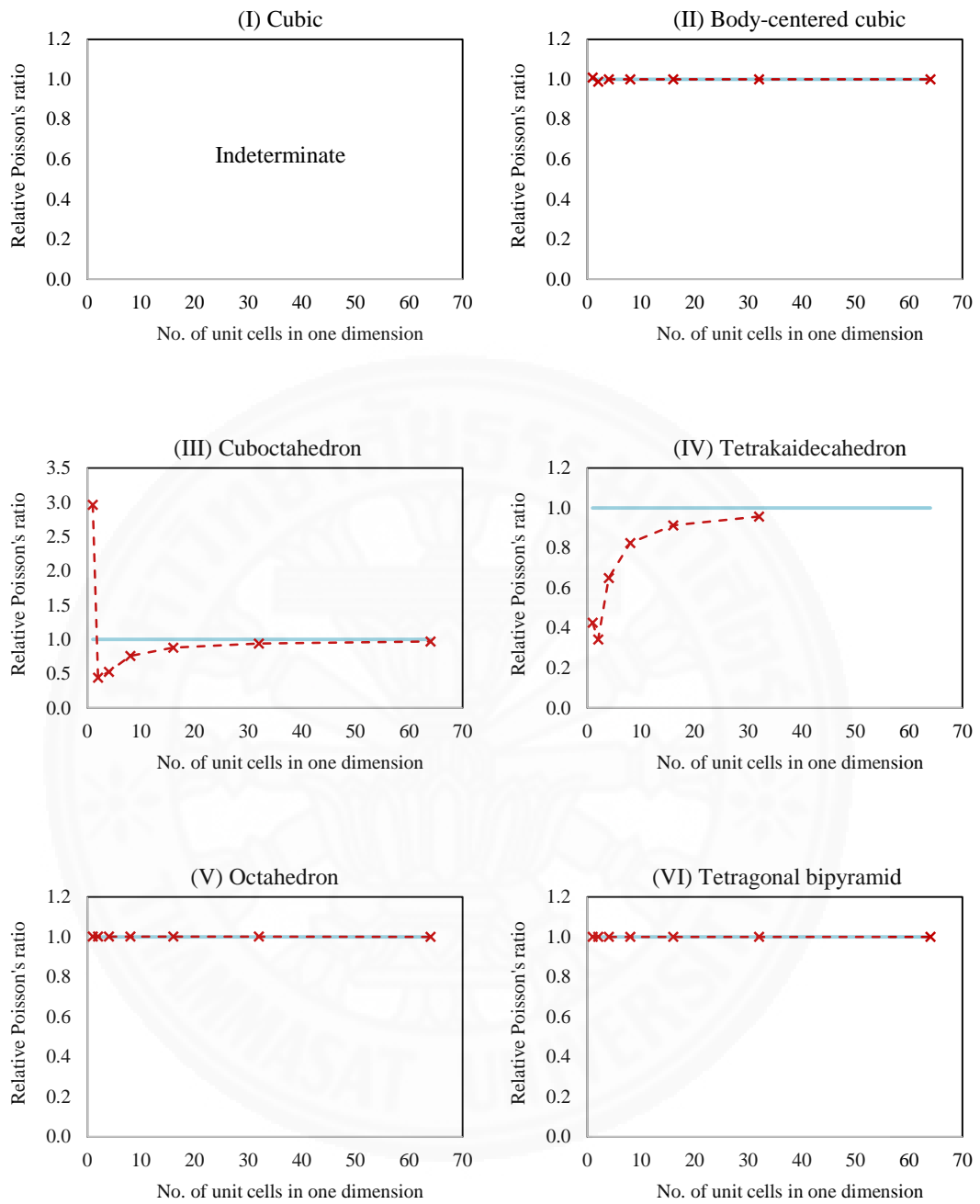
Fig. 19 Convergences of the relative Poisson's ratios of the 3D periodic cellular solids.
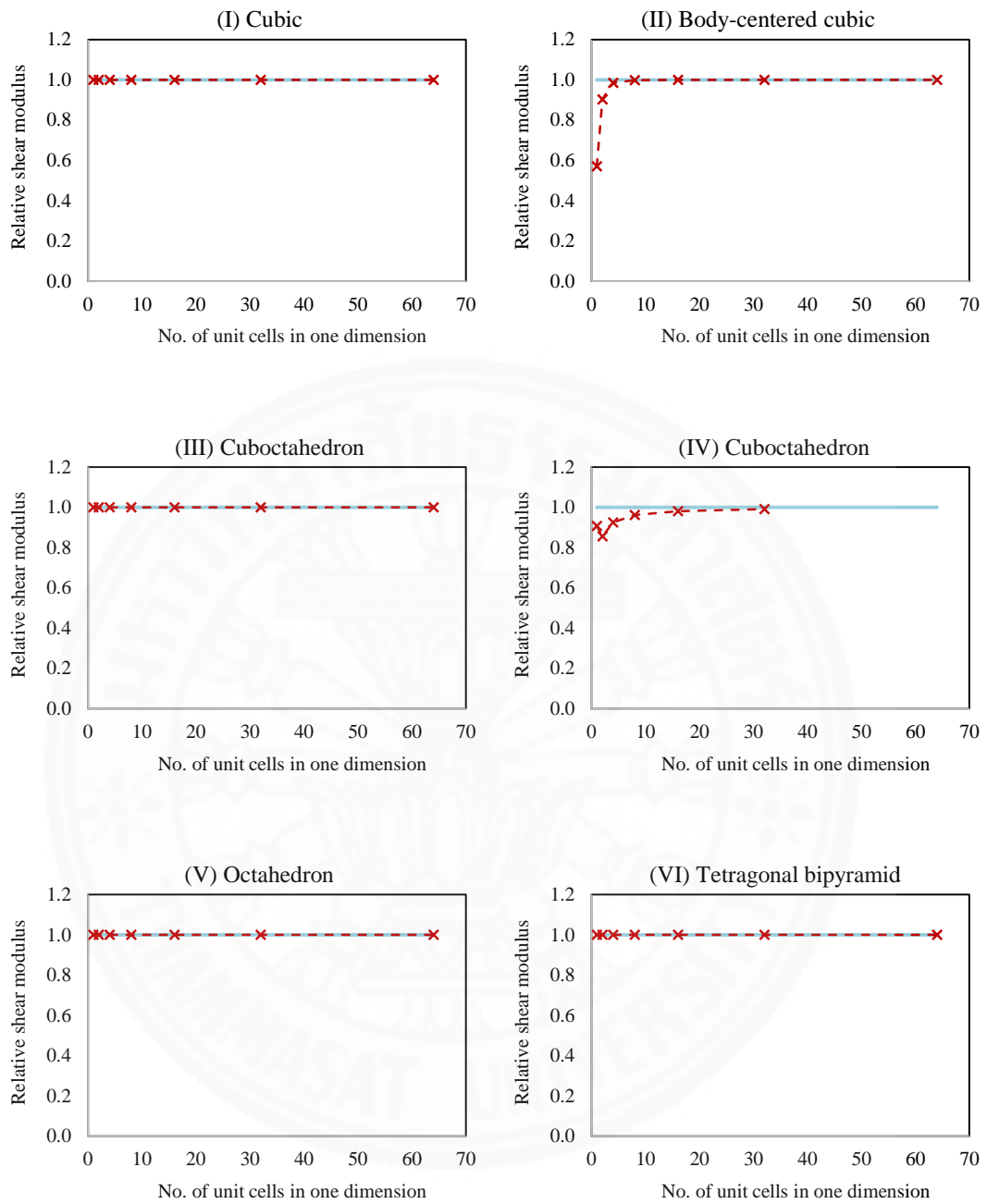
Fig. 20   Convergences of the relative shear moduli of the 3D periodic cellular solids.

Chapter 7
Design for Isotropic Symmetry by Member Sizing

The geometry of unit cells is usually selected in such a way that their equivalent homogeneous materials are orthotropic materials. It is not difficult to arrange unit-cell struts so that the effective elastic properties in all orthotropic directions are the same. A 2D orthotropic material having the same properties in its two orthotropic directions is said to have square symmetry. A 3D orthotropic material having the same properties in its three orthotropic directions is said to have cubic symmetry. Few standard frame-like unit-cell topologies give periodic solids that have isotropic symmetry. Examples include triangular, hexagonal, and kagome unit cells. Isotropic symmetry of periodic solids having these three unit-cell topologies is considered in the works by Srikantha Phani, Woodhouse, and Fleck (2006), Fleck and Qiu (2007), and Srikantha Phani and Fleck (2008). In the work by Srikantha Phani, Woodhouse, and Fleck (2006), wave propagation in these isotropic periodic solids is investigated. The fracture toughness of elastic-brittle periodic solids having these three unit-cell topologies is studied by Fleck and Qiu (2007). In addition, boundary layer phenomena in these isotropic periodic solids are investigated by Srikantha Phani and Fleck (2008). Elastic boundary layers are regions of localized elastic deformations near free edges of periodic solids.

Arranging unit-cell struts to obtain isotropic symmetry intuitively is not easy. It is however possible to create algorithms to find unit-cell topologies that give isotropic symmetry. Quite often, isotropic symmetry is considered as a constraint in topology optimization of unit cells. In the work by Neves, Rodrigues, and Guedes (2000), mathematical programming techniques are used to obtain optimal designs of 2D periodic solids under design constraints on material volume fractions and material symmetry. In their study, 2D periodic solids are treated as 2D continuums. Orthotropic, square, and isotropic types of symmetry are considered as design constraints. In the work by Challis, Roberts, and Wilkins (2008), the level-set method of topology optimization is used to design 3D isotropic two-phase periodic multifunctional composites, and isotropic symmetry is considered as a design constraint. Isotropic symmetry is also considered as a constraint in topology optimization of 2D periodic trusses by Guth, Luersen, and Muñoz-Rojas (2012) and of 3D periodic trusses by Guth, Luersen, and Muñoz-Rojas (2015).

There are also some research works that are concerned with design of periodic solids that are not frame-like for extreme elastic properties (Grima et al., 2012; Shufrin, Pasternak, & Dyskin, 2012; Shan et al., 2015). For example, in the work by Shan et al. (2015), the design of

2D isotropic auxetic periodic solids is considered. The main objective of their work is to demonstrate that 2D auxetic materials with isotropic symmetry can be realized by perforating sheets in periodic cut patterns with either six-fold or three-fold rotational symmetry. Two-dimensional unit-cell designs that yield 2D auxetic structures with isotropic symmetry are also proposed by Shufrin, Pasternak, and Dyskin (2012). In their work, each unit-cell design consists of a flexible arch frame with a sufficiently rigid hexagonal core at the center. In the work by Grima et al. (2012), sheets that are isotropic and auxetic are obtained by connecting rigid triangles in proper arrangements.

For some unit-cell topologies, it is possible to obtain isotropic symmetry by appropriate selection of relative sizes of struts within the unit cells. Generally, these unit cells must have struts that are aligned with the unit cells' orthogonal axes as well as struts that are oblique to the orthogonal axes. Different sizes for struts that are aligned with the orthogonal axes and for struts that are oblique to these axes can be used to adjust the degrees of isotropic symmetry of resulting periodic solids.

This chapter presents a simple strategy to allow some common frame-like unit cells that do not in general yield periodic solids with isotropic symmetry to be used to create periodic solids with isotropic symmetry. The proposed methodology is based on appropriate sizing of unit-cell struts. Frame-like periodic solids are modelled as frames, whose struts are modelled as Euler beams. In the proposed methodology, the unit cell under consideration is set to have two different variable strut sizes. The closed-form effective elastic constants of a periodic solid having the considered unit-cell topology are then derived. By using the closed-form effective elastic constants, an equation to enforce isotropic symmetry can be analytically constructed. This equation is thereafter used to determine the relationship between the two variable strut sizes in the unit cell that results in isotropic symmetry. The closed-form effective elastic constants of periodic solids are derived by the homogenization method based on equivalent strain energy. In the homogenization method based on equivalent strain energy, the effective elastic constants of a periodic solid are derived from strain energy of a unit cell of the solid under various strain modes. These strain modes are contrived by periodic kinematic boundary conditions. In this study, a symbolic FE program written in MATLAB (Sam, 2015) is used to analytically compute strain energy under these strain modes. The employed symbolic FE program is a generic symbolic object-oriented FE program that is capable of performing symbolic FE analysis and generating symbolic results. The obtained analytical expressions of the strain energy are subsequently used to symbolically compute the effective elastic constants. Finally, the proposed methodology is tested with some 2D and 3D frame-like periodic solids with standard unit-cell topologies.

7.1 Isotropic symmetry of elastic solids

As aforementioned, a 3D orthotropic material having the same properties in its three orthotropic directions is said to have cubic symmetry. For a 3D orthotropic periodic solid having cubic symmetry, the effective material constitutive tensor is expressed in matrix form as

$$\boldsymbol{c}^* = \begin{bmatrix} c_{11}^* & c_{12}^* & c_{12}^* & 0 & 0 & 0 \\ & c_{11}^* & c_{12}^* & 0 & 0 & 0 \\ & & c_{11}^* & 0 & 0 & 0 \\ & & & c_{44}^* & 0 & 0 \\ & Sym & & & c_{44}^* & 0 \\ & & & & & c_{44}^* \end{bmatrix}. \tag{70}$$

Note that c_{11}^*, c_{12}^*, and c_{44}^* are three independent material constants. For the material to be isotropic, the ratio $\hat{A}$ shown below must be equal to 1 (Bower, 2010), i.e.

$$\hat{A} = \frac{2c_{44}^*}{c_{11}^* - c_{12}^*} = 1. \tag{71}$$

Eqs. (70) and (71) imply that isotropic elastic materials have only two independent material constants.

For an orthotropic periodic solid under the plane stress condition, the effective material constitutive tensor is expressed in matrix form as

$$\boldsymbol{c}^* = \begin{bmatrix} c_{11}^* & c_{12}^* & 0 \\ & c_{22}^* & 0 \\ Sym & & c_{33}^* \end{bmatrix}. \tag{72}$$

For the above 2D material to be isotropic, the ratio $\hat{A}$ shown below must be equal to 1 (Bower, 2010), i.e.

$$\hat{A} = \frac{2c_{33}^*}{c_{11}^* - c_{12}^*} = 1. \tag{73}$$

Eqs. (71) and (73) are used to enforce isotropic symmetry in this study.

7.2 Design for isotropic symmetry by member sizing

Eqs. (71) and (73) are the conditions for periodic elastic solids to be isotropic. Each equation can be used as a design criterion to obtain isotropic symmetry. In this study, the equations are used to determine relative strut sizes that are required for isotropic symmetry. The proposed design methodology for isotropic symmetry is described below.

7.2.1 Two-dimensional frame-like periodic solids

The proposed methodology to design for isotropic symmetry is introduced using a diamond-square unit cell as an example. Consider a diamond-square unit cell of thickness T shown in Fig. 21. The unit cell contains horizontal, vertical, and diagonal struts, and all struts have rectangular cross sections. Obviously, square symmetry can be easily obtained by using one cross section for all horizontal and vertical struts, and one cross section for all diagonal struts. If all struts have the same cross section, periodic solids having this unit-cell topology will be orthotropic solids with only square symmetry. However, if two different cross sections are used, one for the horizontal and vertical struts and the other for the diagonal struts, it is possible to obtain isotropic symmetry. Using two different cross sections allows the relative stiffness between the horizontal and vertical directions and the diagonal directions to be so adjusted that isotropic symmetry is obtained. Let E denote Young's modulus of the base material. Let L denote the characteristic length of the unit cell as defined in Fig. 21. Let $L_m = \psi_m L$ denote the length of the shortest strut among the horizontal and vertical struts, and let $L_n = \psi_n L$ denote the length of the shortest strut among the diagonal struts. Here, ψ_m and ψ_n are two constants. In addition, let A_m and I_m denote the sectional area and moment of inertia of the horizontal and vertical struts while A_n and I_n denote those of the diagonal struts. The coefficients c_{ij}^* in Eq. (72) can be written as functions of E, L, T, A_m, I_m, A_n, and I_n, i.e.

$$c_{ij}^* = c_{ij}^*(E, L, T, A_m, I_m, A_n, I_n). \tag{74}$$

Let W_m denote the width of the horizontal and vertical struts while W_n denote the width of the diagonal struts. In addition, let $m = W_m/L_m = W_m/(\psi_m L)$ and $n = W_n/L_n = W_n/(\psi_n L)$. By keeping the other parameters constant, the coefficients c_{ij}^* in Eq. (73) become functions of m and n, i.e.

$$c_{ij}^* = c_{ij}^*(m, n). \tag{75}$$

Consequently, the condition of isotropic symmetry in Eq. (73) becomes

$$\frac{2c_{33}^*(m, n)}{c_{11}^*(m, n) - c_{12}^*(m, n)} = 1 \tag{76}$$

It can be seen that, if the value of m is prescribed, then the value of n can be computed from Eq. (76), and vice versa. It is important to note that the values of m and n must not be too large that the resulting struts cannot be represented by Euler beams.
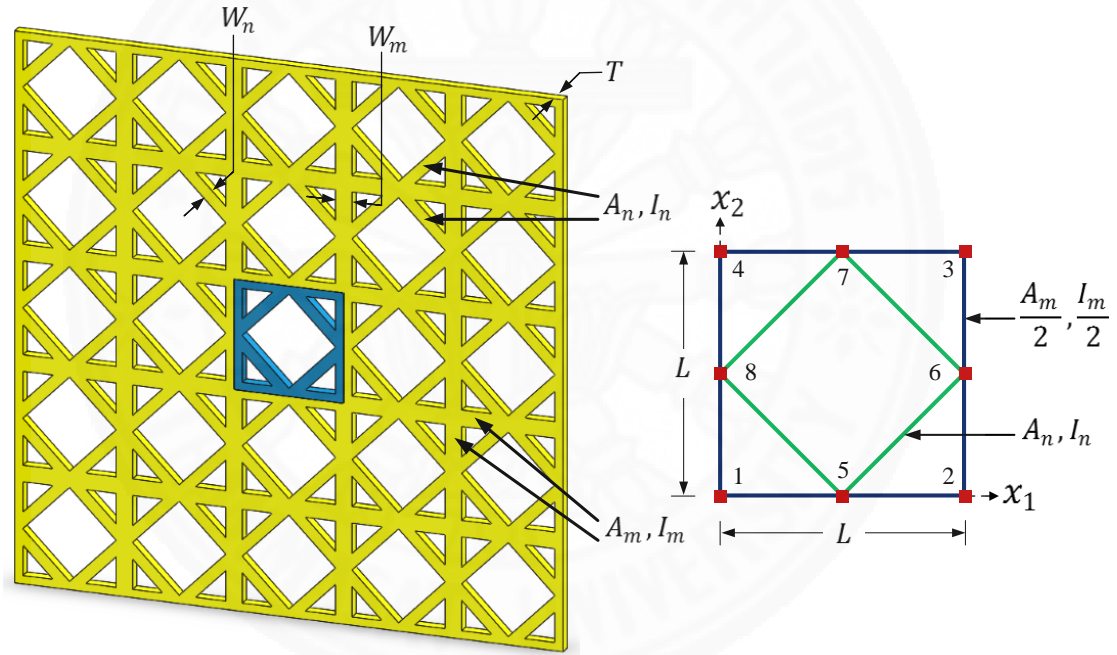
Fig. 21 Diamond-square cellular solid and its beam element unit cell.

7.2.2 Three-dimensional frame-like periodic solids

For 3D frame-like periodic solids, as an example, consider a body-centered cubic unit cell shown in Fig. 22(c). Similar to the diamond-square unit cell, the body-centered cubic unit cell contains horizontal, vertical, and diagonal struts. All struts are set to have circular cross sections. For this unit cell, cubic symmetry can be obtained by using one cross section for all horizontal and vertical struts, and the other cross section for all diagonal struts. If all struts have the same cross section, periodic solids having this unit-cell topology are orthotropic solids with

76

cubic symmetry. Similar to the methodology for 2D periodic solids, in order to obtain isotropic symmetry, two different cross sections are used, one for the horizontal and vertical struts, and one for the diagonal struts Again, let A_m and I_m denote the sectional area and moment of inertia of the horizontal and vertical struts while A_n and I_n denote those of the diagonal struts. The coefficients c_{ij}^* in Eq. (70) can be written as functions of $E, L, T, A_m, I_m, A_n,$ and I_n. Let D_m denote the diameter of horizontal and vertical struts while D_n denote the diameter of diagonal struts. In addition, let $L_m = \psi_m L$ denote the length of the shortest strut among the horizontal and vertical struts, and let $L_n = \psi_n L$ denote the length of the shortest strut among the diagonal struts. Moreover, let $m = D_m/L_m = D_m/(\psi_m L)$ and $n = D_n/L_n = D_n/(\psi_n L)$. By keeping the other parameters constant, the coefficients c_{ij}^* in Eq. (70) become functions of m and n, which can be shown also by Eq. (75). Consequently, the condition of isotropic symmetry in Eq. (71) becomes

$$\frac{2c_{44}^*(m,n)}{c_{11}^*(m,n) - c_{12}^*(m,n)} = 1 \tag{77}$$

Similar to Eq. (76), Eq. (77) allows the value of n to be computed when the value of m is prescribed and vice versa.

(a) Body-centered square   (b) Diamond square

(c) Body-centered cubic   (d) Face-centered cubic
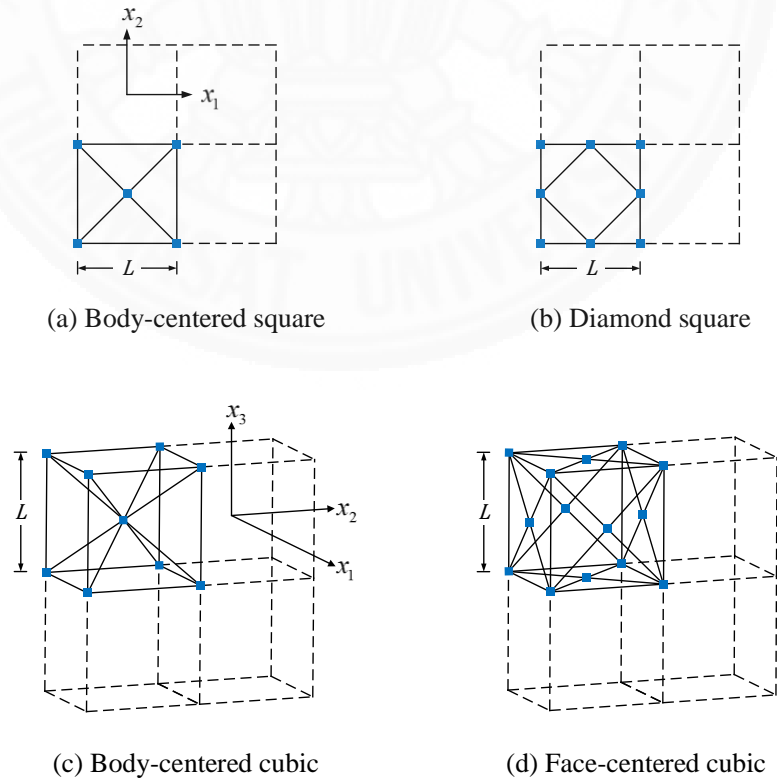
Fig. 22 Considered unit cells.

7.3 Results

To show the validity of the proposed methodology, it is used to design 2D and 3D periodic solids having unit-cell topologies shown in Fig. 22 for isotropic symmetry. The 2D unit cells are set to have rectangular struts with thickness of T while the 3D unit cells are set to have circular struts. In all examples, two different cross sections are used for the unit cell, one for the horizontal and vertical struts, and one for the diagonal struts. In the following derivation, A_m and I_m denote the sectional area and moment of inertia of the horizontal and vertical struts while A_n and I_n denote those of the diagonal struts. As aforementioned, a symbolic FE program is used to determine the analytical expressions of strain energy of the unit cells in Fig. 22 under the strain modes in Eqs. (21) and (25). After that, these analytical expressions of strain energy are used to derive the coefficients c_{ij}^*. The details of each example are shown below.

7.3.1 Body-centered square

The first example is the body-centered square unit cell in Fig. 22. The coefficients c_{ij}^* are obtained from symbolic analysis as

$$c_{11}^* = c_{22}^* = \frac{E}{2L^3 T}\left(2L^2 A_m + \sqrt{2}L^2 A_n + 24\sqrt{2}I_n\right), \tag{78}$$

$$c_{12}^* = \frac{\sqrt{2}E}{2L^3 T}\left(L^2 A_n - 24I_n\right), \tag{79}$$

$$c_{33}^* = \frac{E}{2L^3 T}\left(\sqrt{2}L^2 A_n + 12I_m\right), \tag{80}$$

which, for isotropic symmetry, yield

$$\hat{A} = \frac{\sqrt{2}L^2 A_n + 12I_m}{L^2 A_m + 24\sqrt{2}I_n} = 1. \tag{81}$$

Again, let W_m denote the width of the horizontal and vertical struts, and W_n denote the width of the inclined struts. Also, let $m = W_m/L_m$ and $n = W_n/L_n$. For this unit cell, ψ_m and ψ_n are equal to 1 and $\sqrt{2}/2$, respectively. Substituting $A_m = W_m T = mL_m T = m\psi_m LT$, $A_n = W_n T = nL_n T = n\psi_n LT$, $I_m = W_m^3 T/12 = m^3 L_m^3 T/12 = m^3 \psi_m^3 L^3 T/12$, and $I_n = W_n^3 T/12 = n^3 L_n^3 T/12 = n^3 \psi_n^3 L^3 T/12$ in Eq. (81) yields

$$\hat{A} = \frac{m^3 + n}{n^3 + m} = 1. \tag{82}$$

The above equation is the condition for isotropic symmetry of this unit-cell topology written in terms of m and n. One of the two parameters can be set and the other one can be obtained from the equation. Here, m is set to 0.05, 0.10, 0.15, 0.20, and 0.25, and Eq. (82) is solved for n. The solutions of Eq. (82) include real and complex numbers. The positive real results are shown in Table 30. It can be seen from the table that, for every m, there are two positive real solutions of n. Among the two real solutions of n, the smaller one increases with m while the larger one decreases. It is found that, for each m, the smaller n is the same as m, and the larger n represents a size that is too large for struts. Table 3 also shows the values of the normalized strut widths W_m/L and W_n/L. Note again that, for each m, the larger W_n/L cannot be used. It can be seen that, for isotropic symmetry, the section for the inclined struts is smaller than that for the horizontal and vertical struts.

7.3.2 Diamond square

The second example is the diamond-square unit cell shown in Fig. 22(b). The coefficients c_{ij}^* are found from symbolic analysis to be

$$c_{11}^* = c_{22}^* = \frac{E}{2L^3T}\left(2L^2 A_m + \sqrt{2}L^2 A_n + 24\sqrt{2}I_n\right), \tag{83}$$

$$c_{12}^* = \frac{\sqrt{2}E}{2L^3T}\left(L^2 A_n - 24I_n\right), \tag{84}$$

$$c_{33}^* = \frac{E}{2L^3T}\left(\frac{12I_m{}^2 + \sqrt{2}L^2 A_n I_m + 24\sqrt{2}I_m I_n + L^2 A_n I_n}{2I_m + \sqrt{2}I_n}\right), \tag{85}$$

which give

$$\hat{A} = \frac{24I_m{}^2 + 2\sqrt{2}L^2 A_n I_m + 48\sqrt{2}I_m I_n + 2L^2 A_n I_n}{\left(48\,I_n{}^2 + \sqrt{2}L^2 A_m I_n + 48\sqrt{2}I_m I_n + 2A_m I_n L^2\right)} = 1. \tag{86}$$

For this unit cell, ψ_m and ψ_n are equal to $1/2$ and $\sqrt{2}/2$, respectively. Similar to the previous problem, writing A_m, A_n, I_m, and I_n in Eq. (86) in terms of m, n, L, and T gives

$$\hat{A} = \frac{m^6 + 8n^3 m^3 + 8nm^3 + 16n^4}{4(2n^3 + m)(m^3 + 2n^3)} = 1. \tag{87}$$

Again, m is set to 0.05, 0.10, 0.15, 0.20, and 0.25, and Eq. (87) is solved for n. The solutions of Eq. (87) also include real and complex numbers. Only positive real results are shown in Table 30. Similar to the body-centered square unit cell, for each m, there are two positive real solutions of n and only the smaller n can be used. Among the two real solutions of n, the smaller one increases with m while the larger one decreases. It can be seen from the values of W_m/L and W_n/L in Table 30 that, for isotropic symmetry, the section for the inclined struts is smaller than that for the horizontal and vertical struts. Similar to the body-centered square unit cell, when m is larger, the two real solutions of n move closer to each other.

7.3.3 Body-centered cubic

The third example in the body-centered cubic unit cell shown in Fig. 22(c). The coefficients c_{ij}^* are found to be

$$c_{11}^* = c_{22}^* = c_{33}^* = \frac{E}{9L^4}\left(9L^2A_m + 4\sqrt{3}L^2A_n + 128\sqrt{3}I_n\right), \tag{88}$$

$$c_{12}^* = c_{13}^* = c_{23}^* = \frac{4\sqrt{3}E}{9L^4}\left(L^2A_n - 16I_n\right), \tag{89}$$

$$c_{44}^* = c_{55}^* = c_{66}^* = \frac{2E}{9L^4}\left(2\sqrt{3}L^2A_n + 27I_m + 16\sqrt{3}I_n\right), \tag{90}$$

which yield

$$\hat{A} = \frac{8\sqrt{3}L^2A_n + 108I_m + 64\sqrt{3}I_n}{9L^2A_m + 192\sqrt{3}I_n} = 1. \tag{91}$$

Again, let D_m denote the diameter of the horizontal and vertical struts, and D_n denote the diameter of the inclined struts. Also, let $m = D_m/L_m$ and $n = D_n/L_n$. For this unit cell, ψ_m and ψ_n are equal to 1 and $\sqrt{3}/2$, respectively. Substituting $A_m = D_m^2\pi/4 = m^2L_m^2\pi/4 = m^2\psi_m^2L^2\pi/4$, $A_n = D_n^2\pi/4 = n^2L_n^2\pi/4 = n^2\psi_n^2L^2\pi/4$, $I_m = D_m^4\pi/64 = m^4L_m^4\pi/64 = m^4\psi_m^4L^4\pi/64$, and $I_n = D_n^4\pi/64 = n^4L_n^4\pi/64 = n^4\psi_n^4L^4\pi/64$ in Eq. (91) yields

$$\hat{A} = \frac{9m^4 + 3\sqrt{3}n^4 + 8\sqrt{3}n^2}{3\left(4m^2 + 3\sqrt{3}n^4\right)} = 1. \tag{92}$$

For this problems, m is also set to 0.05, 0.10, 0.15, 0.20, and 0.25, and Eq. (92) is solved for n. The obtained positive real results in Table 30 show that, for each m, only the smaller n is useful. Among the two real solutions of n, the smaller one increases noticeably

with m while the larger one decreases insignificantly. From the values of D_m/L and D_n/L in Table 3, it is found that, for isotropic symmetry, the section for the inclined struts is smaller than that for the horizontal and vertical struts.

7.3.4 Face-centered cubic

The last example in the face-centered cubic unit cell shown in Fig. 22(d). The coefficients c_{ij}^* are as follows:

$$c_{11}^* = c_{22}^* = c_{33}^* = \frac{E}{L^4}\left(L^2 A_m + \sqrt{2}L^2 A_n + 24\sqrt{2}I_n\right), \tag{93}$$

$$c_{12}^* = c_{13}^* = c_{23}^* = \frac{\sqrt{2}E}{2L^4}\left(L^2 A_n + 24I_n\right), \tag{94}$$

$$c_{44}^* = c_{55}^* = c_{66}^* = \frac{E}{2L^4}\left(\sqrt{2}L^2 A_n + 12I_m + 6\sqrt{2}I_n\right), \tag{95}$$

which give

$$\hat{A} = \frac{2\sqrt{2}L^2 A_n + 24I_m + 12\sqrt{2}I_n}{24\sqrt{2}I_n + 2L^2 A_m + \sqrt{2}L^2 A_n} = 1. \tag{96}$$

For this unit cell, ψ_m and ψ_n are equal to 1 and $\sqrt{2}/2$, respectively. Writing A_m, A_n, I_m, and I_n in Eq. (96) in terms of m, n, and L gives

$$\hat{A} = \frac{24m^4 + 3\sqrt{2}n^4 + 16\sqrt{2}n^2}{32m^2 + 6\sqrt{2}n^4 + 8\sqrt{2}n^2} = 1. \tag{97}$$

The positive real solutions of n when m is set to 0.05, 0.10, 0.15, 0.20, and 0.25 obtained from the above equation are shown in Table 30. For this unit cell, for each m, both values of n are found to be larger than m. From the obtained results, only the smaller values of n for m equal to 0.05 and 0.10 can be considered as not too large. Among the two real solutions of n, the smaller one increases noticeably with m while the larger one decreases insignificantly. From the values of D_m/L and D_n/L in Table 30, it is found that, for isotropic symmetry, the section for the inclined struts is larger than that for the horizontal and vertical struts.

Table 30 Member sizes for isotropic symmetry

Unit cell	$\hat{A} = 1$	m	n	$(W_m \text{ or } D_m)/L = m\psi_m$	$(W_n \text{ or } D_n)/L = n\psi_n$
Body-centered square	$\dfrac{m^3 + n}{n^3 + m} = 1$	0.05	0.05000, 0.97406	0.05000	0.03536, 0.68877
		0.10	0.10000, 0.94624	0.10000	0.07071, 0.66909
		0.15	0.15000, 0.91653	0.15000	0.10607, 0.64808
		0.20	0.20000, 0.88489	0.20000	0.14142, 0.62571
		0.25	0.25000, 0.85128	0.25000	0.17678, 0.60195
Diamond-square	$\dfrac{m^6 + 8n^3m^3 + 8nm^3 + 16n^4}{4(2n^3 + m)(m^3 + 2n^3)} = 1$	0.05	0.02499, 0.98729	0.02500	0.01767, 0.69812
		0.10	0.04992, 0.97426	0.05000	0.03530, 0.68891
		0.15	0.07474, 0.96110	0.07500	0.05285, 0.67960
		0.20	0.09939, 0.94801	0.10000	0.07028, 0.67034
		0.25	0.12380, 0.93522	0.12500	0.08754, 0.66130
Body-centered cubic	$\dfrac{9m^4 + 3\sqrt{3}n^4 + 8\sqrt{3}n^2}{3(4m^2 + 3\sqrt{3}n^4)} = 1$	0.05	0.04652, 1.15376	0.05000	0.04029, 0.99919
		0.10	0.09301, 1.15095	0.10000	0.08055, 0.99675
		0.15	0.13943, 1.14625	0.15000	0.12075, 0.99268
		0.20	0.18573, 1.13967	0.20000	0.16084, 0.98698
		0.25	0.23186, 1.13118	0.25000	0.20079, 0.97963
Face-centered cubic	$\dfrac{24m^4 + 3\sqrt{2}n^4 + 16\sqrt{2}n^2}{32m^2 + 6\sqrt{2}n^4 + 8\sqrt{2}n^2} = 1$	0.05	0.08412, 1.63082	0.05000	0.05948, 1.15317
		0.10	0.16845, 1.62428	0.10000	0.11911, 1.14854
		0.15	0.25319, 1.61325	0.15000	0.17903, 1.14074
		0.20	0.33864, 1.59750	0.20000	0.23945, 1.12960
		0.25	0.42514, 1.57668	0.25000	0.30062, 1.11488

Chapter 8
Conclusions

This study employs the homogenization method based on equivalent strain energy to investigate various aspects of the effective elastic properties of frame-like periodic cellular solids. For frame-like periodic cellular solids, Euler beam elements can be used instead of solid elements in the determination of effective properties. The advantages of the Euler beam element in this type of analysis are that FE models using Euler beam elements are easier to create, and require less computational resources. More importantly, it is easier to prescribe periodic boundary conditions when beam elements are used. Since beam elements idealize the domain as connecting lines, models of unit cells that use beam elements must be carefully created. For example, if a strut is split among two unit cells longitudinally to create a unit cell, an Euler beam element with half the axial and bending rigidities must be used to represent the resulting strut in the unit cell. In the determination of the effective elastic properties of a periodic cellular solid by the homogenization method based on equivalent strain energy, periodic boundary conditions must be prescribed correctly as relative displacements between degrees of freedom.

According to the periodic cellular solids investigated in this study, the effective Young's moduli and shear moduli obtained from beam element models are lower than those obtained from solid element models. For the periodic cellular solids whose effective elastic properties are the same in all orthogonal axes and the material volume fractions are approximately 0.1–0.3, the differences of the effective Young's moduli from beam and solid element models are quite low and less than 5%. The differences of the effective shear moduli and the differences of the effective Poisson's ratios are diverse. The differences of all effective elastic constants from beam and solid element models are larger when the material volume fractions are higher.

By using the classical beam theory, the exact forms of the effective elastic properties of frame-like periodic cellular solids can be derived by employing the homogenization method based on equivalent strain energy. The obtained exact forms of the effective elastic constants are in terms of the characteristic length and volume of the unit cell, the area and moment of inertia of the struts, Young's modulus of the base material, and some dimensionless factors. In general, these dimensionless factors can be functions of the area and moment of inertia of the struts. However, for many practical unit-cell topologies, these dimensionless factors are constant. To utilize the proposed exact forms in the determination of the effective elastic constants of periodic cellular solids with a particular unit-cell topology, the dimensionless

factors can first be assumed to be constant. Their values are then determined from exact curve fitting using FE results with different sectional areas and moments of inertia of the struts. From all examples, it is found that the exact solutions of the effective elastic constants obtained from elaborate symbolic FE calculations and/or the literature can always be written in the proposed exact forms. When all dimensionless factors in the proposed exact forms are constant, the effective elastic constants obtained in this study by exact curve fitting are found to be exactly the same as the exact solutions from elaborate symbolic FE calculations and/or the literature.

In this study, a simple methodology to allow some common frame-like unit cells that do not generally yield periodic solids with isotropic symmetry to be used to create periodic solids with isotropic symmetry. The methodology utilizes the fact that individual sizes of struts in a unit cell of a periodic solid affect the resulting effective elastic constants of the periodic solid. As a result, the degree of anisotropy can be adjusted simply by changing relative unit-cell strut sizes. The unit cell under consideration is set to have two different variable strut sizes. By using the closed-form effective elastic constants, an equation to enforce isotropic symmetry is analytically constructed. This constraint equation provides the relation between the two variable strut sizes that is necessary for isotropic symmetry. It is evident that not all unit-cell topologies can be used as starting topologies in the proposed methodology. Unit cells that have struts align only in orthogonal directions are not valid candidates. This is simply because isotropic symmetry requires symmetry beyond orthogonal directions. Struts that are oblique to the orthogonal axes of the unit cell must be available for size adjustment. In this study, two different variable sizes for struts that are aligned with the unit cell's orthogonal axes and for struts that are oblique to the orthogonal axes are used to enforce isotropic symmetry. In each example considered in this study, the section for horizontal and vertical struts is fixed and the section for oblique struts is determined from the constraint equation. The constraint equations for 2D and 3D problems are nonlinear equations whose solutions include real and complex numbers. All examples considered in this study give two solutions that are positive real. In most cases, one of the two positive real solutions represents a section size that can be used for struts while the other solution represents a size that is too large. In a few cases, both positive real solutions represent section sizes that are too big. The obtained results demonstrate that the proposed methodology is a simple and viable method for designing frame-like periodic solids with given topologies for isotropic symmetry.

References

Alzebdeh, K. (2012). Evaluation of the in-plane effective elastic moduli of single-layered graphene sheet. International Journal of Mechanics and Materials in Design, 8(3), 269-278.

Andrews, E.W., Gioux, G., Onck, P., & Gibson, L.J. (2001). Size effects in ductile cellular solids. Part II: experimental results. International Journal of Mechanical Sciences, 43(3), 701-713.

Bower, A.F. (2010) Applied mechanics of solids. Boca Raton: CRC Press.

Challis, V.J., Roberts, A.P., & Wilkins, A.H. (2008). Design of three dimensional isotropic microstructures for maximized stiffness and conductivity. International Journal of Solids and Structures, 45(14-15), 4130-4146.

Dai, G., & Zhang, W. (2009). Cell size effect analysis of the effective Young's modulus of sandwich core. Computational Materials Science, 46(3), 744-748.

Dai, G.M., & Zhang, W.H. (2008). Size effects of basic cell in static analysis of sandwich beams. International Journal of Solids and Structures, 45(9), 2512-2533.

Doyoyo, M., & Hu, J.W. (2006). Multi-axial failure of metallic strut-lattice materials composed of short and slender struts. International Journal of Solids and Structures, 43(20), 6115-6139.

Drago, A., & Pindera, M.-J. (2007). Micro-macromechanical analysis of heterogeneous materials: Macroscopically homogeneous vs periodic microstructures. Composites Science and Technology, 67(6), 1243-1263.

Fang, Z., Starly, B., & Sun, W. (2005). Computer-aided characterization for effective mechanical properties of porous tissue scaffolds. CAD Computer Aided Design, 37(1), 65-72.

Fleck, N.A., & Qiu, X. (2007). The damage tolerance of elastic-brittle, two-dimensional isotropic lattices. Journal of the Mechanics and Physics of Solids, 55(3), 562-588.

Fleck, N.A., & Qiu, X. (2007). The damage tolerance of elastic–brittle, two-dimensional isotropic lattices. Journal of the Mechanics and Physics of Solids, 55(3), 562-588.

Gibson, L.J., & Ashby, M.F. (1999) Cellular Solids: Structure and Properties. Cambridge University Press.

Grenestedt, J.L. (1998). Influence of wavy imperfections in cell walls on elastic stiffness of cellular solids. Journal of the Mechanics and Physics of Solids, 46(1), 29-50.

Grima, J.N., Chetcuti, E., Manicaro, E., Attard, D., Camilleri, M., Gatt, R., & Evans, K.E. (2012). On the auxetic properties of generic rotating rigid triangles. Proceedings of the Royal Society of London A: Mathematical, Physical and Engineering Sciences, 468(2139), 810-830.

Guinovart-Díaz, R., Yan, P., Rodríguez-Ramos, R., López-Realpozo, J.C., Jiang, C.P., Bravo-Castillero, J., & Sabina, F.J. (2012). Effective properties of piezoelectric composites with parallelogram periodic cells. International Journal of Engineering Science, 53(0), 58-66.

Guth, D.C., Luersen, M.A., & Muñoz-Rojas, P.A. (2012). Optimization of periodic truss materials including constitutive symmetry constraints. Materialwissenschaft und Werkstofftechnik, 43(5), 447-456.

Guth, D.C., Luersen, M.A., & Muñoz-Rojas, P.A. (2015). Optimization of three-dimensional truss-like periodic materials considering isotropy constraints. Structural and Multidisciplinary Optimization.

Guth, D.C., Luersen, M.A., & Muñoz-Rojas, P.A. (2015). Optimization of three-dimensional truss-like periodic materials considering isotropy constraints. Structural and Multidisciplinary Optimization, 1-13.

Huang, H.T., Chang, S.L., Chien, C.S., & Li, Z.C. (2009). Superconvergence of high order FEMs for eigenvalue problems with periodic boundary conditions. Computer Methods in Applied Mechanics and Engineering, 198(30-32), 2246-2259.

Huang, X., Radman, A., & Xie, Y.M. (2011). Topological design of microstructures of cellular materials for maximum bulk or shear modulus. Computational Materials Science, 50(6), 1861-1870.

Jang, D., Meza, L.R., Greer, F., & Greer, J.R. (2013). Fabrication and deformation of three-dimensional hollow ceramic nanostructures. Nature Materials, 12(10), 893-898.

Jean, A., & Engelmayr Jr, G.C. (2010). Finite element analysis of an accordion-like honeycomb scaffold for cardiac tissue engineering. Journal of Biomechanics, 43(15), 3035-3043.

Kwon, Y.W., Cooke, R.E., & Park, C. (2003). Representative unit-cell models for open-cell metal foams with or without elastic filler. Materials Science and Engineering A, 343(1-2), 63-70.

Lin, L., Zhang, H., Yao, Y., Tong, A., Hu, Q., & Fang, M., Application of Image Processing and Finite Element Analysis in Bionic Scaffolds' Design Optimizing and Fabrication, in: K. Li, X. Li, G. Irwin, & G. He (Eds.) Life System Modeling and Simulation, Springer Berlin Heidelberg, 2007, pp. 136-145.

Lipperman, F., Ryvkin, M., & Fuchs, M.B. (2008). Crack arresting low-density porous materials with periodic microstructure. International Journal of Engineering Science, 46(6), 572-584.

Liu, T., Deng, Z.C., & Lu, T.J. (2006). Design optimization of truss-cored sandwiches with homogenization. International Journal of Solids and Structures, 43(25-26), 7891-7918.

Luxner, M.H., Stampfl, J., & Pettermann, H.E. (2005). Finite element modeling concepts and linear analyses of 3D regular open cell structures. Journal of Materials Science, 40(22), 5859-5866.

Luxner, M.H., Stampfl, J., & Pettermann, H.E. (2009). Nonlinear simulations on the interaction of disorder and defects in open cell structures. Computational Materials Science, 47(2), 418-428.

Michel, J.C., Moulinec, H., & Suquet, P. (1999). Effective properties of composite materials with periodic microstructure: A computational approach. Computer Methods in Applied Mechanics and Engineering, 172(1-4), 109-143.

Milton, G.W. (1992). Composite materials with poisson's ratios close to — 1. Journal of the Mechanics and Physics of Solids, 40(5), 1105-1137.

Mohsen Karimian, S.A., & Straatman, A.G. (2007). A thermal periodic boundary condition for heating and cooling processes. International Journal of Heat and Fluid Flow, 28(2), 329-339.

Nemat-Nasser, S., & Hori, M. (1999) Micromechanics: Overall Properties of Heterogeneous Materials, Second Edition (North-Holland Series in Applied Mathematics and Mechanics). North Holland.

Neves, M.M., Rodrigues, H., & Guedes, J.M. (2000). Optimal design of periodic linear elastic microstructures. Computers and Structures, 76(1), 421-429.

Onck, P.R., Andrews, E.W., & Gibson, L.J. (2001). Size effects in ductile cellular solids. Part I: Modeling. International Journal of Mechanical Sciences, 43(3), 681-699.

Pindera, M.-J., Khatam, H., Drago, A.S., & Bansal, Y. (2009). Micromechanics of spatially uniform heterogeneous media: A critical review and emerging approaches. Composites Part B: Engineering, 40(5), 349-378.

Sam, P. (2015). Symbolic-numerical object-oriented finite element programming. Master's Degree Thesis. Sirindhorn International Institute of Technology, Thammasat University.

Shan, S., Kang, S.H., Zhao, Z., Fang, L., & Bertoldi, K. (2015). Design of planar isotropic negative Poisson's ratio structures. Extreme Mechanics Letters, 4(96-102.

Shufrin, I., Pasternak, E., & Dyskin, A.V. (2012). Planar isotropic structures with negative Poisson's ratio. International Journal of Solids and Structures, 49(17), 2239-2253.

Sigmund, O. (1994). Materials with prescribed constitutive parameters: An inverse homogenization problem. International Journal of Solids and Structures, 31(17), 2313-2329.

Sigmund, O. (1995). Tailoring materials with prescribed elastic properties. Mechanics of Materials, 20(4), 351-368.

Srikantha Phani, A., & Fleck, N.A. (2008). Elastic boundary layers in two-dimensional isotropic lattices. Journal of Applied Mechanics, Transactions ASME, 75(2), 0210201-0210208.

Srikantha Phani, A., Woodhouse, J., & Fleck, N.A. (2006). Wave propagation in two-dimensional periodic lattices. Journal of the Acoustical Society of America, 119(4), 1995-2005.

Sullivan, R.M., & Ghosn, L.J. (2009). Shear moduli for non-isotropic, open cell foams using a general elongated Kelvin foam model. International Journal of Engineering Science, 47(10), 990-1001.

Sullivan, R.M., Ghosn, L.J., & Lerch, B.A. (2008). A general tetrakaidecahedron model for open-celled foams. International Journal of Solids and Structures, 45(6), 1754-1765.

Suquet, P.M., Elements of Homogenization for Inelastic Solid Mechanics, in: Homogenization techniques for composite media, Springer-Verlag, 1987, pp. 193-278.

Thiyagasundaram, P., Sankar, B.V., & Arakere, N.K. (2010). Elastic properties of open-cell foams with tetrakaidecahedral cells using finite element analysis. AIAA Journal, 48(4), 818-828.

Vigliotti, A., & Pasini, D. (2012). Linear multiscale analysis and finite element validation of stretching and bending dominated lattice materials. Mechanics of Materials, 46(0), 57-68.

Wallach, J.C., & Gibson, L.J. (2001). Mechanical behavior of a three-dimensional truss material. International Journal of Solids and Structures, 38(40–41), 7181-7196.

Wang, A.J., & McDowell, D.L. (2004). In-plane stiffness and yield strength of periodic metal honeycombs. Journal of Engineering Materials and Technology, Transactions of the ASME, 126(2), 137-156.

Wang, H.B., Zhang, W.H., Xu, Y.J., & Zeng, Q.F. (2008). Numerical computing and experimental validation of effective elastic properties of 2D multilayered C/SiC composites. Materials Science and Technology, 24(11), 1385-1398.

Xia, Z., Ju, F., & Sasaki, K. (2007). A general finite element analysis method for balloon expandable stents based on repeated unit cell (RUC) model. Finite Elements in Analysis and Design, 43(8), 649-658.

Xu, Y., & Zhang, W. (2011). Numerical modelling of oxidized microstructure and degraded properties of 2D C/SiC composites in air oxidizing environments below 800 °C. Materials Science and Engineering: A, 528(27), 7974-7982.

Yan, J., Cheng, G., Liu, S., & Liu, L. (2006). Comparison of prediction on effective elastic property and shape optimization of truss material with periodic microstructure. International Journal of Mechanical Sciences, 48(4), 400-413.

Yeong, W.Y., Sudarmadji, N., Yu, H.Y., Chua, C.K., Leong, K.F., Venkatraman, S.S., Boey, Y.C.F., & Tan, L.P. (2010). Porous polycaprolactone scaffold for cardiac tissue engineering fabricated by selective laser sintering. Acta Biomaterialia, 6(6), 2028-2034.

Zhang, W., Dai, G., Wang, F., Sun, S., & Bassir, H. (2007). Using strain energy-based prediction of effective elastic properties in topology optimization of material microstructures. Acta Mechanica Sinica, 23(1), 77-89.

Zhang, W., Dai, G., Wang, F., Sun, S., & Bassir, H. (2007). Using strain energy-based prediction of effective elastic properties in topology optimization of material microstructures. Acta Mechanica Sinica/Lixue Xuebao, 23(1), 77-89.

Zhang, W., Wang, F., Dai, G., & Sun, S. (2007). Topology optimal design of material microstructures using strain energy-based method. Chinese Journal of Aeronautics, 20(4), 320-326.

Zhu, H.X., Knott, J.F., & Mills, N.J. (1997). Analysis of the elastic properties of open-cell foams with tetrakaidecahedral cells. Journal of the Mechanics and Physics of Solids, 45(3), 319-343.